HIGHWAY RESEARCH RECORD

Number 428

Bridge Evaluation and Analysis

7 reports
prepared for the
52nd Annual Meeting

Subject Area

27 Bridge Design

HIGHWAY RESEARCH BOARD
DIVISION OF ENGINEERING NATIONAL RESEARCH COUNCIL
NATIONAL ACADEMY OF SCIENCES—NATIONAL ACADEMY OF ENGINEERING
Washington, D.C. 1973

NOTICE

The studies reported herein were not undertaken under the aegis of the National Academy of Sciences or the National Research Council. The papers report research work of the authors that was done at the institutions named by the authors. The papers were offered to the Highway Research Board of the National Research Council for publication and are published here in the interest of the dissemination of information from research, one of the major functions of the Highway Research Board.

Before publication, each paper was reviewed by members of the HRB committee named as its sponsor and accepted as objective, useful, and suitable for publication by the National Research Council. The members of the review committee were chosen for recognized scholarly competence and with due consideration for the balance of disciplines appropriate to the subject concerned.

Responsibility for the publication of these reports rests with the sponsoring committee. However, the opinions and conclusions expressed in the reports are those of the individual authors and not necessarily those of the sponsoring committee, the Highway Research Board, or the National Research Council.

Each report is reviewed and processed according to the procedures established and monitored by the Report Review Committee of the National Academy of Sciences. Distribution of the report is approved by the President of the Academy upon satisfactory completion of the review process.

ISBN 0-309-02157-X
Library of Congress Catalog Card No. 73-7058
Price: $2.20
Available from
Highway Research Board
National Academy of Sciences
2101 Constitution Avenue, N. W.
Washington, D. C. 20418

CONTENTS

FOREWORD

The seven papers contained in this RECORD report on analytical and experimental research on bridge components as well as full-scale field testing. The information will be of particular interest to those having responsibility for evaluation of bridge performance and the development of design specifications. Included also is information related to assessing the aesthetic appeal of bridge designs.

By using a sequence of paired line drawings in which one visual factor is varied at a time and a panel of people selects the preferred one, Zuk has developed a systematic methodology to rationally determine the aesthetic appeal of bridges. The study indicated that aesthetic preference is given to such factors as simplicity, slimness, symmetry, conformity to the site, and expression of out-of-the-ordinary characteristics.

Ramey and Tattershall report on the use of the finite element technique to assess the effects of large web openings in the bent cap region of concrete box girder highway bridges. The size, shape, and location of openings were varied, and it was concluded that a design based on a single rectangular opening would be satisfactory when separated by at least half the depth of the member. Methods are presented for designing the reinforcing around openings.

The response of concrete box girder bridges to AASHO design loadings and a specific overload vehicle is the subject of the paper by Scordelis, Bouwkamp, and Wasti. Results of a large-scale model study indicate that this type of bridge has excellent load distribution properties. However, total stresses in the steel and concrete under three lanes of AASHO trucks or one lane of the overload vehicle were found to exceed allowable values. No distress in the bridge was observed under either loading.

The paper by Zundelevich, Hamada, and Chiu reports the results of a study on the time-dependent behavior of Hawaii aggregate lightweight concrete. The two-part study covers both the creep characteristics under uniaxial compression of cylinders and the camber and deflection characteristics under repeated flexural loads of prestressed beams. Mathematical models for creep, camber, and deflections are discussed, and a statistical evaluation of deflection data is presented.

Stress ranges caused by normal traffic on six bridges are summarized by Goodpasture and Burdette, and these are compared with calculated stresses using two AASHO design vehicles. Stresses calculated for the AASHO loadings are shown to exceed almost all stress ranges measured in the field, and one-half of this stress is shown to compare favorably with a significant number of stress ranges encountered on the most highly stressed girder.

Peterson and Kostem present the findings of an analytical study on the determination of vehicle-induced dynamic response of highway bridge superstructures. The investigators use the finite element displacement approach, which assumes the superstructure to be two-dimensional, a composition of discrete beam and slab elements. Good correlation was observed when analytical results using the AASHO design vehicle were compared with data obtained from field tests performed on the actual bridge.

The final paper by Bowers reports on the testing of two single-span bridges to determine the magnitude and frequency of stress ranges induced by normal live loading. The study was undertaken as a result of a catastrophic failure of a cover-plated steel beam that fractured along the toe of the fillet weld at the end of the primary cover plate. Results of tests on both bridges showed that a majority of stress ranges at cover plate ends fell within 0.60- to 1.95-ksi levels and a very limited number exceed 3.0. The authors raise the question of whether low-level stress ranges can perhaps drastically shorten the service life of welded cover-plated members.

METHODOLOGY FOR EVALUATING THE AESTHETIC APPEAL OF BRIDGE DESIGNS

William Zuk, Virginia Highway Research Council

Presented is a systematic methodology for rationally determining the aesthetic appeal of bridge designs by the use of paired line drawings where one visual factor at a time is varied. These paired drawings are then judged by either a preselected or randomly selected group of people. An example (using a standard bridge overpass) is selected as a vehicle to explain the method. The method is such that conclusions can be clearly drawn from the judgments of the example. The results show that aesthetic preference is generally given to such factors as simplicity, slimness, symmetry, conformity to the site, and expression of out-of-the-ordinary characteristics. Other more detailed conclusions are also determined and presented in the body of the report.

•THE APPEARANCE of bridges has always commanded the interest of not only bridge builders but also most people who see them.. In designing bridges for safety, engineers are guided by precise codes, yet in their designs few of them are guided by any sort of aesthetic rationale. In some recent references (1 through 10) a number of characteristics and illustrations are given to depict bridges that are said to be pleasing in appearance. Unfortunately, the authors offer no validation of their statements concerning aesthetic content except the force of their own convictions. This is not to question their conclusions but to suggest that there might be an alternate way to evaluate the appearance of bridges more systematically, a way that puts aesthetic judgments on a broad base and is supported by rational data.

The testing procedure presented is dependent on the fact that in bridges relatively few elements are involved (supports, span, end abutments, and railings) in contrast to other works of art (as architecture, painting, and sculpture) where the constraints are few and the elements are many. However, even with only four basic visual elements of bridges, countless variations and combinations are possible. But, once again, the economic and technological constraints imposed on bridges reduce the number of variations to a manageable level.

It is known that decisions can most easily be made by comparing one situation or object with another. In the case of bridges, if the difference between two relates to one particular feature, that feature can be isolated (relative to the whole) and evaluated on its effect on appearance. In this way, preferences for different features and combinations of features can be systematically evaluated, always in a set of two.

It is also well known that decisions on the appearance of an object depend on who is doing the judging. One person may like an object, whereas another may dislike it. For this study two groups were used. Group I included people such as artists, architects, and landscape architects who have been formally trained in aesthetics. The second group included a random assortment of people, professional and nonprofessional, young and old, who have not had formal training in the arts. The majority opinion of each group is used to establish the preference position.

Sponsored by Committee on Bridge Design.

METHODOLOGY AND EXAMPLE

The specifics of the methodology described will be illustrated by example. The example is a short-span overpass highway bridge as might be seen on many of today's Interstate highways. The view is that of one driving at highway speeds, such that detail cannot be observed. All bridges shown are simple line drawings so that only the essential elements can be presented (avoiding distractions) and the controlled features can be easily varied. Line drawings are also useful to a bridge designer in that he does not have to construct models or build the actual bridge before an aesthetic evaluation can be made. Certain computers equipped with "light-pens" can be used to make line drawings that can be quickly changed.

Features that are varied include the piers, the spanning element, the end aubtments, and the rail. The proportions of these elements are varied along with their interrelationships with one another, as pier to span, abutment to span, or rail to span. The relation of the bridge form to the site and the color of the bridge as related to its environment are other factors varied.

All possible proportions or relationships have not been included in this example; however, should need arise to include other variables, no change in the basic methodology is needed.

In application, a copy of a brochure was given to a subject with instructions to compare the two diagrams on each page and indicate which one he found more pleasing visually at a quick glance. The subject was asked to disregard as much as possible any concern about the functionality of the bridge. The reasons for choices were not asked, although in some cases the subject volunteered such information.

Due to lack of space, only a few of the figures are included. Figure 1 shows the control bridge and some of the variations presented. The subject was presented with the control and a variation of the control and was asked to indicate of the two which he found more aesthetically pleasing. Figure 2 shows the control and a variation of it as they were presented. In regard to variations, six basic categories are believed to have relevance to aesthetic bridge design: (a) proportion of elements, (b) relation of elements, (c) degree of visual complexity, (d) site compatibility, (e) color, and (f) expression of out-of-the-ordinary characteristics. Expression of functionality and safety was omitted inasmuch as it was not considered a basis for aesthetic appeal.

In most of the comparative figures, one of the categories predominated as the variant, although in a few cases two categories may be suggested. For purposes of analysis, however, only one was listed for each pair. Table 1 gives the results of the survey. The reasons for choices were not asked, but in some cases the subjects volunteered such information.

The population interviewed in Group I included 29 architects, two landscape architects, and one artist (30 males and two females) ranging in age from 19 to 47. The population in Group II included 18 nonprofessional females, seven professional females, seven nonprofessional males, and 12 professional males, ranging in age from 16 to 55. The nonprofessional category included occupations such as homemaker, secretary, and laborer, and the professional category included occupations such as teacher, engineer, and medical doctor.

ANALYSIS AND CONCLUSIONS

The conclusions for the entire set of figures, derived from data given in Table 1, are as follows:

1. Groups I and II both like simplicity of form and simple relationships of elements.
2. Groups I and II both like slimly proportioned elements as piers, abutment, span, and rail.
3. Groups I and II both overwhelmingly favor symmetrical relationships of elements over unsymmetrical relationships.
4. Groups I and II both like bridges with some out of the ordinary characteristics, in particular, forms such as arches or those suggesting arches.
5. Groups I and II both like bridge forms that conform to the dominant features of the site.

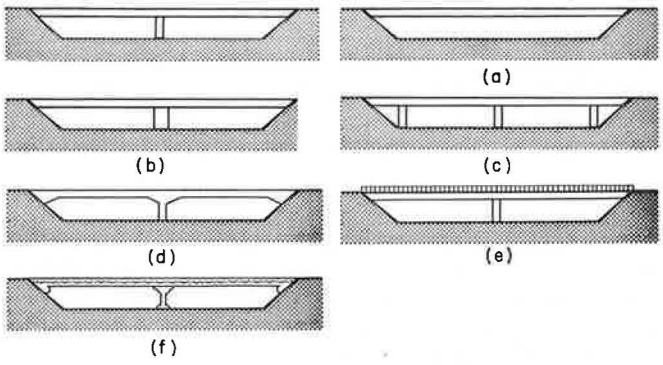

Figure 1. Control bridge (a) without pier, (b) with widened pier, (c) with two additional piers, (d) with haunches, (e) with open rail, and (f) with decorative embellishments.

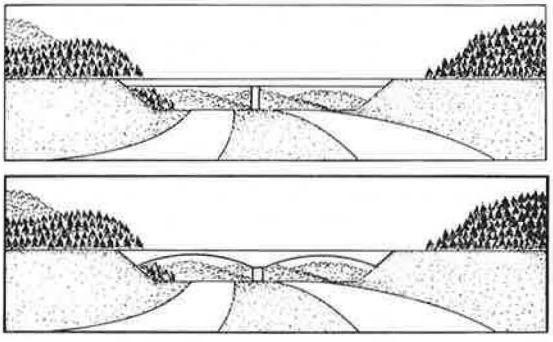

Figure 2. Control bridge and control bridge with arch variation both set in rural environment.

Table 1. Survey results.

Principal Variant[a]	Percentage for Control and Variable		Comments
	Group I	Group II	
c	6-94	54-46	Group I prefers extreme simplicity of no piers, whereas Group II is about evenly divided
a	69-31	75-25	Preference toward slim spanning element
a	69-31	61-39	Preference toward slim pier
b	69-31	61-39	Preference toward overall slim proportions
b	75-25	72-28	Preference toward simple relation of piers to span (few piers)
b	75-25	82-18	Preference for few piers
c	72-28	75-25	Preference toward simply shaped piers (no visible base)
c	47-53	70-30	Group II prefers simply shaped piers (no capitals), whereas Group I is about evenly divided
f	44-56	28-72	Preference toward simple pier but with special character
f	35-65	43-57	Preference toward span with special character
b	88-12	95-5	Overwhelming preference for symmetry
c	53-47	84-16	Group II strongly prefers simple lines of span, whereas Group I is about evenly divided
b	50-50	57-43	Generally evenly divided, but somewhat in favor of no exposed end abutment
a	41-59	34-66	Preference toward modest-sized abutment
b	78-22	57-43	Preference for "invisible rail"
a	38-62	43-57	Preference for slim rail appearance
f	4-94	23-77	Preference for bridge form of special character
b	60-40	52-48	Preference for simple relation between pier and span (arch form)
c	66-34	70-30	Dislike of superficial decorative elements
d	31-69	32-68	Preference for bridge form in harmony with site
e	44-56	48-52	Slight preference for bridge color (gray) contrasting with concrete pavement (white)
e	53-47	45-55	About evenly divided on bridge color contrasting or blending with bituminous (gray) pavement
e	19-81	77-23	Group I strongly prefers bridge color contrasting with environment, whereas Group II prefers blending color

[a]a = proportion of elements; b = relation of elements; c = degree of visual complexity; d = site compatibility; e = color; f = expression of out-of-the-ordinary characteristics.

6. Group I strongly prefers a bridge color that contrasts with the environment, whereas Group II strongly prefers a bridge color that blends with the environment.

7. Group I is somewhat influenced in aesthetic judgment by the preference for a clear expression of functionality, and Group II is similarly influenced by an appearance of structural adequacy or safety. (Both factors are related, but because of eductional and training differences they are seen and expressed differently.)

Considered as an example of the methodology, the described procedure and results are believed to have accomplished the goal intended: that of systematically evaluating the aesthetic appeal of different bridge designs and rationally determining patterns of preference. The example used was not designed to arrive at one specific most pleasing bridge form, although by the same technique of comparative designs one form could have been so determined. However, by inference, it appears that arch related forms are generally preferred over all others presented, including the control bridge form.

Interestingly, the results of Groups I and II are dissimilar on only one point, that of color contrast or harmony. On points of form, the two groups are generally in agreement. The latter conclusion is reassuring in that the position of "taste-makers" and that of the general public are essentially the same on most issues, provided a large enough sampling is made. (It is to be noted that there was no figure in the brochure that was unanimously selected or rejected by all.)

ACKNOWLEDGMENTS

Appreciation is extended to all those who participated in this survey and generously gave of their time for discussion of their opinions on bridge aesthetics in general.

REFERENCES

1. Wegenroth, R. H. Bridge Engineer Looks at Esthetics of Structures. Jour. Structural Div., Proc. ASCE, Vol. 97, No. ST4, Proc. Paper 8074, April 1971, pp. 1227-1237.
2. Prize Bridges of 1971. AISC, New York, 1971.
3. Visual Values for Highways. Graduate School of Design, Harvard Univ., Sept. 1970.
4. The Highway and Its Environment. Third Annual Awards Competition, Federal Highway Administration, U.S. Dept. of Transportation, 1970.
5. Prize Bridges of 1970. AISC, New York, 1970.
6. Concrete Bridge Design. ACI, SP-23, 1969, pp. 1-18.
7. The Appearance of Bridges. Ministry of Transport, Great Britain, 1969.
8. Leonhardt, F. Aesthetics of Bridge Design. PCI Jour., Feb. 1968, pp. 14-31.
9. The Freeway in the City. U.S. Govt. Print. Office, Washington, D.C., 1968.
10. Appleyard, D., et al. View From the Road. M.I.T. Press, Cambridge, 1966.

REINFORCING REQUIREMENTS FOR CONCRETE BEAMS WITH LARGE WEB OPENINGS

Melvin R. Ramey, University of California, Davis; and
Delbert W. Tattershall, Dravo Corporation, Pittsburgh, Pennsylvania

The finite element technique was used to assess the effects of large web openings in the bent cap region of concrete box girder highway bridges. Bent caps were modeled that contained openings ranging in size from 0.21 to 0.625 of the member depth. The shape and location of the opening were varied. Sixty simply supported beams were also analyzed to provide the basis for a working stress design procedure suggested for use in determining the reinforcing requirements in the vicinity of the opening. The analyses showed that a design based on a single rectangular opening would be satisfactory as long as adjacent openings were separated by at least half the depth of the member. The Vierendeel method was found to be acceptable for designing the reinforcing in the chord regions of the opening, whereas special curves were developed to permit the design of the reinforcing needed to resist the stress concentrations at the corners. Twelve laboratory specimens were designed in accordance with the suggested design procedure. Subsequent testing indicated that the reinforcing provided around the opening adequately strengthened this portion of the member so that the load-carrying capacity was governed by the behavior of the solid part of the beam. /AUTHOR/

•INCREASINGLY, beams and girders are being designed with large web openings to provide passage for service conduits that, for either aesthetic reasons or headroom problems, cannot be suspended below the girder. Such openings alter the stress distribution significantly and usually require special reinforcing around their periphery. In highway construction this technique has been employed to place pipelines, electrical conduits, and drainage systems inside concrete box girder bridges. The cellular nature of the box girder highway bridge is particularly well suited for carrying service conduits; however, to provide an unobstructed pathway through the bridge requires that large holes be built into the bent caps (Fig. 1).

This paper presents the results of a study aimed at developing a suitable working stress design procedure for determining the reinforcing requirements around the web openings used in concrete box girder highway bridge bent caps. The finite element method was used to obtain the elastic stress distribution around various sizes, shapes, and locations of these holes, and a limited experimental program was undertaken to test the suitability of a proposed design procedure.

The analytical technique often used to determine the elastic stress distribution around holes in beams evolves from elasticity theory that uses conformal mapping techniques (1, 2, 3). In general the solutions apply to members where the opening is small in comparison to the face of the beam in which the opening is placed. Further, when this method is used, it is usually difficult to treat complicated boundary conditions and oddly shaped holes.

A different but common analytical method used to determine the stresses in the vicinity of the opening is the Vierendeel truss technique. This technique has been used

Sponsored by Committee on Concrete Superstructures.

Figure 1. Cutaway view of box girder highway bridge.

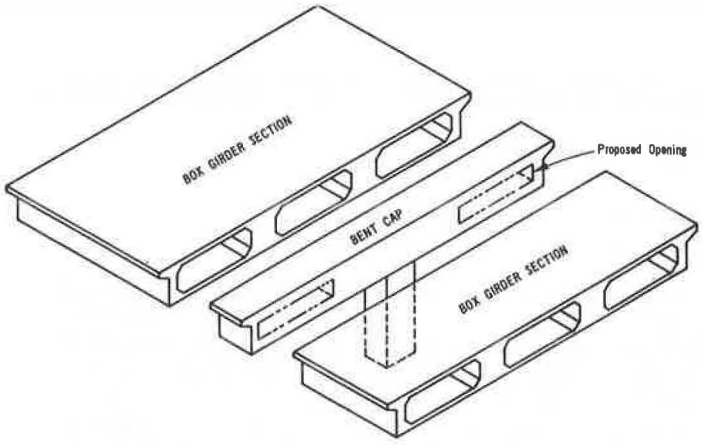

Figure 2. Cross section and dimensions of cantilever and two-column box girder highway bridge.

TABLE 1 BENT CAPS ANALYZED

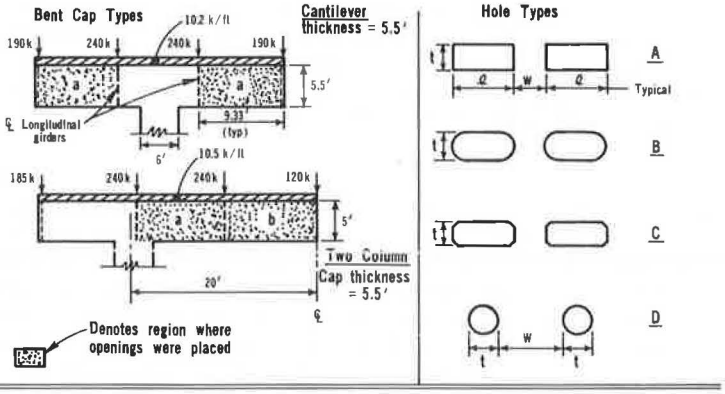

Mark	Bent Type	Location of Opening (s)	No. Opening per bay	Hole Type	ℓ (ft)	W (ft)	t (ft)
B-0	Cantilever	None	–	–	–	–	–
B-1		a	1	A	4.0	0	2.0
B-2		a	2	A	2.0	2.75	2.0
B-3		a	2	A	2.0	1.0	2.0
B-4		a	1	A	6.0	0	2.5
B-5		a	2	A	3.0	1.0	2.5
B-6		a	1	C	6.0	0	2.5
B-7		a	1	B	6.0	0	2.5
B-8		a	2	D	–	2.0	2.25
C-1	Cantilever	a	1	A	7.0	0	0.5
↕	↕	↕	↕	↕	↕	↕	↕
C-8	Cantilever	a	1	A	7.0	0	4.5
D-0	Two Column	None	–	–	–	–	–
D-1		a	1	A	6.0	0	3.0
D-2		b	1	A	6.0	0	3.0
D-3		a, b	1	A	6.0	0	3.0
D-4		a	1	C	6.0	0	3.0
D-5		b	1	C	6.0	0	3.0
D-6		a, b	1	C	6.0	0	3.0
D-7		a	1	B	6.0	0	3.0
D-8		b	1	B	6.0	0	3.0
D-9		a, b	1	B	6.0	0	3.0
D-10		a	1	A	4.0	0	2.0
D-11		b	1	A	4.0	0	2.0
D-12		a, b	1	A	4.0	0	2.0
D-13		a	2	D	–	2.75	2.0
D-14		b	2	D	–	2.75	2.0
D-15		a, b	2	D	–	2.75	2.0
D-16		a	1	D	–	0	3.0
D-17		b	1	D	–	0	3.0
D-18	Two Column	a, b	1	D	–	0	3.0

Varies in 0.5-ft. intervals

to proportion reinforcements surrounding the openings in steel beams (5) and has been compared to a classical elasticity solution for both round and rectangular openings in steel beams (3). In his study, Bower (4) found that the Vierendeel analysis did not predict the stress concentrations that occurred at the corners of the holes, whereas the elasticity analysis did. Further investigation showed, however, that the simpler Vierendeel analysis was adequate for most design problems in steel inasmuch as local yielding of the material at the corners was permissible.

Previous experimental data on both steel and concrete members clearly indicate that, if properly reinforced, the region of the beam containing the opening does not prevent the member from supporting the same loads as when the hole was not present (4 through 13). Many of the tests were performed on beams subjected to pure flexure or flexure and small shear forces. It was generally concluded that a beam loaded to provide pure flexure in the region of an unreinforced central opening is as strong as a similar beam without a hole. However, under combined shear and flexure, the presence of an unreinforced opening often causes a reduction in beam strength. In a study of the effects of the interaction between two or more holes, it was concluded that adjacent, identical circular openings did not reduce steel I-beam capacities for the spacings tested, but identical, adjacent rectangular openings had a substantial effect when their spacing was less than one-half their depth (13).

The use of the finite element technique permitted an analysis to be made of the member where the following parameters were varied:

1. Magnitude of the shear and moment at the opening,
2. Size and shape of the opening, and
3. Influence of adjacent openings.

A subsequent review of these results was used to suggest a working stress design method to proportion the reinforcing around the web opening.

METHOD OF ANALYSIS

The various bent cap configurations were modeled on an IBM 7044 digital computer using a plane stress finite element computer program developed by E. L. Wilson (14). The material properties were assumed to be linearly elastic, homogeneous, and isotropic. The original program was slightly modified to provide for automatic finite element mesh generation. A contour plotting program (15) was used to generate contours of maximum principal tensile stresses. This was a convenient way to survey the entire stress field and find areas of particularly high stress.

Two groups of structures were analyzed. The first group consisted of 35 bent caps subjected to the HS20-44 live load as specified by AASHO and the state of California (16). The most severe loading condition was a standard lane load plus a concentrated load rider for shear. The bent caps were supported with either a single column at midspan (cantilever type) or two columns spaced 40 ft apart (Fig. 2). In both cases the loads and openings were symmetrically arranged. The overall geometry and loads for the cantilever cap were based on the example found in Chapter 6 of the California Division of Highways Manual of Bridge Design Practice, 2nd Edition. The loads used in the two-column bent cap were derived from a three-span continuous box girder structure having equal spans of 90 ft.

In practice the bent caps are often subjected to torsional effects due to asymmetrical loadings on spans adjacent to the cap. In the present study, such torsional effects are not included.

The second group of structures analyzed consisted of 60 simply supported beams containing one or two openings. Concentrated loads were applied at specified locations to produce desired moments and shears at the mid-length of the opening. All beams were the same overall size (11 ft long and 2 ft deep) and contained 2-ft long openings. Of the 60 beams, 44 were simply supported on 10-ft centers, whereas the remaining 16 were supported on $8\frac{1}{2}$-ft centers with a 2-ft cantilever (Fig. 3). The variables considered are as follows:

1. Ratio of beam depth h to hole depth t,
2. Shear-to-moment ratio M/V at the mid-length of the opening, and
3. Interaction of adjacent openings.

All openings were located at mid-depth of the beams.

ANALYTICAL RESULTS

Region Affected by the Opening

The principal tensile stress contours for representative cantilever bent cap configurations are shown in Figure 4. Comparison of the principal tensile stress patterns in the solid member (Fig. 4a) to similar members containing large web openings illustrates the vast alteration of the stress distribution. First, note that inflection points occur approximately at the midspan of the chords, particularly for those members with a single rectangular opening. These inflection points are key factors in the design of the chords where a Vierendeel analysis is used. Second, for all but the circular openings, stress concentration patterns were evident at each corner of the hole. As reported by Nasser, Acavalos, and Daniel (8) and predicted by the Vierendeel analysis, corners along a common diagonal have the same stress sign. For example, in the cantilever bent cap shown in Figure 4b the stresses in corners A and C are tensile, whereas those in B and D are compressive.

An examination of tne principal tensile stress contours and the computer output showed that the disturbance caused by the addition of square, rectangular, and nearly rectangular openings was limited to a small region around the opening. For a bent cap of depth h, the stress approximately 0.46h from the edge of the hole was found to be essentially the same as in the solid member. Similar results were obtained from the analyses of the simply supported beams.

Effect of Size and Shape of the Opening

The effect of various hole sizes was studied by increasing the depth of a 7-ft long rectangular hole in a cantilever bent cap from 0.5 to 4.5 ft in 0.5-ft increments (Fig. 2). The resulting principal tensile stress contours showed that, as the depth of the hole increased relative to the height of the bent cap, the stress concentrations at the corners and the stresses in the chords also increased. The same effect has been reported by others for different geometries and loading conditions (1).

To study the effect that shape of the opening had on the magnitude and distribution of the stress concentrations around the corners of the opening, we analyzed members with rectangular, square, or circular holes. Additionally, analyses were done on rectangular openings with small corner fillets and openings having an oval shape. Holes of these shapes were selected because they are representative of those currently being placed in the web regions of flexural members.

Analyses showed that the stress concentrations for the rectangular holes were not significantly different from the rectangular openings with filleted corners or those with rounded ends. For example, one may compare the stress contours in Figures 4b, 4d, and 4e. Not only did the circular openings have smaller stress concentrations, but also the distance affected by the opening was smaller than the same size rectangular openings. Compare Figures 4c and 4f.

The results suggest that a design procedure based on rectangular openings will be satisfactory for the usual shapes of holes and that the size of the opening, as represented by the depth, is a significant variable.

Effect of Adjacent Openings

The large spacing between the longitudinal girders of the bridge makes it possible to consider locating either one large opening or several smaller ones in the bent cap. To study the latter situation, we placed two holes in a member and varied the distance between them. Figure 5 shows how the stress distribution around a single hole, L, changed when a second hole, R, was introduced and moved closer.

Figure 3. Beam configurations and hole types.

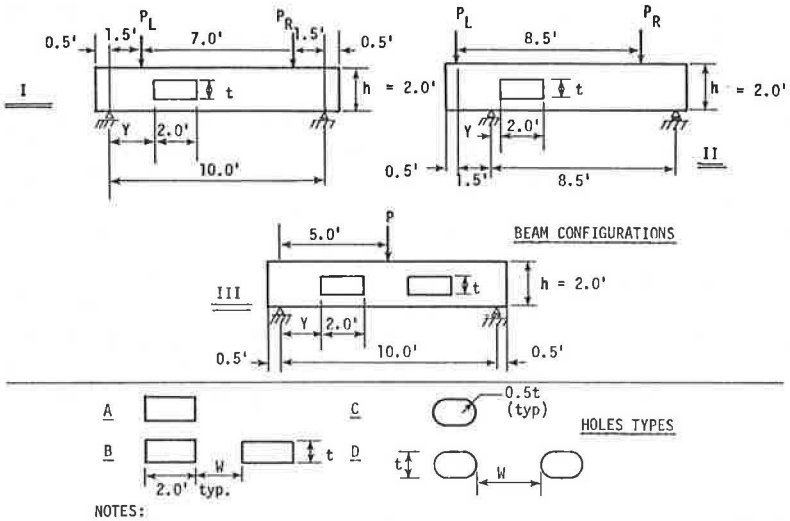

NOTES:

1. t/h varies from 0.21 to 0.625.
2. M/Vh varies from 0.1 to 6.48, obtained by using different values of P, P_L and P_R.
3. W varies from 0.5'to 2.0'.
4. Y varies from 0.5' to 4.5'.
5. See reference 17 for additional details.

Figure 4. Principal tension stress contours.

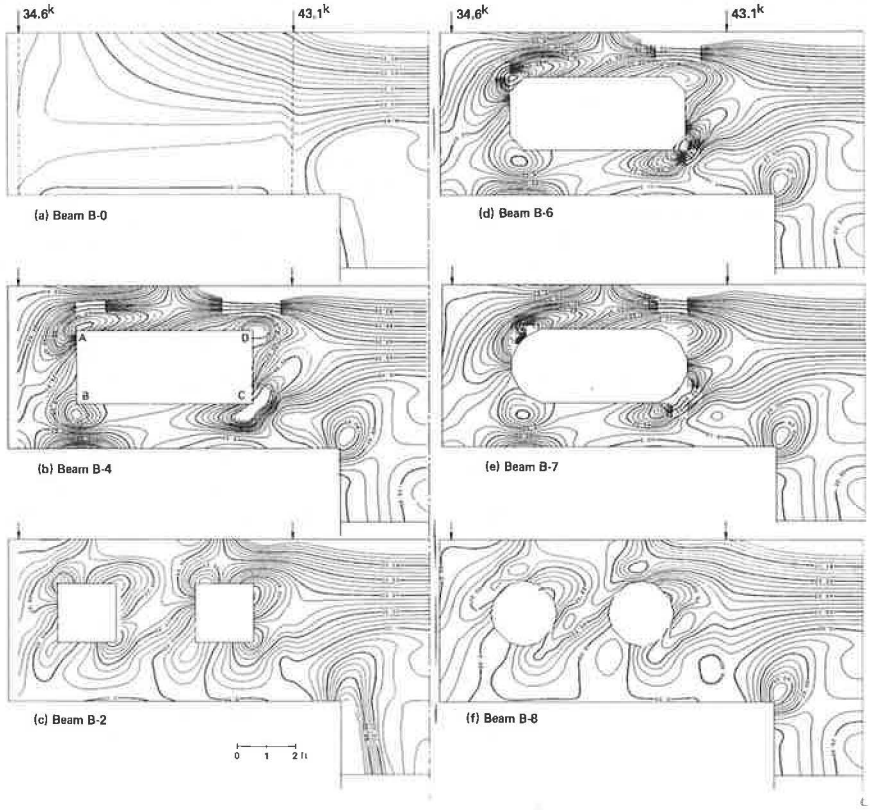

When hole R was farther than 0.5h away from hole L, the magnitude and distribution of the stresses around the corners of hole L changed very little from their values when hole R was not present. When hole R was closer than 0.5h the stress distribution around hole L changed significantly, particularly on the side closest to hole R. Similar results have been reported for experimental tests on steel wide-flanged sections (13).

Studies of the effects of multiple web openings in steel beams have shown that the resulting interaction equations for the shear and moment in the web post separating closely spaced holes are quite complex (7). Nevertheless, the equations were found to be conservative, and the single-hole analysis was found to be sufficient for the prediction of the failure load. Similar results for concrete members are not available, but it is clear that, when the holes are close (less than 0.5h separating them), special attention must be given to the design of the web post.

In the development that follows, it is assumed that adjacent holes are separated by at least 0.5h so that the design may be based on a single-hole analysis. In most situations, a single opening of the desired size can be more easily designed and fabricated than two separate openings.

Comparison of Finite Element and Vierendeel Solutions

The Vierendeel method is most often used to design the chord regions of beams containing large openings. In this study, the finite element and Vierendeel solutions were compared to determine whether the Vierendeel method could be used satisfactorily for different load and geometry variations. Fourteen of the simply supported beams were used in this case, and the resultant forces and moments occurring at the ends of the chords were determined by each method. Concentrated loads were applied in varying magnitudes to produce different moment-to-shear ratios at the middle of the opening.

A classical Vierendeel analysis assumes inflection points at the midspan of the upper and lower chords. The total shear acting at the vertical plane through the inflection points is assumed to be distributed to the two chords in proportion to their respective areas. Moments at the ends of the chords are determined from the combined effects of the external moment at the midspan of the chords and the product of the shears and the half-chord lengths (4).

Empirical evidence indicates that the assumption of the midspan inflection point location may be significantly in error. Experiments by Nasser, Acavalos, and Daniel (8) demonstrated that the point of inflection might occur in locations between the chord midspan and 40 percent of the chord length away from that point.

The finite element analysis confirmed this variation in inflection point location as a function of load and size of opening. Figure 6 shows these indicated variations in location as functions of the ratio of hole depth to beam depth t/h, with M/Vh ratio parametric. It is seen that the inflection point moves away from the midspan of the chord with decreasing t/h and also with decreasing M/Vh ratios.

Tests were made of two variations that departed from the classical assumptions of the Vierendeel analysis, and the resulting stresses were compared with those from tests that used those assumptions and with values from the finite element analysis. In the first variation, the moment at the end of the chord was determined from the combined effects of the external moment at the midspan of the chord and the product of the midspan shear and the distance from the end of the chord to the point of inflection established by the finite element analysis. In the second variation, the moment at the end of the chord was determined from the combined effects of the external moment at the inflection point established by the finite element analysis and the product of the shear at the point and the distance from that point to the end of the chord.

Table 1 gives the results where all values have been normalized by dividing by the corresponding values from the finite element solution. It is seen that the values for axial force and the moment on the right end of the chord are close to the finite element solution for all variations of the Vierendeel technique. The moment at the left end is generally quite low for the two variations of the Vierendeel analysis, whereas the classical Vierendeel analysis gives results much closer to the elastic analysis.

Figure 5. Principal tension stress contours for single-hole and two-hole beams.

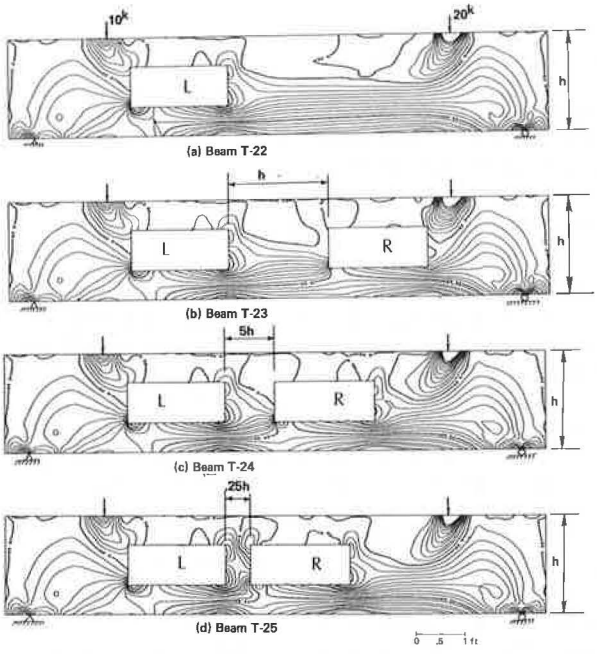

Figure 6. Position of point of inflection in chord.

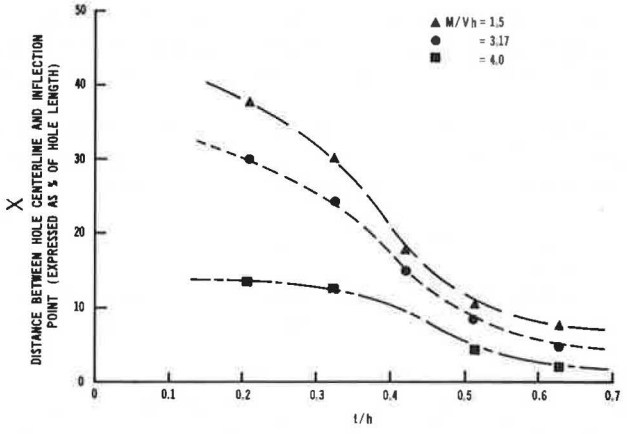

Table 1. Beam chord end forces normalized by their respective finite element values.

Beam	M/Vh	t/h	Finite Element			Classical Vierendeel			Vierendeel, Variation 1			Vierendeel, Variation 2		
			F	M_R	M_L	F	M_R	M_L	F	M_R	M_L	F	M_R	M_L
T-11	0.098	0.417	1.0	1.0	1.0	1.11	0.90	0.88	1.11	0.90	0.88	1.11	0.90	0.88
T-22	6.33	0.417	1.0	1.0	1.0	1.00	0.70	0.94	1.00	0.97	0.16	0.96	0.96	0.18
T-26	4.0	0.417	1.0	1.0	1.0	1.04	0.81	1.03	1.04	1.05	0.54	1.05	1.05	0.56
T-30	3.17	0.417	1.0	1.0	1.0	1.06	0.86	1.07	1.06	1.09	0.66	1.01	1.09	0.67
T-34	4.0	0.625	1.0	1.0	1.0	1.05	1.07	1.09	1.05	1.07	0.78	1.03	1.07	0.78
T-35	4.0	0.521	1.0	1.0	1.0	1.04	0.87	0.91	1.04	1.03	0.69	1.02	1.03	0.69
T-36	4.0	0.313	1.0	1.0	1.0	1.04	0.76	1.32	1.04	1.11	0.03	0.96	1.09	0.09
T-42	3.17	0.625	1.0	1.0	1.0	1.07	0.98	0.99	1.07	0.98	0.88	1.05	0.97	0.89
T-43	3.17	0.521	1.0	1.0	1.0	1.09	0.94	0.99	1.08	1.10	0.80	1.06	1.09	0.80
T-44	3.17	0.313	1.0	1.0	1.0	1.06	0.81	1.26	1.06	1.13	0.38	0.98	1.11	0.41
T-57	1.5	0.625	1.0	1.0	1.0	0.97	1.02	1.06	0.97	1.06	0.96	0.96	1.06	0.96
T-58	1.5	0.521	1.0	1.0	1.0	0.90	0.90	0.93	0.90	0.98	0.84	0.87	0.98	0.84
T-59	1.5	0.313	1.0	1.0	1.0	0.92	1.17	1.04	0.92	1.44	0.73	0.84	1.43	0.74
T-60	1.5	0.208	1.0	1.0	1.0	0.89	0.77	1.15	0.89	0.96	0.75	0.81	0.94	0.77

Note: F = axial force; M_L = moment, left end; and M_R = moment, right end.

The results given in Table 1 indicate that there is no significant advantage of using either of the two variations of the Vierendeel technique to ascertain the moments and axial forces at the ends of the chords. Thus, once these values from the usual Vierendeel technique have been obtained, the reinforcing for the chords can be determined using standard design techniques.

Effect of Shear and Bending Moment on the Design of Corner Reinforcing

The magnitudes of the shear and bending moment at the opening are known to affect the design of the chords and alter the stress concentration at the corners. To investigate the latter situation, we used finite element solutions of the simply supported beams to develop curves showing the variation of net resultant tensile force T_n occurring at the corners as a function of the shear and bending moment present at the mid-length of the opening. For the corner on the compressive side of the beam, T_n was obtained along a 45-deg plane extending from the corner of the opening to the surface of the member. Stresses from the finite element solution were resolved normal to this plane, after which a regression analysis by least squares was performed to establish a third-order polynomial fitting these stresses. Functions were integrated within the limits of the tensile stresses to assess a resultant force at each tensile corner. The plane chosen in this instance was based on experimental results showing that cracking around the corners occurs at approximately 45 deg.

For corners on the tensile side of the beam, T_n was obtained as the difference between the resultant tensile force with and without the hole being present. These force resultants were designated T_{an} and T_{bn} respectively. This procedure was necessary in order to reflect the fact that the reinforcing provided in the solid portion of the beam would support a significant portion of the tensile force and that any special corner reinforcing would only be required to resist the stresses caused by the stress concentration.

T_{an} was obtained from the integration of the finite element stress distribution resolved normal to a 45-deg plane; T_{bn} was obtained from an integration of the usual bending stresses ($\sigma = M'y/I$) and the shearing stresses ($\tau_{xy} = V'Q/I_b b$) in the solid member, which were resolved to normal stresses along the same plane. Here M' is the bending moment at the edge of the opening, V' is the shear at the edge of the opening, and I_b is the moment of inertia of the gross beam cross section. The finite element and beam theory stress distributions were integrated from the corner of the hole to the point where their stresses were equal, and the difference was taken to obtain T_n (Fig. 7b).

Curves showing the variation of the net tensile stress resultant as a function of moment M and shear V occurring at the middle of the opening were plotted for five hole sizes: t/h = 0.21, 0.312, 0.417, 0.52, and 0.625. Figure 7 shows the variation of T_n for the tensile corners on the compression and tension sides of the beam. Note that, for a given value of M/Vh, as t/h increases T_n/V also increases. The variation reflects the fact that the stress concentration becomes larger as the size of the hole increases.

These curves may be used to design the reinforcing required to resist the increased stresses due to the stress concentration. For example, if one desires to use special corner reinforcing in the form of bars close to the corners sloping at 45 deg (a commonly used technique), the bars can be proportioned to carry all of T_n. If, instead, vertical bars are to be used close to the side of the opening, they can be proportioned to carry $0.707T_n$ with the horizontal component carried by the reinforcing in the chord.

SUGGESTED DESIGN PROCEDURE TO PROPORTION THE REINFORCING AROUND RECTANGULAR OPENINGS LOCATED AT MID-DEPTH

Based on the previous analytical results, the suggested procedure for designing the reinforcing around a single rectangular web opening is as follows (working stress design techniques to be used):

1. Design the reinforcing for the main sections of the member, where there is no opening, in the usual manner.
2. Determine the amount and distribution of reinforcing in the chord regions of the opening by using the classical Vierendeel analysis. Often this results in reinforcing the chords with both tension and compression reinforcing as well as stirrups.
3. Obtain a value of T_n/V from Figure 7b for the size of opening desired (t/h) and the value of M/Vh occurring at the mid-length of the opening.
4. Calculate T_n from the value of T_n/V.
5. Provide special corner reinforcing to resist the net tensile force T_n.

This procedure, when used to provide reinforcing around all of the corners, means that all corners will be reinforced to resist the forces in the most highly stressed corner (the tensile corner on the tension side of the beam). If the tensile corner on the compressive side of the beam were desired to have a different amount of reinforcing, the curves of Figure 7a would then be used. From a practical point of view, it is often easier to provide the same reinforcing around all corners and limit mistakes that can occur during construction. Additionally, however, the laboratory tests to be described later showed that the measured stresses in the compressive side of the member were sometimes larger than those predicted by using Figure 7a.

EXPERIMENTAL STUDY

The suggested design procedure was based on the results of an analysis that includes many assumptions about the behavior of the materials and that does not fully model many other variables (i.e., cracking). To test the suitability of the design procedure, we conducted a limited number of laboratory tests on beams designed on the basis of the suggested method. The purpose was to determine whether the reinforcing around the hole was sufficient to force the failure to occur in the solid portion of the beam before it occurred around the opening.

Tests were done on 12 simply supported reinforced concrete beams arranged in a series of four groups having M/Vh ratios ranging from 0.0 to 5.4. Each group of beams consisted of from one to four beams that were identical with the exception of the manner in which the corners were reinforced. The beams were all 13 ft long, 20 in. deep, 8 in. wide and, with one exception, simply supported on a 12.0-ft span. The remaining beam was supported on a 9.0-ft span with a 3.0-ft cantilever. All but one beam had a 10-in. high by 24-in. long web opening. (Details of the beams are found in Fig. 8.) The concrete used in the beams was a seven-sack mix with $\frac{3}{8}$-in. maximum size aggregate and a mean 21-day compressive strength of 4,200 psi. Curing was done under wet burlap for 14 days, and all tests were conducted between 14 and 21 days after casting.

Three types of special corner reinforcing were used: (a) bars placed 45 deg to the horizontal and proportioned to resist the entire tensile force resultant; (b) vertical bars placed close to the ends of the hole and proportioned to resist the vertical component of the tensile force resultant; and (c) a combination of vertical bars and 45-deg bars, each proportioned to take one-half the total tensile force resultant.

The corner reinforcing was designed to resist the total tensile force resultant occurring at the corner instead of the net tensile force resultant as outlined in the design procedure. This was done because the curves showing the variation of the net tensile force were not developed at the time of the design and fabrication of the specimens. The total tensile force resultant T was obtained from an integration of the finite element stresses resolved on a 45-deg plane extending from the edge of the opening to the surface of the member. A graph of T versus M/Vh was obtained for the specimen hole size of t/h = 0.417 (Fig. 9). Thus, in step 4 of the suggested design procedure, Figure 9 was used to determine the tensile force resisted by the corner reinforcing. It was later found that providing corner reinforcing to resist the total tensile force instead of the net tensile force, as suggested, overreinforced the corners substantially.

Strain measurements were obtained from resistance strain gauges attached to selected reinforcing bars in five of the beams. Most of the instrumentation was on the bars surrounding the opening. Deflections of the beams were measured at midspan with a mechanical scale.

Figure 7. Effect of hole size on net tensile force resultant in corners.

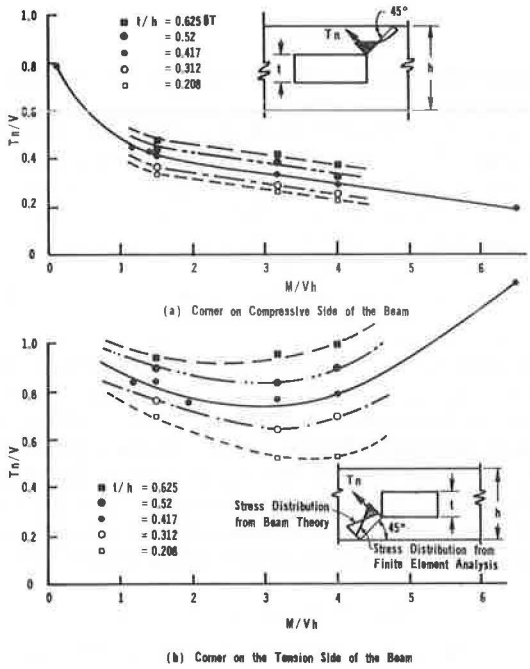

Figure 8. Beam details.

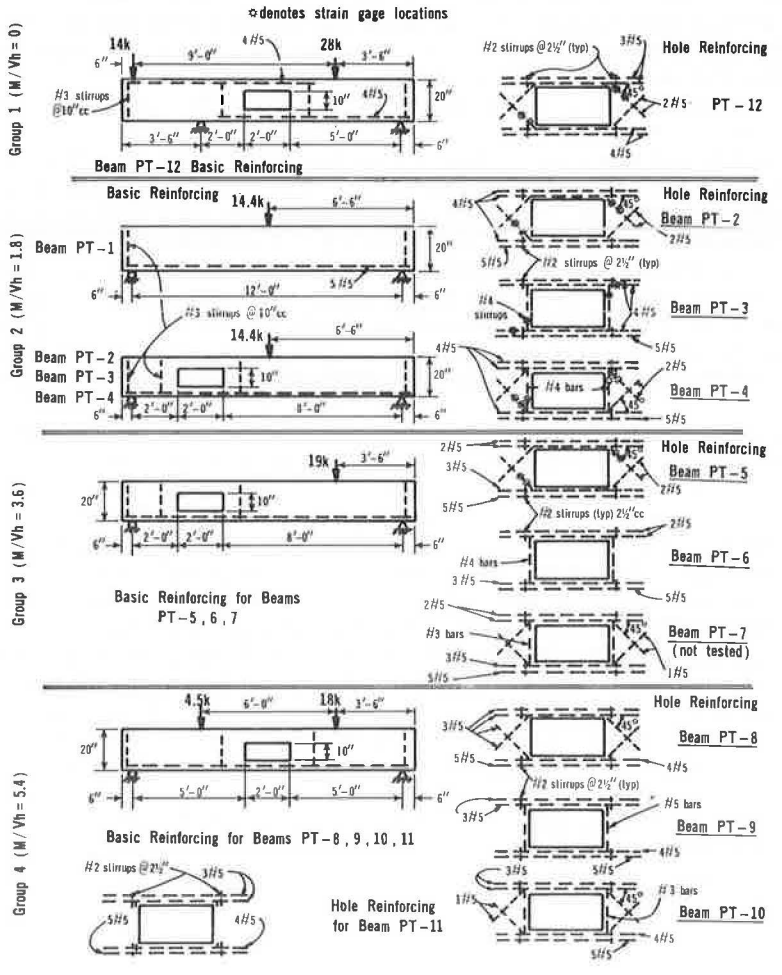

The load was applied by one or two hydraulic rams (50 and 100 kip) controlled by a closed-loop testing machine (Fig. 10). The number of loads and their relative proportions were adjusted to produce a desired M/Vh ratio at the mid-length of the opening. Each load was increased from zero to the maximum value in proportion to the original design load ratio.

Test Results

The results showed that, of the nine members tested that contained the special corner reinforcing, seven failed due to distress in the main portion of the beam. Figure 11, a photograph taken during the test of beam PT-4, shows the typical type of cracking pattern that occurred. The two beams that failed as a result of cracks originating in the corners were found to be improperly detailed. These two members had the 45-deg bars located so that cracks initiated at the corners were able to bypass the reinforcing. Evidence of this type of behavior is shown in Figure 12 for beam PT-2.

The chord regions of the opening were found to be adequately reinforced inasmuch as no subsequent failures occurred in this region. There were flexural cracks in the tensile chord at loads approaching ultimate, but they were well controlled by the reinforcing designed by the Vierendeel method.

A measure of the forces present in the corner portion of the openings was obtained from the strain gauges mounted on the special corner reinforcing in several of the beams. Figure 13 is typical of these forces as recorded in the test and as predicted using the suggested design procedure. For the lower levels of loading, the predicted and observed values of the corner tensile force were substantially the same in the upper right corner (tensile corner in the compression side of the beam). However, at this corner, as the load increased, the observed value exceeded the predicted value, which was obtained from Figure 7a. The predicted value obtained for the lower left corner (tensile corner on the tension side of the member) was always greater than the observed value. In this instance the predicted value was obtained from Figure 7b as suggested in the design procedure. The fact that this latter predicted value was greater than the observed value is significant inasmuch as it is suggested that all corners be designed and reinforced in accordance with the data provided from this region of the opening.

SUMMARY AND CONCLUSIONS

The finite element technique was used to provide elastic stress analyses of beams with large, centrally placed web openings, where the loads, geometry of the beams, and configurations of the web openings were varied. The analyses showed that, for working stress design purposes, a standard Vierendeel analysis was satisfactory for the determination of axial forces and moments on which the reinforcing requirements of the chords are based. It was observed that, as long as the adjacent openings were no closer than half the depth of the member, a single-hole analysis was satisfactory and that for most cases the design based on a rectangular hole was sufficient. The laboratory tests indicated that vertical bars, diagonal bars placed at a 45-deg angle, or a combination of both can adequately restrain corner cracking.

The reinforcing needed to resist the stress concentrations was obtained from the curves developed that gave the net tensile force in the corners. It is worth noting that, for the corner on the tension side of the beam, as the shear V tends toward zero (i.e., $M/Vh \rightarrow \infty$) the amount of reinforcing required becomes very large (T_n/V increases as M/Vh increases). This is shown in Figure 7b. This particular result is inconsistent with the results of others (13) who have noted that, for openings in a zero-shear region of a beam, the stress concentrations at the corners of the opening are small and that the effect of the opening on the strength of the member is minimal.

It is felt that the inconsistency occurring in this case is due to the fact that the design curves shown in Figure 7b were based on a resolution of the forces along a 45-deg plane. For situations where the shear is reasonably high, this direction is close to the direction of the principal tensile stresses around the corner and, hence, describes the effect of the stress concentration in an adequate manner. On the other hand, when the shear is small, the principal tensile stresses are not so oriented, and the resolution of forces

Figure 9. Variation of the total tensile force resultant.

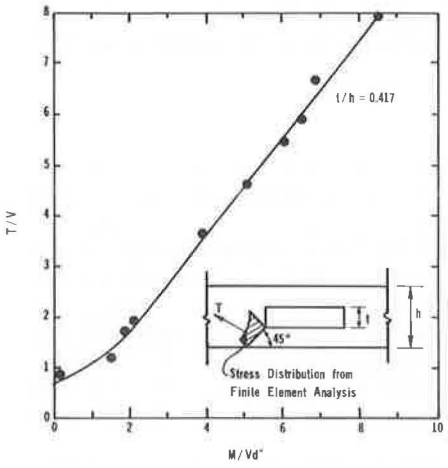

Figure 10. Test configuration.

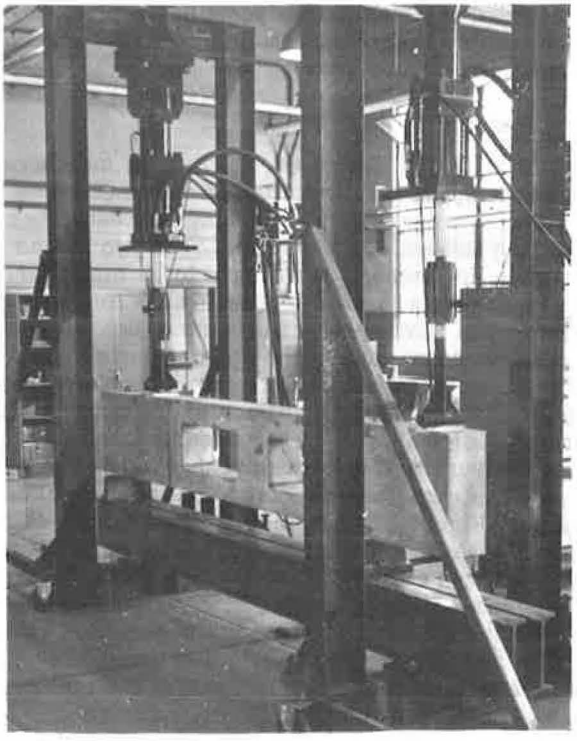

Figure 11. Testing of beam PT-4, nearly at maximum load.

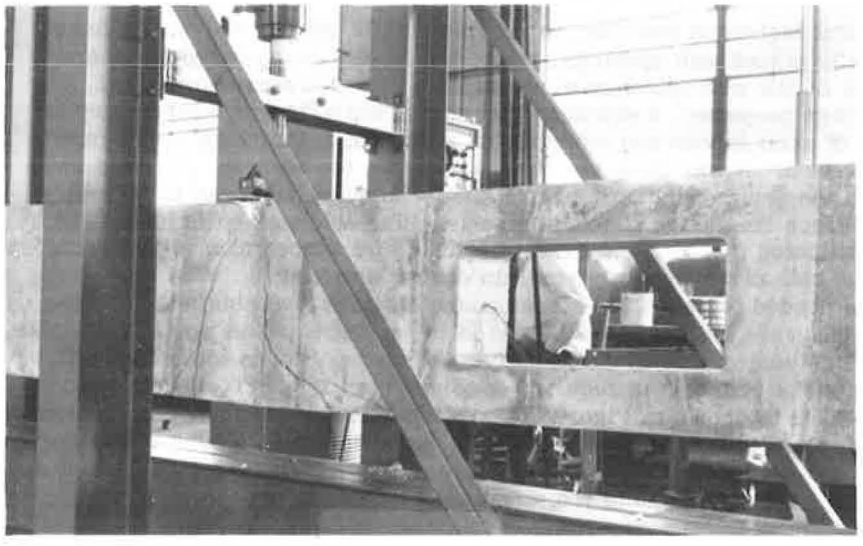

Figure 12. Testing of beam PT-2.

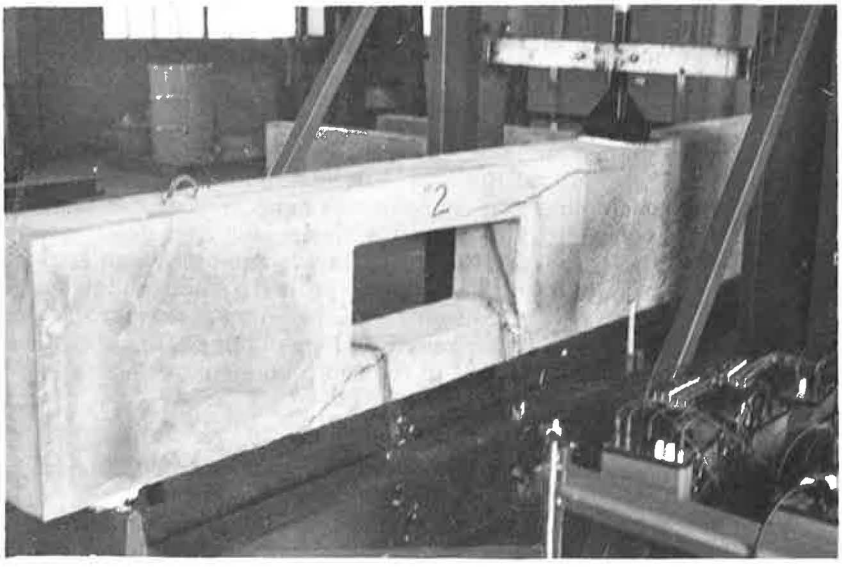

Figure 13. Corner bar tension forces, beam PT-3.

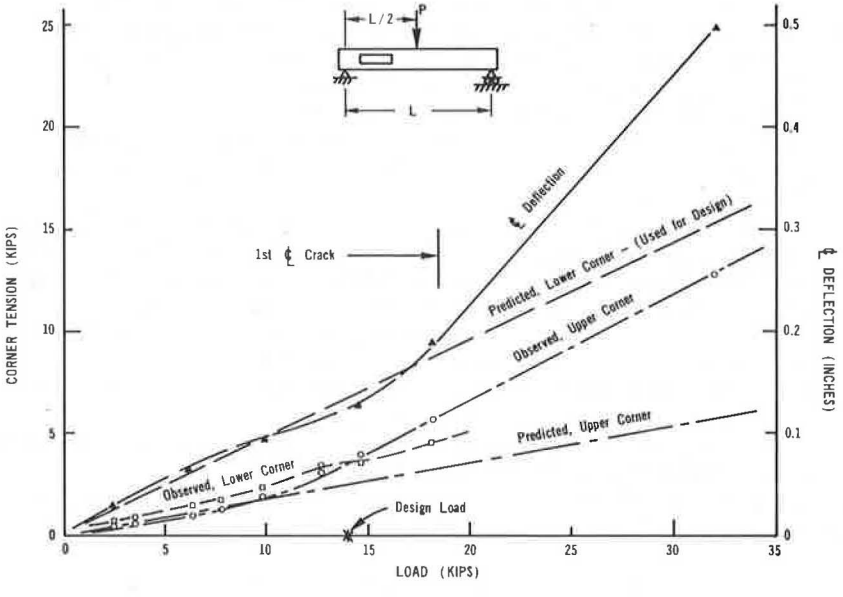

along a 45-deg line does not correctly indicate the effect of the stress concentration. It is felt, for this reason, that the data shown in Figure 7b for values of M/Vh up to approximately 4 will give suitable estimates of the amount of special corner reinforcing. For values in excess of M/Vh ≃ 4, the design curves will be conservative.

ACKNOWLEDGMENTS

This research was sponsored by the Division of Highways, Department of Public Works, State of California, and the Federal Highway Administration, U.S. Department of Transportation. The opinions, findings, and conclusions expressed in this paper are those of the authors and not necessarily those of the sponsoring agencies.

The authors wish to express their gratitude to R. E. Davis, Senior Bridge Engineer, California Division of Highways, for his assistance in the project. A special acknowledgment is due D. W. Spannagel who developed several of the computer programs and L. R. Herrmann of the Civil Engineering Department, University of California, Davis, for his assistance in the development of portions of the finite element programs.

REFERENCES

1. Savin, G. N. Stress Concentrations Around Holes. Pergamon Press, London, 1961.
2. Heller, S. R., Brock, J. S., and Bart, R. The Stresses Around a Rectangular Opening With Rounded Corners in a Beam Subjected to Bending With Shear. David Taylor Model Basin, Rept. 1311, March 1959.
3. Bower, J. E. Elastic Stresses Around Holes in Wide-Flange Beams. Jour. Structural Div., Proc. ASCE, Vol. 92, No. ST2, Proc. Paper 4773, April 1966.
4. Bower, J. E. Experimental Stresses in Wide-Flange Beams With Holes. Jour. Structural Div., Proc. ASCE, Vol. 92, No. ST5, Oct. 1966, pp. 167-186.
5. Segner, E. P. Reinforcement Requirements for Girder Web Openings. Jour. Structural Div., Proc. ASCE, Vol. 90, No. ST3, June 1964, pp. 147-164.
6. Bower, J. E. Ultimate Strength of Beams With Rectangular Holes. Jour. Structural Div., Proc. ASCE, June 1968, pp. 1315-1337.
7. Bower, J. E. Analysis and Experimental Verification of Steel Beams With Unreinforced Web Openings. In Design of Beams With Web Openings, Univ. of Wisconsin Institute, Milwaukee, Jan. 22-23, 1970.
8. Nasser, K. W., Acavalos, A., and Daniel, H. R. Behavior and Design of Large Openings in Reinforced Beams. ACI Jour., Vol. 64, No. 1, Jan. 1967, pp. 25-33.
9. Ragan, H. S., and Warwaruk, J. Tee Members With Large Web Openings. Prestressed Concrete Institute Jour., Vol. 12, No. 4, Aug. 1967, pp. 52-65.
10. Carpenter, J. E., and Hanson, N. W. Tests of Reinforced Concrete Wall Beams With Large Web Openings. ACI Jour., Sept. 1969, pp. 756-766.
11. Hanson , J. M. Square Openings in Webs of Continuous Joists. Portland Cement Assn., Res. and Development Bull., RD001.01D, 1969.
12. Lorentsen, M. Holes in Reinforced Concrete Girders. Byggmastaren, Stockholm, Vol. 41, No. 7, July 1962; Trans. by Portland Cement Assn.
13. Redwood, R. G., and McCutcheon, J. E. Beam Tests With Unreinforced Web Openings. Jour. Structural Div., Proc. ASCE, Vol. 94, No. ST1, Jan. 1968, pp. 1-16.
14. Wilson, E. L. Finite Element Analysis of Two-Dimensional Structures. Univ. of California, Berkeley, PhD thesis, 1963.
15. Calcomp General Purpose Contouring Program. California Computer Products, Inc., Anaheim, 1968.
16. Bridge Planning and Design Manual. California Department of Public Works, Sacramento, Vol. 1, Section 2.
17. Ramey, M. R. Vierendeel Bent Caps. Civil Engineering Dept., Univ. of California, Davis, Rept. 72-1, July 1972.

DISCUSSION

John M. Hanson, Wiss, Janney, Elstner and Associates, Inc., Northbrook, Illinois

The authors have presented an interesting paper that demonstrates the applicability of the Vierendeel method of analysis to openings in reinforced concrete bent caps. Their paper also provides analytical confirmation of experimental data (18) showing that multiple openings separated by posts with a width equal to more than half the depth of the member do not reduce ultimate strength.

However, the authors' conclusion that special corner reinforcing is needed to resist stress concentrations may be fallacious and is not supported by the experimental evidence in the paper.

In the first place, openings formed in concrete beams often develop shrinkage cracks along their sides and particularly in their corners. The presence of these random shrinkage cracks will significantly alter the stresses computed by the authors' elastic analysis. Cracking due to stress will also generally occur below the working stress design load, further limiting the applicability of the analysis.

In the second place, columns, piers, spandrels, and other members may be subjected to force systems similar to those in the chords above or below an opening. These members frequently have a reentrant corner where they frame into another member, and it is standard practice to design these members without regard to the effect of stress concentrations. There is no evidence that the strength of these members is reduced by the reentrant corner.

Experimental studies by the writer (11) have indicated that the first prominent cracking observed at an opening can be satisfactorily related to tensile stresses computed from forces obtained from a Vierendeel analysis, without regard to stress concentration. Accordingly, the writer contends that an opening reinforced with adequate vertical stirrups along its side will cause the beam to behave as if two subbeams were bridging the opening and that the strength of this system depends only on the ultimate strength of the subbeams. Of course, the behavior of the subbeams will depend on their reinforcement.

The authors point to their 12 test beams and indicate that the special corner reinforcement provided adequately strengthened the members. However, the nine beams with corner reinforcement either failed in the main portion of the beam or were improperly detailed. Therefore, it cannot be concluded that this reinforcement was necessary. The only evidence intended to support the authors' contention that corner reinforcement is needed is provided by Figure 13. However, the example shown in Figure 13 is for a beam that contains horizontal and vertical bars along the sides of the opening, and the relationship presented between the observed and the predicted stresses is certainly not convincing.

Of the three remaining beams, one did not contain openings (PT-1), one was not tested (PT-7), and the other did not contain vertical reinforcement along the sides of the opening (PT-11). The writer inquires about the behavior of PT-1 and PT-11 and requests a comparison of the maximum moment at failure in these two beams with the others in the test program.

In the remainder of this discussion, the writer would like to comment on several other points in the paper. The authors indicated that, in a classical Vierendeel analysis, the total shear acting at the vertical plane through the inflection points at the mid-length of the upper and lower chords is assumed to be distributed to two chords in proportion to their respective areas, and they note that their analysis and test results support this method of analysis. However, the writer would like to point out that the authors' experimental and analytical program was based on an opening located at mid-depth of a rectangular member. This is a special case in which, at least until cracking, the distribution of shear is independent of the sectional properties of the chords. When the opening is not at mid-depth, or the member is not rectangular, the distribution of shear will be related to the span-to-depth ratio of the chords and, after cracking, to the reinforcement in the chords. For low span-to-depth ratios, the shear distribution will depend on the areas of the top and the bottom chord, and, for high span-to-depth ratios, the shear distribution will depend on the flexural stiffnesses of the chords.

The authors indicate that Figure 6 shows variation in location of the inflection position as a function of the ratio of the hole depth to beam depth. Is this ratio the same for both the top and bottom chords above and below the opening?

From the description of the manner in which the force T_n was obtained on the tensile side of a beam with an opening, the writer gained the impression that T_{an} was computed from normal stresses acting on a 45-deg plane through the corner, whereas T_{bn} was computed by resolving stresses on a vertical plane through the corner to an angle of 45 deg. The writer would like to see a more rigorous explanation of this approach. Furthermore, the curves for T_n shown in Figure 7 appear to be independent of the horizontal dimension of the hole. Is this actually the case, or are these curves restricted to the specified 2-ft length of hole investigated by the authors? The writer notes that the authors have used these curves in their recommended design procedure, which does not contain any restriction about the horizontal length of the opening.

References

18. Hanson, J. M., Corley, W. G., and Hognestad, E. Evaluation of Structural Concrete Members Penetrated by Service Systems. Bureau of Standards, Spec. Publ. 361, Vol. 1, Feb. 1972, pp. 545-556.

AUTHORS' CLOSURE

The writers appreciate the in-depth discussion by Hanson. He noted that, in tests of his own on joints containing rectangular openings, reinforcing close to the opening would be sufficient to prevent cracking around the corners. In his discussion he points out that an "adequately" designed vertical stirrup would suffice for reinforcing the corners of the opening. The writers believe that the word "adequately" is a key term here because few studies show the manner by which the design engineer determines how much reinforcing is "adequate." In fact, in the reference cited by Hanson it is merely stated that a No. 3 stirrup placed close to the side of the opening was used to reinforce the corners, and no mention was made of the design procedure used to proportion this stirrup. We feel that an important contribution of this paper is a method by which the design engineer can determine what is adequate.

The basis of the development rests on using an elastic analysis of the member that indicates that there are stress concentrations at the corners of the opening. It is recognized that the analysis shows larger stress concentration values than are no doubt present; however, tests on concrete elements containing variously shaped openings clearly show that such increased stresses do exist (1). In the proposed design method the resultant of these stress concentrations is used as a measure of the reinforcing required at the opening. This technique is similar to that used to determine the reinforcing requirements in the end zones of prestressed concrete beams to prevent tensile splitting.

Hanson raised some other points that the writers would briefly like to comment on. As noted in his discussion, most of the beams used in the limited experimental program failed in the main portion of the beam. This was as desired inasmuch as we did not want the opening to weaken the member. Tests by others, including Hanson, showed that an unreinforced opening in a high shear region weakens the beam and that some corner reinforcing is required. Beam PT-12 (Fig. 12) shows significant corner cracking in a member with a rectangular opening in a high shear region and the corner reinforcing improperly placed. It is easy to see that a similar result might be obtained if the corner reinforcing were absent.

The usual assumptions of the Vierendeel analysis pertaining to the shear distribution in the chord members was found to be valid based on the elastic finite element analyses

reported in the paper as long as the opening was centrally placed with respect to the depth of the member. It is clearly stated that no other hole placements were considered. The writers are aware that other parameters influence the shear distribution between the chords when the openings are not centrally located and make reference to a brief discussion of this point (17).

Although the finite element analyses showed that the location of the points of contraflexure in both chords varied with the loading and the size of the opening, this fact was shown to be of little consequence in developing the suggested working stress design procedure and was not used.

The method described in the paper to estimate the net tensile force around the corner of the opening on the tensile side of the member considered the fact that the 45-deg line on which the stresses were resolved extended into the solid portion of the beam. Recognizing that there usually is tensile reinforcing provided to carry stresses that are present when the opening is absent, additional stresses introduced by the opening must be carried by the corner reinforcing. In the paper the stresses from the usual beam theory and those obtained from the finite element analyses were each resolved normal to a 45-deg line originating from the corner of the opening and extending to the surface of the beam. The net tensile force T_n was obtained as the integral of the difference between these stresses, with the integration being done from the corner of the opening to the intersection of the stress distributions plotted along the 45-deg line. Figure 7b shows the region taken as T_n.

It was correctly noted that the curves showing T_n are not a function of the length of the opening. It is our judgment that one of the more important variables in the analysis is the length-to-depth ratio of the chords of the opening rather than the absolute length of the opening. T_n was thus presented as a function of the depth of the opening relative to the depth of the beam, which, in effect, reflected a variation of length-to-depth changes in the chord members.

Hanson cited some important experimental work done by others, and a survey of the literature (20) will show that limited research has been done on this subject of web openings in concrete flexural members. Further studies dealing with both the theoretical and experimental aspects of the problem are obviously needed.

Reference

20. Imbert, I. D. C. The Effect of Holes on Tensile Deformations in Plain Concrete. Highway Research Record 324, 1970, pp. 54-65.

STUDY OF AASHO LOADINGS ON A CONCRETE BOX GIRDER BRIDGE MODEL

A. C. Scordelis and J. G. Bouwkamp, University of California, Berkeley; and S. T. Wasti, Middle East Technical University, Ankara, Turkey

A brief description of the instrumentation, construction, and testing of a large-scale, two-span, four-cell, reinforced concrete box girder bridge model is presented. Tested in the laboratory, the model was a 1:2.82 scale of a typical prototype bridge found in the California highway system. The overall plan dimensions of the model and the prototype were 12 by 72 ft and 34 by 203 ft respectively. The research program included a study of the theoretical and experimental response of the bridge to dead load, live loads at working stress and overstress levels, and ultimate loading to failure. However, this paper presents only the results of the investigation dealing with an evaluation of present AASHO loadings on bridges of this type and the response of the bridge to actual scaled loads of AASHO HS20-44 trucks placed in two or three lanes and of a proposed class I overload construction vehicle placed in one lane only. Results indicate that concrete box girder bridges have excellent load distribution properties; however, the present AASHO empirical formula, which ignores the number of lanes on the bridge, underestimates the true value for three lanes of trucks. Total stresses in the steel and concrete under three lanes of AASHO trucks or one lane of the overload vehicle exceed allowable values, but no distress in the bridge was observed. /AUTHOR/

•IN 1971, approximately 80 percent of the concrete bridges (computed on the basis of deck area) in California were multicell concrete box girder bridges. These cast-in-place structures are usually constructed as reinforced concrete bridges with spans ranging between 60 and 100 ft and as post-tensioned prestressed bridges for longer span lengths.

Because of their large use in California, a continuing program of research on box girder bridges, directed toward improved design methods, has been conducted at the University of California, Berkeley, since 1965. Simple and continuous straight bridges, skew bridges, and curved bridges are successively being studied through use of analytical and experimental methods.

As part of this research program, an extensive investigation was carried out on the structural behavior of the large-scale, two-span, reinforced concrete box girder model shown in Figures 1 and 2. The model, having overall plan dimensions of 12 by 72 ft, was a 1:2.82 scale replica of a typical prototype bridge, 34 by 203 ft, found in today's California highway system. It had four cells: a center bent with a single column support, two end diaphragms, and, for purposes of comparison, a midspan diaphragm at section X but not at section Y. The large scale of the model enabled the use of standard high-strength (60-ksi yield) deformed steel bars as reinforcement and concrete with $\frac{3}{8}$-in. aggregate rather than a mortar mix for the model material. The model was tested in the Structures Laboratory at the University of California.

Three research reports (1, 2, 3) describe in detail the model dimensions and reinforcement, method of construction, instrumentation, automatic data recording and

Sponsored by Committee on Concrete Superstructures.

Figure 1. Dimensions of box girder bridge model with transverse locations.

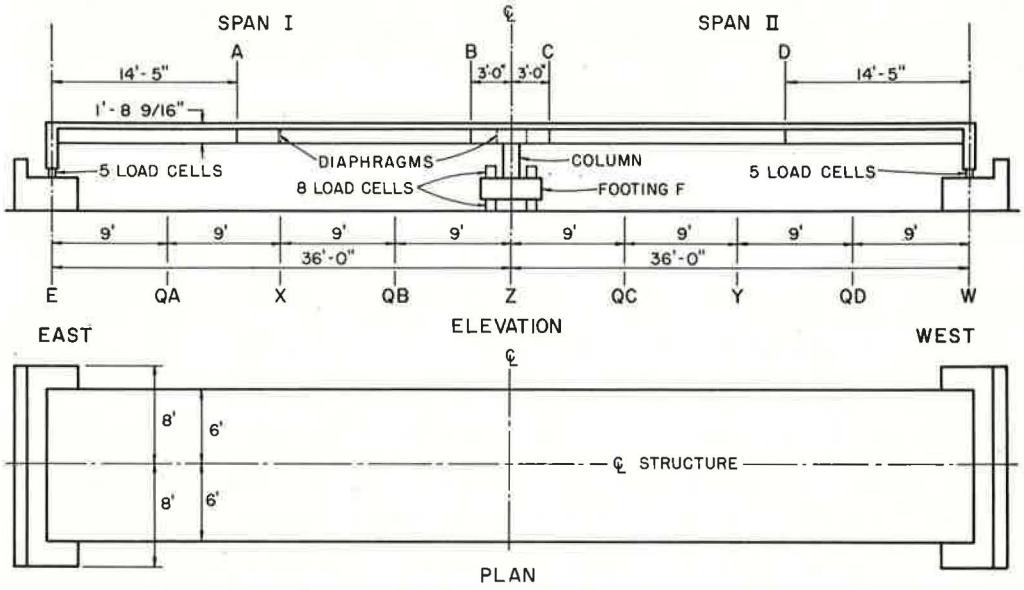

Figure 2. Cross section of box girder bridge model.

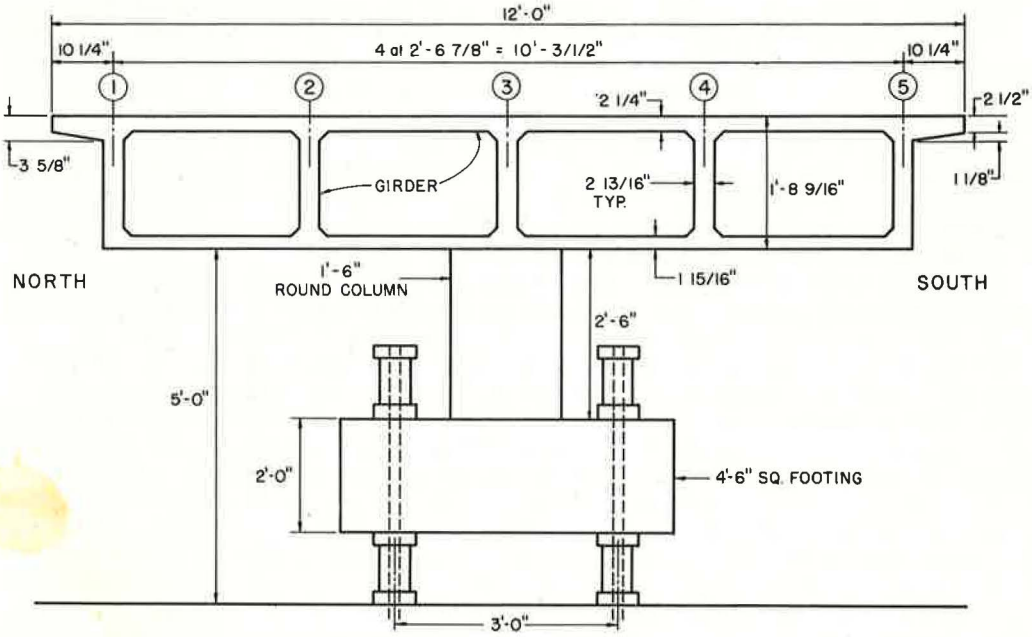

reduction system, and test program. Also presented are theoretical and experimental results for the response of the bridge to dead load, live loads at working stress and overstress levels, and ultimate loading to failure. Theoretical results for working stress loads were based on a finite element analysis assuming the structure to be an uncracked, homogeneous, elastic structure.

The purpose of this paper is to present only the results of the investigation dealing with an evaluation of the present AASHO loadings on bridges of this type.

EXPERIMENTAL PROGRAM

The same procedure used in the field on prototype structures was used to construct the model. The two end abutments and the center column and footing were cast first. Subsequently, the bottom slab, girder webs, and diaphragms at section X and at the center bent Z were formed, reinforced, and cast. At this stage, to satisfy similitude for dead load, we placed extra dead weight in the form of steel billets in the cells. The billets plus the dead load of the model resulted in the required model-prototype weight ratio of 1:2.82. The top slab was then formed, reinforced, and cast.

Instrumentation was designed to measure reactions, deflections, and strains in the concrete and the steel reinforcement. Reactions were measured by load cells at each of the five girders, numbered 1 to 5 (Fig. 2) at the two end abutments and at four locations under the central footing. Vertical deflections were measured by potentiometers at each girder web at transverse sections X, QB, Z, QC, and Y (Fig. 1). Longitudinal strain was measured with strain meters in the concrete and with weldable waterproof gauges on the steel reinforcement at sections A and D in the maximum positive moment region and at sections B and C near the center support in the negative moment region. All data recording and reduction were automated as much as possible using available computer systems.

The main objective of the test program was to obtain information on load distribution in reinforced concrete box girder bridges under conditions of working loads. Working loads would result in total design stresses of 24 ksi in the tensile steel at the sections of loading. Bearing in mind, however, that the tensile stresses in the tensile reinforcement at these sections due to their own weight and extra dead load of the bridge model alone were about 12 ksi, we decided to consider two levels of working loads: those producing total stresses in the steel of 24 ksi and those resulting in total tensile steel stresses of 30 ksi at the sections of loading. The advantage of the latter stress level was that 50 percent higher live load stress and strain values could be registered for a total increase in the bridge model stresses of only 6 ksi.

In terms of actual experimental data, it was convenient to divide the experimental program into seven phases, from the dead load condition (phase 0) through the 24, 30, 40, 50, and 60 ksi stress levels (phases 1 to 5) to the failure condition (phase 6).

The box girder bridge model had a loading frame at midspan sections X and Y enabling live loads to be applied at each of the girders 1 to 5 by means of jacks singly and in various combinations (Fig. 3). Each phase of the experimental program for live loads comprised first the application of equal loads on each girder at both midspans to produce the same order of nominal steel stress at sections of maximum positive and negative moment. These loads were termed "conditioning loads." Subsequently, after the removal of the conditioning loads, point loads were applied in several combinations. The conditioning loads were chosen to produce nominal total tensile steel stresses of 24, 30, 40, 50, and 60 ksi at the sections of loading and to represent the successive deterioration of the box girder bridge model due to the effects of overload. The point loads, however, were chosen in all cases to produce stresses where applied on the order of the working stresses, i.e., 24- and 30-ksi total tensile stress in the reinforcement.

The working load phase, which involved the application of the conditioning loads to produce the 30-ksi tensile steel stress, was chosen as the most representative from the point of view of assessing actual box girder bridge behavior for design purposes. Following the conditioning loads, 19 separate single or combined point load combinations were applied to the bridge model at midspan sections X and Y. Results from these point loads could then be used to develop influence tables for reactions, deflections,

strains, stresses, and moments. In addition, during this working load phase, the model was subjected to scaled-down versions of the wheel loads from standard AASHO HS20-44 trucks and a proposed class I overload construction vehicle. Dimensions and wheel loads of prototype and model vehicles are shown in Figures 4 and 5. Six AASHO trucks and two construction vehicles were fabricated using a system of statically determined beams. Figure 6 shows a three-lane AASHO truck loading on the bridge model and indicates how the resultant of each truck's wheel loads was applied through a single jack. A variety of vehicle loading patterns was used and will be described in detail later.

MAXIMUM NUMBER OF WHEEL LOADS CARRIED BY A GIRDER

Present AASHO specifications prescribe a design method wherein a box girder bridge is considered to be made up of a number of identical I-shaped interior girders plus two exterior girders. According to these specifications, each girder is designed as a separate member by applying to it a certain fraction of a single longitudinal line of wheels from the standard truck. This fraction, known as the number of wheel loads N_{WL}, is given for interior girders as

$$N_{WL} = S/7$$

and for exterior girders as

$$N_{WL} = S_1/7$$

where S is the flange width in feet of the interior girder, which is equal to the average width of the cell, and S_1 is the top flange width in feet of the exterior girder, which is equal to half the cell width plus the cantilever overhang. In December 1967 the state of California put forward a design specification in which the distinction between S_1 and S was abolished and the total value of the distribution factor N_{WL} for the "whole-width unit" was given by

$$N_{WL}(\text{total}) = \frac{\text{deck width in feet}}{7}$$

It has been pointed out (2) that the most important variable not taken into account by the AASHO specifications is the number of traffic lanes on the bridge. Other factors such as span, total width, number of cells, and continuity or fixity at the supports also influence the load distribution.

The prototype bridge represented by the model could be either two- or three-lane depending on the choice of barrier curb and railing used. Theoretical and experimental load distributions were determined as described below.

The actual box girder cross section was first divided into three interior girders (2, 3, and 4) and two exterior girders (1 and 5). The girder moment at any section taken by an individual girder was found by integrating the longitudinal stresses over the proper slab, web, or reinforcement areas to obtain forces and then by multiplying these forces by their respective lever arms to the neutral axis of the gross uncracked section. The girder moments, at a particular section, were summed to determine the total moment on an entire cross section. Each girder moment was then divided by the total moment at a section to determine the percentage distribution to each girder.

Theoretical and experimental percentages of the total moments at sections A, D, B, and C carried by each girder were computed for all 19 point load combinations applied at midspan sections X and Y. These gave essentially influence tables, which at a glance enabled determination of the load-distributing properties of the bridge. For an optimum load distribution, a uniform stress would exist across the entire section, and the percentage distributions to girders 1 to 5 would be 16.5, 22.4, 22.4, 22.4, and 16.5 percent respectively. These values are directly proportional to the gross moments of inertia of the interior and exterior girders.

To determine the maximum number of wheel loads carried by an interior or exterior girder at sections A, B, C, and D shown in Figure 1, we used the influence tables. Each

Figure 3. Loading frames with jacks in position.

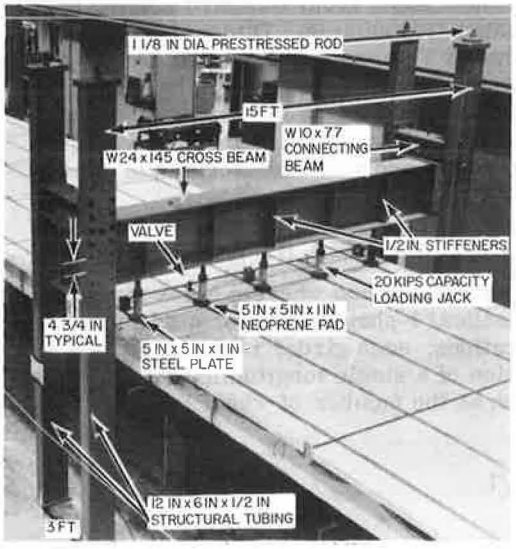

Figure 4. Wheel loads and dimensions of prototype and model AASHO HS20-44 truck.

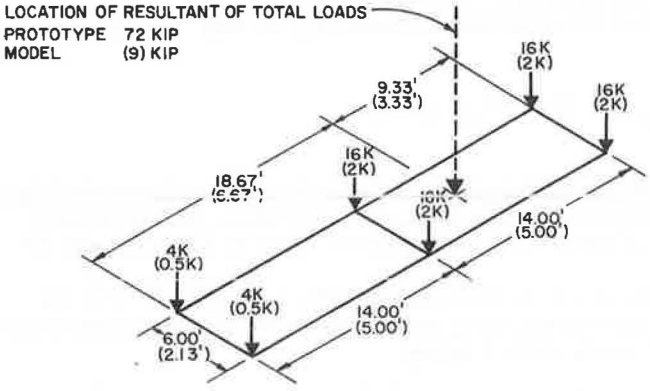

Figure 5. Wheel loads and dimensions of prototype and model overload construction vehicle.

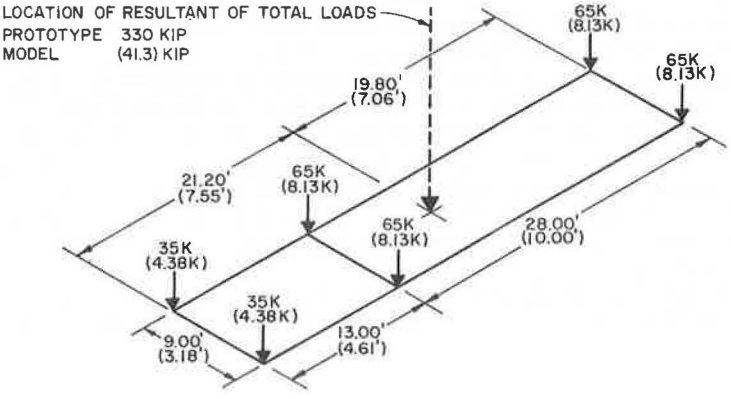

prototype AASHO truck was assumed to occupy a 10-ft traffic lane and have wheels spaced transversely at 6 ft. For simplicity, only a single transverse series of wheels at midspan sections X and Y were considered. For maximum positive moments at sections A and D only one span was loaded, whereas for maximum negative moments at sections B and C both spans were loaded.

Table 1 gives a summary of the results for the maximum number of wheel loads to be carried by interior or exterior girders at sections A, B, C, and D. Line 1 gives values computed from the AASHO formulas. The remaining lines give values for two lanes of trucks (total of four wheel lines on bridge) and for three lanes of trucks (total of six wheel lines on bridge). The uniform stress values (lines 2 and 5) are obtained by multiplying the total number of wheel lines on the bridge by 22.4 and 16.5 percent for the interior and exterior girders respectively. Theoretical values (lines 3 and 6) and experimental values (lines 4 and 7) are found by using influence ordinates as described above. Finally lines 8, 9, and 10 are given because AASHO specifies a 10 percent reduction for three lanes of loading. It is important to note that, in using the S/7 AASHO empirical formula, no reduction should be made for more than two lanes of loading because this is assumed to have been included already in the development of the formula.

A study of Table 1 reveals several interesting facts for the bridge under consideration:

1. The AASHO formulas are conservative for two-lane truck loading but unconservative for three-lane truck loading. The latter is especially true for interior girders, even with the 10 percent reduction, where AASHO underestimates the load by about 18 to 23 percent.
2. When theoretical and experimental values are compared, experimental values are 1 to 5 percent higher for interior girders at sections A, C, and D and 10 percent higher at section B. For exterior girders, differences of 2 to 3 percent exist at sections B and C and 5 to 14 percent at sections A and D.
3. When both theoretical and experimental values are compared with optimum uniform stress values, the former are generally only 2 to 8 percent higher than the latter, with three-lane truck loading being the closest. This emphasizes the excellent load-distributing properties of concrete box girder bridges.

AASHO TRUCK AND CONSTRUCTION VEHICLE LOADS

As described earlier, the model was loaded by scaled-down versions of the standard AASHO HS20-44 truck (total load = 72 kip) as shown in Figure 4 and a proposed class I overload construction vehicle (total load = 330 kip) as shown in Figure 5. All linear dimensions were reduced by the scale factor 1:2.82. Similitude required that the loads be reduced by a factor of 1:8 to produce the same stresses in the model as in the prototype. Thus, for the model the total load for each truck was 9.0 kip and for each construction vehicle was 41.3 kip. With these loads, a study could be made of the bridge response due to actual design truck live loads placed at various positions on the bridge.

Figure 7 shows the various positions and directions of the truck and construction vehicle loads on the bridge. A total of 11 combinations of two-lane truck loadings, three combinations of three-lane truck loadings, and seven combinations of construction vehicle loading were used. For the AASHO truck loadings it was assumed that one, two, three, four, or six trucks could occupy any of the positions shown in Figure 7. However, it was assumed that no more than one overload construction vehicle could be in each span at any one time because this would be a controlled loading. Reactions, girder moments, deflections, strains, and stresses were determined experimentally for all load combinations and theoretically for selected cases through use of a finite element analysis.

Reactions

Excellent static checks were obtained, with the ratios of the sum of the reactions to the sum of applied loads varying from 0.97 to 1.01 for all cases. The agreement between theoretical and experimental total reactions at the east, center, and west supports was very close (Table 2) for several typical cases of AASHO truck loadings.

Figure 6. Three-lane truck loading on bridge deck model.

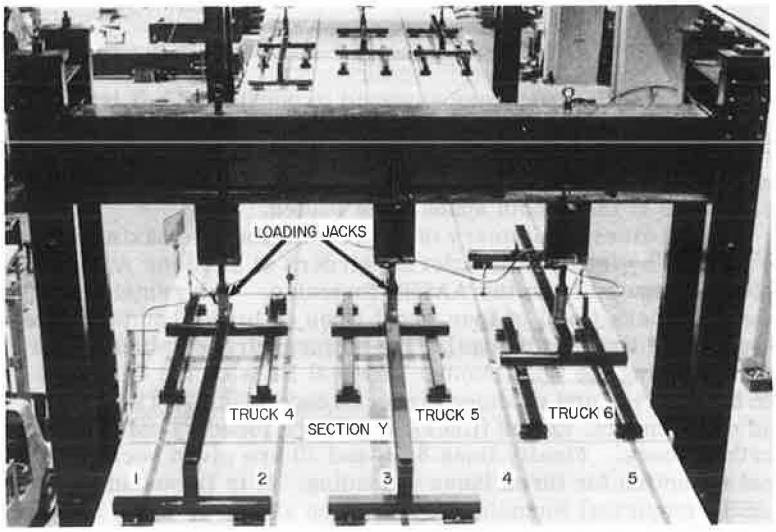

Table 1. Maximum number of wheel loads for interior and exterior girders.

Girder	Line	Load Case	Section A	B	C	D
Interior	1	AASHO specifications	1.04	1.04	1.04	1.04
	2	Two-lane (uniform stress)	0.90	0.90	0.90	0.90
	3	Two-lane (theoretical)	0.96	0.95	0.99	0.99
	4	Two-lane (experimental)	0.98	1.06	1.00	1.04
	5	Three-lane (uniform stress)	1.34	1.34	1.34	1.34
	6	Three-lane (theoretical)	1.37	1.38	1.40	1.39
	7	Three-lane (experimental)	1.42	1.54	1.45	1.47
	8	0.90 x three-lane (uniform stress)	1.21	1.21	1.21	1.21
	9	0.90 x three-lane (theoretical)	1.23	1.24	1.26	1.25
	10	0.90 x three-lane (experimental)	1.27	1.39	1.31	1.32
Exterior	1	AASHO specifications	0.88	0.88	0.88	0.88
	2	Two-lane (uniform stress)	0.66	0.66	0.66	0.66
	3	Two-lane (theoretical)	0.67	0.67	0.71	0.71
	4	Two-lane (experimental)	0.73	0.65	0.70	0.61
	5	Three-lane (uniform stress)	0.99	0.99	0.99	0.99
	6	Three-lane (theoretical)	0.96	0.95	0.97	0.97
	7	Three-lane (experimental)	1.02	0.94	0.99	0.84
	8	0.90 x three-lane (uniform stress)	0.89	0.89	0.89	0.89
	9	0.90 x three-lane (theoretical)	0.86	0.86	0.87	0.87
	10	0.90 x three-lane (experimental)	0.92	0.84	0.89	0.76

Figure 7. Positions and directions of truck and construction vehicle loadings on bridge.

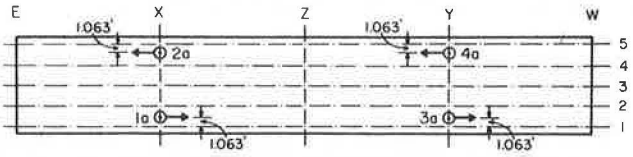

(a) TWO-LANE TRUCK LOADING (EACH TRUCK = 9.0 KIP NOMINAL)

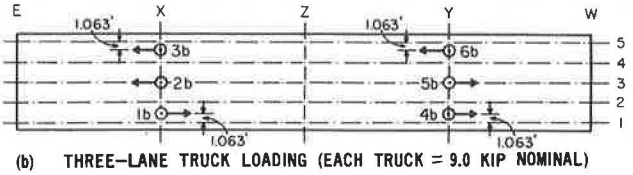

(b) THREE-LANE TRUCK LOADING (EACH TRUCK = 9.0 KIP NOMINAL)

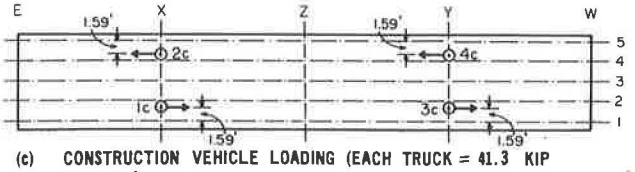

(c) CONSTRUCTION VEHICLE LOADING (EACH TRUCK = 41.3 KIP NOMINAL)

The good agreement indicates that the theory can also be used to accurately predict the total moment at any section of the bridge based on external reactions.

Girder Moments

Girder moments, total section moments, and percentage distributions to each girder were evaluated for the various vehicle load combinations using the procedure described earlier. Critical design vehicle positions for maximum experimental girder moments at each section are given in Table 3 together with the maximum moments in exterior and interior girders and their ratio. The following conclusions can be drawn:

1. As would be expected the maximum moments get progressively larger as one proceeds from two-lane truck to three-lane truck to construction vehicle loading because of the greater total load across the bridge width in each case.
2. When we consider positive moments at sections A and D, maximum moments are produced when only one span is loaded with as many vehicles as possible across the width of the bridge. Single vehicles in one span in an extreme eccentric position do not produce maximum effects.
3. When we consider negative moments at sections B and C, maximum moments are produced when both spans are loaded, again with as many vehicles as possible across the width of the bridge.
4. With the exception of two-lane AASHO loading for section D, where the exterior girder moment appears questionable, the ratios of maximum exterior to interior girder moments range from 0.61 to 0.76. For a uniform stress distribution across the bridge width this ratio would be 16.5/22.4 = 0.74.

Deflections

Experimental deflections are shown in Figure 8 for vehicle loadings that produce maximum values at diaphragmed section X and undiaphragmed section Y. For the two- and three-lane truck cases, the loading is relatively uniform across the width of the bridge (Fig. 7), which results in a uniform distribution of deflection also. For the construction vehicle, only one lane is loaded, which results in a larger deflection under girder 5. By comparing results at sections X and Y, these loadings also demonstrate the effect of the diaphragm.

It is of interest to compute the maximum deflection-span ratios for each of these design live loadings inasmuch as they would be the same in a full-scale prototype structure because of similitude. For the two-lane truck, three-lane truck, and construction vehicle loadings the maximum deflections are respectively 0.17, 0.25, and 0.51 in., which when divided by the span of 432 in. (36 ft) give deflection-span ratios of 1/2,600, 1/1,770, and 1/870, all of which are quite small.

A comparison of theoretical and experimental deflections, not shown, indicates that the theory predicts the general distribution of deflections quite well if the theoretical values based on an uncracked section are multiplied by a factor of about 1.5 to account for cracking at the working stress level.

Maximum Stresses

The maximum live load experimental stresses in the concrete and the steel reinforcement for all vehicle load positions considered are given in Table 4. These were obtained by searching all the measured strain values at each section under all vehicle load combinations studied to determine the absolute maximum strains. These were then multiplied by the appropriate moduli of elasticity to determine maximum live load stresses.

The bridge model was designed by the Bridge Department of the California Division of Highways using the "whole-width unit" concept described earlier. The allowable steel stress was 24.0 ksi to be produced by dead load, live load, and impact (22 percent for this bridge). For comparison, one can take 1.22 times the measured live load stresses given in Table 4 and add the nominal dead load stresses to see what total stresses are produced under two-lane AASHO truck loading, three-lane AASHO truck

Table 2. Theoretical and experimental reactions at east, center, and west supports.

Truck Position	No. of Lanes Loaded	No. of Spans Loaded	Theoretical Reaction (kip)			Experimental Reaction (kip)		
			East Support	Center Support	West Support	East Support	Center Support	West Support
3a + 4a	2	1	-1.4	12.3	7.1	-1.4	12.6	7.1
1a + 2a + 3a + 4a	2	2	5.7	24.6	5.7	5.4	24.3	5.7
4b + 5b + 6b	3	1	-2.1	18.4	10.7	-2.0	18.8	10.5
1b + 2b + 3b + 4b + 5b + 6b	3	2	8.6	36.8	8.6	8.2	36.8	8.6

Table 3. Maximum girder moments for vehicle loadings.

Section	Vehicle Positions	Maximum Girder Moments (ft-kip) M_{ext}	M_{int}	M_e/M_i
Two-Lane AASHO				
A	1a + 2a	16	21	0.76
B	1a + 2a + 3a + 4a	13	21	0.62
C	1a + 2a + 3a + 4a	13	20	0.65
D	3a + 4a	24	24	1.00
Three-Lane AASHO				
A	1b + 2b + 3b	21	30	0.70
B	1b + 2b + 3b + 4b + 5b + 6b	20	32	0.63
C	1b + 2b + 3b + 4b + 5b + 6b	20	29	0.69
D	4b + 5b + 6b	25	37	0.68
Construction Vehicle				
A	2c	36	54	0.67
B	1c + 3c	31	42	0.74
C	1c + 3c	21	49	0.65
D	4c	30	49	0.61

Figure 8. Experimental deflections at transverse midspan sections for various vehicle loadings.

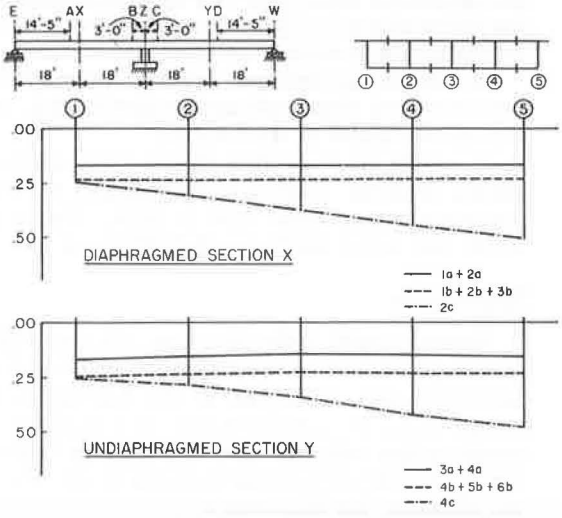

Table 4. Maximum live load experimental stresses for truck and construction vehicle loadings.

Material	Section	Two-Lane Truck Loading (psi)	Three-Lane Truck Loading (psi)	Construction Vehicle Loading (psi)
Concrete	A	207	276	516
	B	235	351	510
	C	241	346	514
	D	249	383	440
Steel	A	8,030	9,980	17,000
	B	3,710	5,850	10,200
	C	3,860	5,830	9,370
	D	6,640	10,700	13,000

loading, and one-lane overload construction vehicle loading. The nominal dead load stresses at positive moment sections A and D are 12.8 ksi and at negative moment sections B and C are 8.9 ksi. The resulting total stresses for the two-lane and three-lane AASHO truck loadings and the one-lane construction vehicle loading are 22.6, 25.9, and 33.5 ksi respectively at sections A and D and 13.6, 16.1, and 21.4 ksi at sections B and C, which are 3 ft from the centerline of the bent support. If the latter values are extrapolated to the centerline of the bent the total stresses are 21.3, 24.9, and 32.4 ksi.

The allowable concrete stress was 1.3 ksi. As can be seen from Table 4, the measured live load concrete stresses were quite low. The total concrete stresses at section A or D and B or C were below the allowable value; however, values extrapolated to the centerline of the bent were greater than the allowable value for the three-lane truck loading and the overload construction vehicle loading.

It is of interest to note from a design standpoint that, for both steel and concrete stresses, the dead load may contribute half or more to the total stress. Thus an error in the live load distribution factors of say 30 percent might give an error in the total stress of only 15 percent.

Finally, under all the vehicle loadings placed on the bridge, no visual signs of distress were observed. The crack patterns developed consisted of hairline cracks with widths of less than 0.01 in.

CONCLUSIONS

The most important conclusions from the study reported in this paper are as follows:

1. Both theoretical and experimental results show that for the bridge tested the AASHO empirical formula $N_{WL} = S/7$ overestimates the actual value of the girder moment slightly for a two-lane truck loading but underestimates it by as much as 23 percent for a three-lane truck loading on the bridge.
2. Concrete box girder bridges have excellent load-distributing properties because, under the most critical truck load positions, the transverse distribution of girder moments approaches that found for an optimum uniform stress distribution.
3. Steel and concrete stresses produced by dead load, live load, and impact are less than allowable values for two lanes of AASHO HS20-44 trucks but are greater for three lanes of AASHO HS20-44 trucks or for one lane of the class I proposed overload construction vehicle. However, none of these vehicle loadings produced any distress in the bridge.

ACKNOWLEDGMENT

This investigation was sponsored by the Division of Highways, State of California, and the Federal Highway Administration. The opinions, findings, and conclusions expressed are those of the writers and not necessarily those of the sponsors.

G. D. Mancarti and R. E. Davis of the Research and Development Section provided close liaison from the Bridge Department, Division of Highways, State of California.

REFERENCES

1. Bouwkamp, J. G., Scordelis, A. C., and Wasti, S. T. Structural Behavior of a Two Span Reinforced Concrete Box Girder Bridge Model, Volume 1. Univ. of California, Berkeley, Structural Eng. and Structural Mech. Rept. 71-5, April 1971.
2. Scordelis, A. C., Bouwkamp, J. G., and Wasti, S. T. Structural Behavior of a Two Span Reinforced Concrete Box Girder Bridge Model, Volume 2. Univ. of California, Berkeley, Structural Eng. and Structural Mech. Rept. 71-6, Oct. 1971.
3. Scordelis, A. C., Bouwkamp, J. G., and Wasti, S. T. Structural Behavior of a Two Span Reinforced Concrete Box Girder Bridge Model, Volume 3. Univ. of California, Berkeley, Structural Eng. and Structural Mech. Rept. 71-7, Oct. 1971.

TIME-DEPENDENT BEHAVIOR OF HAWAIIAN AGGREGATE CONCRETE TO REPEATED LOADINGS

Samuel Zundelevich, Harold S. Hamada, and Arthur N. L. Chiu,
Department of Civil Engineering, University of Hawaii

The results of experimental studies on axially loaded cylinders and the camber and deflection of simply supported rectangular prestressed concrete beams are reported. The cylinders and beams were initially loaded for a period of 450 days. Subsequently, the loads were removed, and the beams and cylinders were left without loads for 90 days and then were reloaded to the original stress for 90 days. This sequence was repeated for another cycle. The modulus of elasticity is observed at different times. Values for ultimate shrinkage strains as well as ultimate creep coefficients are suggested. Mathematical models for creep, camber, and deflections are discussed. The effect of loading age is observed, and a statistical evaluation of deflection data is performed.

• A PROGRAM has been started at the University of Hawaii with the cooperation and support of the Hawaii Department of Transportation to evaluate Hawaiian aggregate lightweight concrete used in structural systems. The objective of the program is to gather experimental data that will be directly applicable to current design procedures. As part of the program, concrete cylinders were tested in uniaxial compression at constant stress, and simply supported prestressed concrete beams were loaded with dead weights to study the time-dependent behavior of Hawaiian aggregate lightweight concrete. This paper reports on the preliminary findings of the experimental data and is divided into two parts: concrete cylinders and prestressed concrete beams.

The following notation will be used:

- A_g = beam cross-sectional area, neglecting the steel;
- $C.F._{L.A.}$ = correction factor for delayed time of loading;
- C_t = creep coefficient at time t;
- C_{t_1} = creep coefficient for the noncomposite beam due to subsequently applied loads (first loading);
- C_{t_2} = creep coefficient for second loading;
- C_{t_3} = creep coefficient for third loading;
- $C_{t_{N1}}$ = creep coefficient for first unloading;
- $C_{t_{N2}}$ = creep coefficient for second unloading;
- $C_{t_{N3}}$ = creep coefficient for third unloading;
- C_u = ultimate creep coefficient;
- $C_{u_{L.A.}}$ = ultimate creep coefficient for specimen loaded at age L.A.;
- C_{u7} = ultimate creep coefficient for specimen loaded at age 7 days;
- D = parameter in creep equation;
- DL = script denoting dead weight;
- e = eccentricity of prestressing steel;
- $(E_c)_t$ = concrete modulus of elasticity at time t;
- E[ ] = expected value of [ ];

Sponsored by Committee on Concrete Superstructures.

$(f'_c)_t$ = concrete compressive strength at time t;
F_o = prestressing force at transfer (after elastic loss);
ΔF_t = total loss of prestress at time t minus the initial elastic loss;
G_o = elastic change in prestress caused by lengthening (or shortening) of the steel due to additional loading (or unloading);
ΔG_t = time-dependent change in prestress caused by lengthening (or shortening) of the steel due to additional loading (or unloading);
I_g = moment of inertia of the gross section;
K = constant;
L = subscript denoting additional loading (also span length);
LA = subscript denoting loading age;
P = applied transverse load;
v = coefficient of variation;
W = unit weight of concrete, pcf;
Var [ ] = variance of [ ] (also [^{v}]);
α = empirical constant;
$\Delta(t)$ = deflection or camber at any time t;
$\Delta_i(t)$ = ith deflection component at time t;
$(\Delta_i)_{F_o}$ = initial camber due to the initial prestressing force, F_o;
$(\Delta_i)_{DL}$ = initial dead load deflection;
$(\Delta_i)_L$ = elastic deflection due to additional loading;
$(\Delta_i)_{CP}$ = elastic deflection due to change in prestress;
$[(\Delta_i)_L]_N$ = initial deflection caused by the nth loading or unloading;
ϵ_{axial} = strain at beam neutral axis;
ρ = correlation coefficient; and
σ = standard deviation.

UNIAXIALLY LOADED CONCRETE CYLINDERS

The time-dependent behavior of Hawaiian aggregate concrete in uniaxial compression was investigated by loading concrete cylinders at constant stress. The experimental results from this simple stress state were used to construct a mathematical model for creep and to supplement data derived from simply supported prestressed concrete beams.

Laboratory Procedures

Standard 6-in. diameter concrete cylinders were loaded in uniaxial compression in accordance with ASTM C 512-69 recommendations. The constant axial load was maintained by placing steel coil springs in series with the concrete specimens.

The initial load was applied on the 28th day after casting and was maintained for 450 days. Subsequently, the cylinders were unloaded and left stress-free for a period of 90 days and loaded for a second time for a period of 90 days. This unloading and loading sequence was continued for another cycle, but this paper considers data for the initial loading, unloaded stress-free state, and second loading.

The concrete specimens were moist-cured for the first 7 days after casting and housed in a controlled-environment room thereafter. The room temperature was maintained at 73 ± 2 F and the relative humidity was maintained at 50 ± 4 percent.

Concrete Mixes

The nominal compressive strength selected was 5,000 psi. Three coarse aggregates were selected: basalt rock from Kapaa Quarry, Oahu; lightweight volcanic cinder, commercially called cinderlite, from Molokai; and lightweight trachyte pumice, commercially called volcanite, from Hawaii. Concrete made from the basalt rock weighed approximately 152 lb/cu ft, whereas concretes made from the other two aggregates were lighter (124 lb/cu ft for cinderlite and 121 lb/cu ft for volcanite) and hereafter will be referred to as lightweight concrete.

The design mixes and actual 28-day compressive strengths have been reported by Hamada, Zundelevich, and Chiu (9).

Mathematical Expressions for Creep

The rate of creep phenomenon diminishes with the passing of time. Many mathematical equations have been proposed to characterize the observed physical phenomenon. Ross (1) and Lorman (2) suggest a hyperbolic formula; Shank (3) proposes the power function, Thomas (4), Hansen (5), and McHenry (6) recommend the logarithmic function. Other forms have also been proposed, but they will not be enumerated here. Usually, the equations are arbitrarily selected to explain experimental data. For the concrete mixes of this study, Watari (7) investigated the various equations presented in the literature. The "best" equation, given by Branson (16), was selected on the basis of minimum residual after least-squares curve fitting:

$$C_t = \frac{t^{0.6}}{t^{0.6} + D} C_u \qquad (1)$$

where C_t is the creep coefficient, defined as the ratio of the strain at time t to the initial strain, C_u is the ultimate creep coefficient, or the limit value of C_t as t gets large, and D is a constant. The two parameters C_u and D are used to characterize the concrete mixes, and it is thought that they differ for each mix.

On the basis of data obtained from the prestressed concrete beams, it was found that Eq. 1 models well the behavior beyond the initial loading.

Test Results

The test data from the cylinders were used to determine the parameters in the creep equation on the basis of least-squares curve fitting techniques. The ultimate creep coefficient and the parameter D are given in Table 1 for the initial loading. It is noted here that D was assigned a value of 10, as recommended by Branson (16), for the prestressed concrete beam calculations. It was found that accurate prediction of time-dependent displacements can be made by using a value of 10. The prediction technique is not sensitive to the value of D provided it is restricted in the range of 10 to 20. The information given in Table 1 was reported previously by Hamada, Zundelevich, and Chiu (9) on the basis of 325 days of sustained loading. The information in Table 1, revised for 450 days of loading, differs slightly from that reported previously.

Figure 1 shows the curves for creep strain versus time after loading for the three aggregates subjected to three stress levels. These curves are presented to demonstrate the degree to which the creep equation fits the experimental data. Each data point, a triangle, square, or circle, represents the average value from nine samples. The nine samples were from three cylinders in which three gauge lines were attached to each cylinder.

To determine if the ultimate creep coefficient is stress-dependent, we generated the following curve. For each stress level, the creep strain was normalized by dividing it by the applied stress. The quotient is called specific creep. If the ultimate creep coefficient is stress-dependent, then it was anticipated that the data from the different stress levels would show a definite pattern when specific creep was plotted as a function of time after loading. Shown in Figure 2 is the result for cinderlite concrete. The graphs for basalt and volcanite concretes are similar and will not be presented. On the basis of Figure 2, it is speculated that, for the aggregates investigated, the ultimate creep coefficient is stress-independent inasmuch as no obvious pattern for the triangles, circles, or squares emerges. The squares, circles, and triangles represent the stress levels of Figure 1b. The data shown in Figure 2 also serve as an indication of the spread in the experimental data.

After the 450th day of loading, the specimens were unloaded and left stress-free for a period of 90 days and then reloaded for a period of 90 days. The maximum creep strains for each period of either loading or unloading are given in Table 2. In the stress-free state the recovery of creep strains is very small. It is noted that the value of one standard deviation of the experimental data is much larger than the average value. This undesirable result occurs because the recovery strain is determined by taking small differences of two large numbers. In fact, the average difference given

Figure 1. Creep strain versus time after loading.

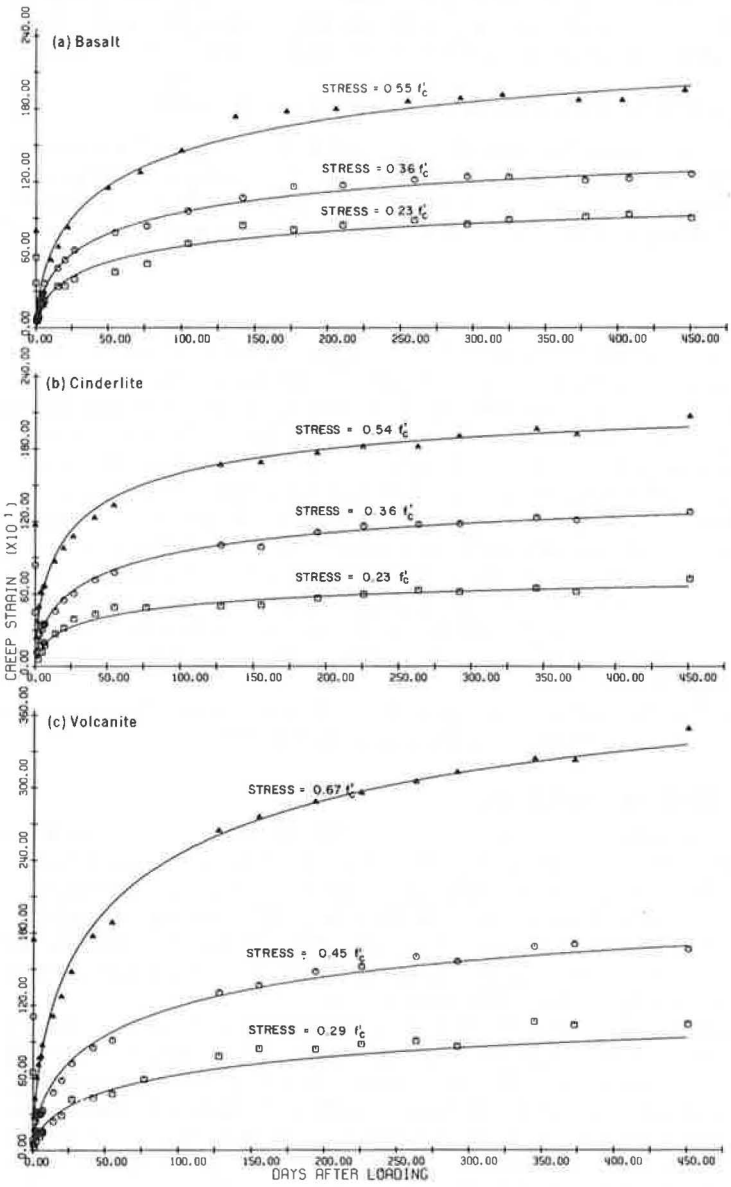

in Table 2 is smaller than the measurement errors. Therefore, no definite conclusions may be drawn. It is noted, however, that the data are consistent in that the concrete expands during the stress-free state and contracts when loaded in compression. The data are being analyzed further, and a model will be postulated to explain the data.

SIMPLY SUPPORTED PRESTRESSED CONCRETE BEAMS

Simply supported prestressed concrete beams were used to investigate the camber, deflection, camber recovery, and deflection recovery behavior in order to assess the time-dependent characteristics of concrete made with Hawaiian aggregates. Information from this portion of the study supplements the data derived from uniaxially loaded cylinders.

Laboratory Procedures

The beams were manufactured with the same types of aggregates as used for the cylinders by using type I standard cement and plastiment as retardant admixture.

Using the different mixes with a nominal strength f'_c = 5,000 psi, we cast separately three sets of seven beams per set. Each set consisted of three beams to study deflection and deflection recovery and three beams to study camber. One unstressed beam 7 by 9 ft long was poured for each set to determine shrinkage strains. The beams were 4 by 6 in. in cross section, 15½ ft long, and simply supported over a 15-ft span. Two ⅜-in., 7-wire, 270-ksi strands located 1.75 in. from the bottom were used. In addition to their own weights, the deflection specimens support two concentrated 750-lb loads at one-third points of the span, as shown in Figure 3 (9). The beams were moist-cured until stressed at age 7 days, placed in the controlled-atmosphere room afterward, loaded at age 28 days, unloaded at age 478 days, then reloaded and unloaded for two cycles at 90-day intervals.

Strain readings were taken with a Whittemore gauge at different times in accordance with ASTM 69. (The gauge point locations are shown also in Figure 5.)

Mathematical Model for Camber and Deflection

Camber and deflection histories for each beam measured with dial gauges are shown in Figure 4. Camber and deflection values from dial gauge readings compared very well with values calculated from strain gauge point readings (9). The average measured camber and deflection can be modeled as shown in Figure 5a, which is the sum of the various camber and deflection components shown in Figure 5b. These data will be used to assess the creep coefficient at different times of loading and to evaluate the accuracy of the various suggested methods for calculating deflections.

Several mathematical expressions are available to model the deflection behavior of prestressed concrete members. The expression suggested by ACI Committee 435 (10) is a simplified version from the more accurate expression developed by Branson (11). This expression can be expanded to take into account the effects of further loading and unloading. The terms in this expression can be rearranged, and the total deflection at any time, excluding the effects of nonprestressed reinforcement, can be expressed as the sum of different components shown in Eq. 2 and Figures 5a and 5b (camber is positive):

$$\Delta(t) = \Delta_1 + \Delta_2(t) + \Delta_3 + \Delta_4(t) + \Delta_5 + \Delta_6(t) + \Delta_7 + \Delta_8(t) + \Delta_9 + \Delta_{10}(t) + \Delta_{11} + \Delta_{12}(t) + \Delta_{13} + \Delta_{14}(t) \quad (2)$$

where

$$\Delta_1 = (\Delta_i)_{Fo} - (\Delta_i)_{DL}$$

is the result of the initial camber due to the initial prestressing force and the initial deflection due to the beam's own weight;

Figure 2. Specific creep versus time after loading for cinderlite concrete.

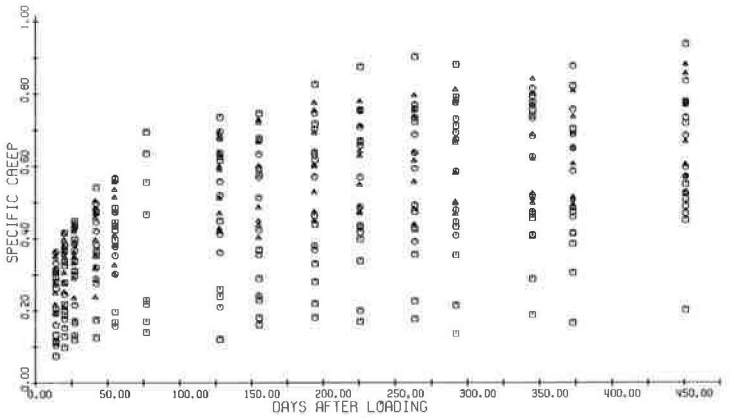

Table 1. Ultimate creep coefficients for initial loading.

Aggregate	Applied Stress (psi)	Ultimate Creep Coefficient	Constant D for Creep Equation	Age at Loading (day)
Basalt	1,230	3.37	13.69	28
	2,040	3.22	14.20	28
	2,720	4.94	20.27	28
Cinderlite	1,260	2.08	10.16	38
	1,980	2.07	12.68	38
	2,990	2.23	7.75	38
Volcanite	1,260	2.53	20.91	28
	1,980	2.40	17.33	28
	2,990	2.69	13.54	28

Figure 3. Details of prestressed concrete beams.

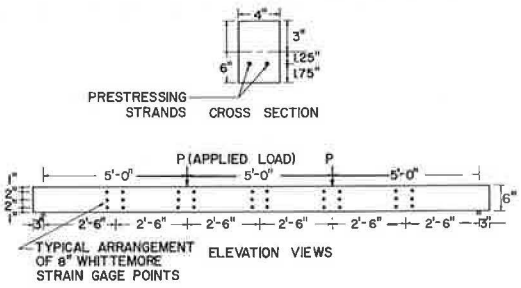

Table 2. Maximum creep strains for loading and unloading phases.

Aggregate	Stress (psi)	First Loading (μin./in.)	First Unloading (μin./in.)	Second Loading (μin./in.)
Basalt	1,230	1,300 ± 156	14 ± 160	75 ± 123
	2,040	1,627 ± 114	14 ± 70	102 ± 82
	2,720	2,101 ± 602	100 ± 76	88 ± 64
Cinderlite	1,260	633 ± 204	4 ± 65	42 ± 60
	1,980	982 ± 221	54 ± 79	120 ± 93
	2,990	1,585 ± 309	114 ± 179	—
Volcanite	1,260	1,124 ± 121	50 ± 85	94 ± 84
	1,980	1,319 ± 403	44 ± 70	54 ± 102
	2,990	3,352 ± 1,296	64 ± 77	—

Figure 4. Beam deflection versus time.

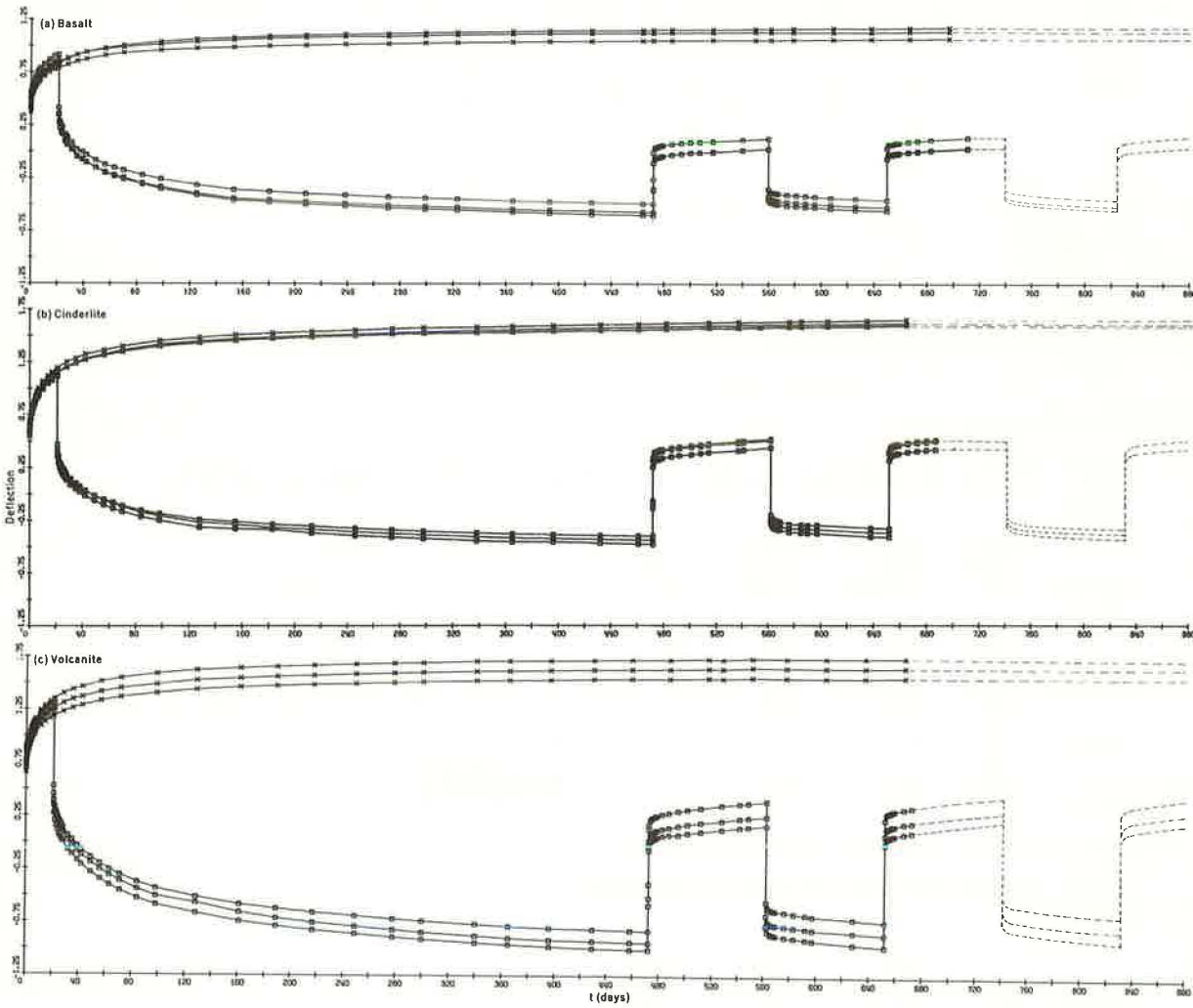

$$\Delta_2(t) = \left[- \frac{\Delta F_t}{F_o} + \left(1 - \frac{\Delta F_t}{2F_o}\right) C_t \right] (\Delta_1)_{F_o} - (\Delta_1)_{DL} C_t \qquad t \geq 0$$

is the result of time-dependent effect due to initial camber;

$$\Delta_3 = - (\Delta_1)_L + (\Delta_1)_{CP} \qquad t \geq t_1$$

is the instantaneous change in deflection due to the first loading (additional dead weights) and subsequent loadings will be the same;

$$\Delta_4(t) = \left[\frac{\Delta G_t}{G_o} + \left(1 + \frac{\Delta G_t}{2G_o}\right) C_{t_1} \right] (\Delta_1)_{CP} - (\Delta_1)_L C_{t_1}$$

$$= C_{t_1} \left[\left(2 + \frac{C_{t1}}{2}\right) (\Delta_1)_{CP} - (\Delta_1)_L \right] \qquad t \geq t$$

is the time-dependent effect on deflection due to first loading;

$$\Delta_5 = (\Delta_1)_L - (\Delta_1)_{CP} \qquad t \geq t_{n_1}$$

is the instantaneous change in deflection due to first unloading;

$$\Delta_6(t) = C_{t_{n_1}} \left[- \left(2 + \frac{C_{t_{n_1}}}{2}\right) (\Delta_1)_{CP} + (\Delta_1)_L \right] \qquad t \geq t_{n_1}$$

is the time-dependent effect on deflection due to first unloading;

$$\Delta_7 = - (\Delta_1)_L + (\Delta_1)_{CP} \qquad t \geq t_2$$

is the instantaneous change in deflection due to second loading;

$$\Delta_8(t) = C_{t_2} \left[\left(2 + \frac{C_{t_2}}{2}\right) (\Delta_1)_{CP} - (\Delta_1)_L \right] \qquad t \geq t_2$$

is the time-dependent effect on deflection due to second loading;

$$\Delta_9 = (\Delta_1)_L - (\Delta_1)_{CP} \qquad t \geq t_{n_2}$$

is the instantaneous change in deflection due to second unloading;

$$\Delta_{10}(t) = C_{t_{n_2}} \left[- \left(2 + \frac{C_{t_{n_2}}}{2}\right) (\Delta_1)_{CP} + (\Delta_1)_L \right] \qquad t \geq t_{n_2}$$

is the time-dependent effect on deflection due to second unloading;

$$\Delta_{11} = - (\Delta_1)_L + (\Delta_1)_{CP} \qquad t \geq t_3$$

is the instantaneous change in deflection due to third loading;

$$\Delta_{12}(t) = C_{t_3}\left[\left(2 + \frac{C_{t_3}}{2}\right)(\Delta_1)_{CP} - (\Delta_1)_L\right] \qquad t \geq t_3$$

is the time-dependent effect on deflection due to third loading;

$$\Delta_{13} = (\Delta_1)_L - (\Delta_1)_{CP} \qquad t \geq t_{n_3}$$

is the instantaneous change in deflection due to third unloading; and

$$\Delta_{14}(t) = C_{t_{n_3}}\left[-\left(2 + \frac{C_{t_{n_3}}}{2}\right)(\Delta_1)_{CP} + (\Delta_1)_L\right] \qquad t \geq t_{n_3}$$

is the time-dependent effect on deflection due to third unloading.

Equation 2 will adequately model the deflection behavior of a prestressed concrete member if proper values for concrete strength, modulus of elasticity, ultimate shrinkage strain, and ultimate creep coefficients are used.

Test Results

Modulus of Elasticity—The value of the modulus of elasticity will greatly influence the magnitude of the elastic and time-dependent deflections. The following expression can be used to calculate the modulus of elasticity, as suggested in ACI 318-71:

$$(E_c)_t = 33\ W^{1.5}\sqrt{(f'_c)t} \tag{3}$$

The compressive strength, as it varies with age $(f'_c)_t$, can be calculated as (8, 16)

$$(f'_c)_t = \frac{t}{4.00 + 0.85t}(f'_c)_{28} \tag{4}$$

The values of the modulus of elasticity were determined by using

1. Cylinders to determine the stress-strain diagrams,
2. Values from the elastic camber measured at the release of the prestressing force from the formula

$$\Delta_1 = (\Delta_1)_{F_o} - (\Delta_1)_{DL} = \frac{F_o e L^2}{8(E_c)_7 I_g} - \frac{5\omega L^4}{384(E_c)_7 I_g} \tag{5}$$

3. Measured elastic strains at different gauge points on the beam at the release of the prestressing force from the formula

$$\epsilon_{axial} = \frac{F_o L}{A(E_c)_7} \tag{6}$$

4. The elastic response at loading and subsequent unloading and reloading from the formula

$$(\Delta_1)_{L_N} = \frac{KPL^3}{(E_c)_t I} \tag{7}$$

The experimental results are given in Tables 3 and 4 and Figure 6, and they are compared with calculated values:

1. Basalt—At age 7 days, the mean modulus of elasticity determined from measured camber (Eq. 5) at the release of prestress agrees well with values calculated from the formula recommended in ACI 318-71 (Eq. 3). The mean value determined from measured axial shortening at the release of prestress (Eq. 6) is 12 percent less than the calculated value; however, the standard deviation for this latter case is twice of that obtained from measured camber. As time progressed, measured values were approximately 5 percent below the predicted values. The coefficient of variation of the measured modulus at different times ranged between 0.06 and 0.136. Mean measured values from cylinders were 10 to 20 percent less than measured values from beams.
2. Cinderlite—At age 7 days, the mean modulus of elasticity from measured camber at the release of prestress is slightly below values predicted from ACI 318-71. The mean value obtained from axial shortening at the release of prestress is about 10 percent higher than the mean value from camber and just above the predicted value. The standard deviation for this latter case was higher than that obtained from camber values. As time progressed, measured values were smaller than the predicted values (about 80 percent of the predicted modulus at age 480 days). The coefficient of variation for the measured modulus at different times ranged between 0.04 and 0.07. Averaged measured values from cylinders were always 10 to 20 percent less than the measured values from beams.
3. Volcanite—At age 7 days, the mean value obtained from measured camber at the release of prestress as well as the mean value measured from the axial shortening are approximately 20 percent less than the value calculated using ACI 318-71. The standard deviation for the values obtained from strain is 60 percent higher than the standard deviation for the values obtained from measured axial strains. As time progressed, the difference between mean measured values and predicted modulus of elasticity became larger. The elastic modulus showed a decrease with time instead of the expected increase. The coefficient of variation for the measured modulus at various times ranged between 0.07 and 0.11. The mean measured values from cylinders were 10 percent below measured values for beams.

It can be concluded that the modulus of elasticity of concrete made with basalt increases with age, and it can be closely predicted. The modulus of elasticity of concrete made with lightweight aggregate increased up to 28 days, approximately, and then decreased slightly with age or remained almost constant. The initial modulus is overestimated by ACI 318-71, and the gap becomes wider with time.

Creep Coefficient—Deflection equations will be adequate only if proper values for the various parameters are used. Of particular importance are the values of creep coefficients at any time after any age of loading under any conditions. Correction factors (8) are available to account for conditions other than standard. Creep coefficient at any time is given as (8)

$$C_t = \left(\frac{t^{0.6}}{10 + t^{0.6}}\right) C_u \tag{1}$$

The correction factor due to age at loading other than 7 days (for moist-cured concrete) can be given as (8)

$$CF_{LA} = 1.25 t_{LA}^{-0.118} \tag{8}$$

or (12)

$$CF_{LA} = \left(\frac{7}{t_{LA}}\right)^{\alpha} \tag{9}$$

Figure 5. Camber and deflection versus time.

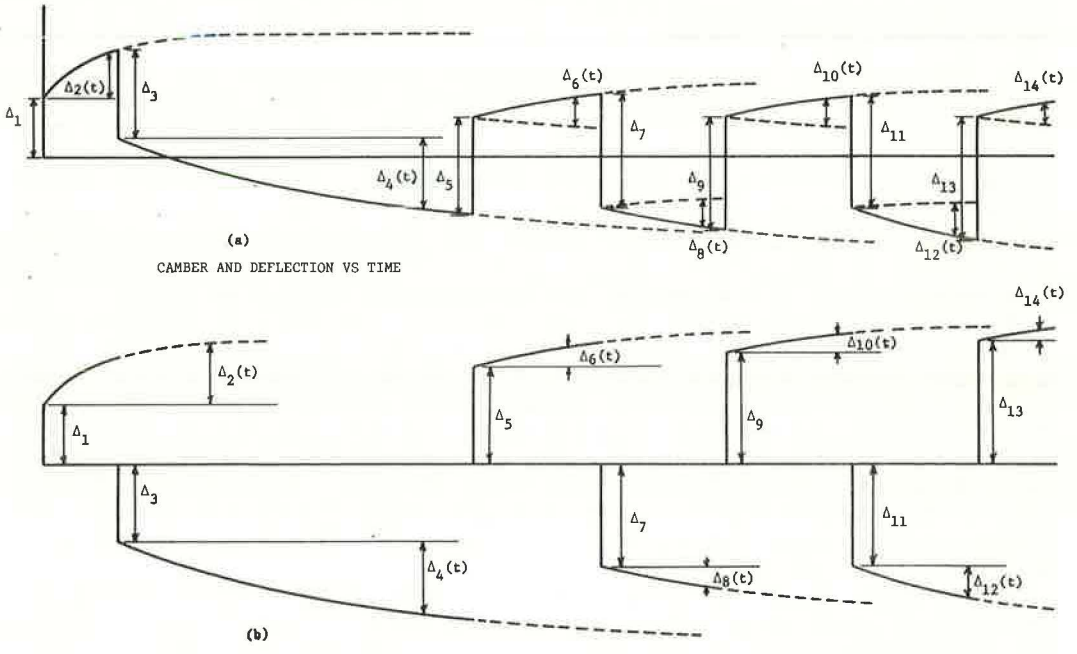

Table 3. Modulus of elasticity at 7 days.

Aggregate	Assessed E_c in Beams (ksi)				Calculated E_c (ACI 318-71)
	From Strain[a]		From Camber[b]		
	Average	σ	Average	σ	
Basalt	3,152	426	3,661	229	3,623
Cinderlite	2,808	198	2,591	81	2,794
Volcanite	2,087	238	2,077	146	2,632

[a]Equation 6, measured strain. [b]Equation 5, from camber.

Table 4. Measured modulus of elasticity at loading and unloading (ksi).

Item	First Loading (28 days)	First Unloading (478 days)	Second Loading (568 days)	Second Unloading (658 days)
Basalt				
I-A	4,162	4,289	4,378	4,272
I-B	4,434	4,539	4,628	4,529
I-C	4,178	4,324	4,387	4,254
Measured average	4,360(±156)	4,487(±138)	4,571(±145)	4,455(±158)
From cylinders	3,500	3,580	4,100	—
ACI 318-71	4,342	4,673	4,676	4,680
Cinderlite				
II-A	3,026	2,860	2,928	2,884
II-B	2,920	2,773	2,810	2,784
II-C	2,949	2,845	2,904	2,856
Measured average	3,057(±57)	2,911(±54)	2,971(±64)	2,930(±53)
From cylinders	3,000	2,230	2,530	—
ACI 318-71	3,350	3,603	3,605	3,609
Volcanite				
III-A	2,382	2,208	2,225	2,199
III-B	2,415	2,206	2,197	2,147
III-C	2,676	2,158	2,190	2,145
Measured average	2,570(±165)	2,264(±29)	2,277(±19)	2,235(±32)
From cylinders	2,100	1,900	2,000	—
ACI 318-71	3,154	3,394	3,396	3,399

Figure 6. Modulus of elasticity versus time.

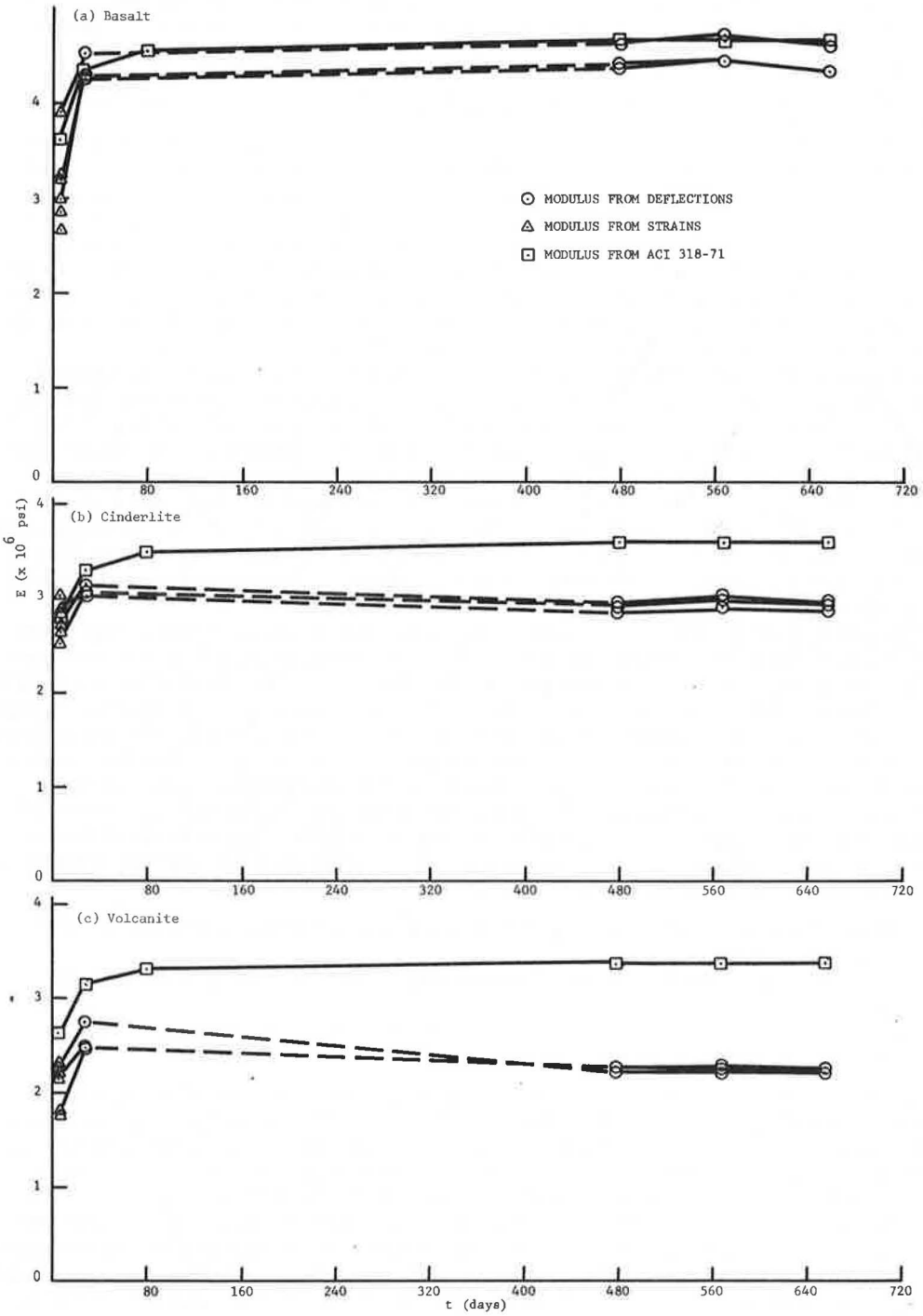

Measured deflection components can be used to evaluate the ultimate creep coefficient provided the uncertainty in the modulus of elasticity is minimized or eliminated. For this, it is necessary to normalize the time-dependent camber and the time-dependent effects on deflection with respect to instantaneous behavior. Plots of $\frac{\Delta_1 + \Delta_2(t)}{\Delta_1}$, $\frac{\Delta_3 + \Delta_4(t)}{\Delta_3}$, $\frac{\Delta_5 + \Delta_6(t)}{\Delta_5}$, and so on are shown in Figure 7. Using Eq. 2 with different values for ultimate creep coefficients and selecting the values that will show the best visual fit of the normalized deflection components result in values for ultimate creep coefficients at various loading ages. Calculated values for the normalized components of deflection using the values selected for the ultimate creep coefficients together with Eq. 1 compared very well with measured values, as shown in Figure 7. Values for ultimate creep coefficients obtained from the beams and from the cylinders as well as ultimate shrinkage values are shown in Table 5. If the curing conditions had been different, it is speculated that similar values would have been obtained. Also, the creep behavior is similar to that reported in the literature (17).

The values of the correction factor at various loading ages are shown in Figure 8 and are compared with Eq. 8 as well as upper and lower bounds suggested by Meyers et al. (8) and by Eq. 9. The results show that Eq. 8 does not satisfactorily predict the effect of loading age for the aggregates used in this study. However, it should be noted that Eq. 8 is the result of careful evaluation of data with loading ages ranging from 7 to 60 days (Fig. 7, 8) and that it is quite adequate for that period. Equation 9 shows a closer fit. In this program, data were taken at loading ages of 7, 28, and 478 days and later on, leaving the values of ultimate creep coefficients at loading ages from 28 to 478 days with uncertainty. Further studies are needed to obtain a solution with sufficient statistical confidence.

Statistical Analysis—Concrete members under nominally identical conditions show large variability in their deflection behavior (13); therefore, it is of importance to assess the variability (14). In prestressed concrete members, the total deflection is the sum of different components, i.e., $\Delta(t) = \Delta_1 + \Delta_2(t) + \Delta_3 + \Delta_4(t) + \ldots$. It is possible then that similar prestressed concrete beams may show the same total deflection even though the magnitude of the various deflection components is quite different. For this reason, it is necessary to study the variability of each deflection component. Some of these deflection components are time-dependent and therefore are stochastic processes (15). However, for a first approximation, their variability could be studied at fixed times.

A simple statistical analysis of these components was performed, and the results are given in Table 6. The following can be observed:

1. The coefficient of variation for the various deflection components has a value between 2 and 10 percent,
2. The time-dependent deflection components for later loading ages show less variation, and
3. The variation of the deflection components for lightweight concrete is smaller than that for basalt (particularly for cinderlite).

A variety of equations as well as recommendations for the values of the constants involved are available for forecasting the deflection of a simply supported prestressed concrete member. All of these yield a single number that is either smaller or larger than the deflection that would be likely to occur in the actual member. As stated by the ACI committee (14): "If the variability of actual deflections with respect to calculated deflections was sufficiently small, the engineer could use calculated values with a high degree of confidence. However, the variability of actual deflections under nominally identical conditions is often large rather than small." It is desirable then to have a range of possible actual deflection values centered around the calculated deflection. Some ideas (14) will be expanded to the case of uncracked, simply supported prestressed concrete beams.

The measured deflection at any time can be expressed as

$$\Delta(t) = \Delta_{1_{calc}} \frac{\Delta_{1_{meas}}}{\Delta_{1_{calc}}} + \Delta_2(t)_{calc} \frac{\Delta_{2_{meas}}(t)}{\Delta_2(t)_{calc}} + \Delta_{3_{calc}} \frac{\Delta_{3_{meas}}}{\Delta_{3_{calc}}} + \Delta_4(t)_{calc} \frac{\Delta_{4_{meas}}(t)}{\Delta_4(t)_{calc}}$$

Substituting $r_i = \frac{\Delta_{i_{meas}}}{\Delta_{i_{calc}}}$, where r_i is a random variable that takes into account the variability of the measured i th component with respect to calculated values, gives a total deflection of

$$\Delta(t) = \sum_{i=1}^{N} \Delta_{i_{calc}} r_i$$

where N = total number of deflection components.

If it is assumed that the random variables r_i are normally distributed, then the expected total deflection is

$$E[\Delta(t)] = \overline{\Delta(t)} = \sum_{i=1}^{N} \Delta_{i_{calc}} \overline{r_i}$$

The variance of the total deflection is

$$Var[\Delta(t)] = \sum_{i=1}^{N} \Delta_{i_{calc}} \overset{v}{r_i} + 2 \sum_{i=1}^{N} \sum_{i<j\leq N}^{N} \rho_{ij} \sigma_{r_i} \sigma_{r_j} \Delta_{i_{calc}} \Delta_{j_{calc}}$$

and

$$ST\ DEV\ [\Delta(t)] = \sigma_{\Delta(t)} = \sqrt{Var[\Delta(t)]}$$

The estimates of the mean, variance, and correlation coefficients for the random variables r_i (i = 1, 2, 3, 4) at different times are given in Tables 7 and 8. Using these estimates, we can assess the variability of actual deflections with respect to calculated values. These estimates are derived from only three samples, but they could be re-evaluated as more data are obtained.

As an example, for N = 4:

$$\overline{\Delta(t)} = \Delta_{1_{calc}} \overline{r_1} + \Delta_{2_{calc}}(t) \overline{r_2(t)} + \Delta_{3_{calc}} \overline{r_3} + \Delta_{4_{calc}}(t) \overline{r_4(t)}$$

and

$$\begin{aligned}
\overset{v}{\Delta}(t) = {} & \Delta_{1_{calc}}^{2} \overset{v}{r_1} + \Delta_{2_{calc}}(t)^2 \overset{v}{r_2}(t) + \Delta_{3_{calc}}^{2} \overset{v}{r_3} + \Delta_{4_{calc}}(t)^2 \overset{v}{r_4}(t) \\
& + \rho_{12} \sigma_{r_1} \sigma_{r_2} \Delta_{1_{calc}} \Delta_{2_{calc}}(t) \\
& + \rho_{13} \sigma_{r_1} \sigma_{r_3} \Delta_{1_{calc}} \Delta_{3_{calc}} \\
& + \rho_{14} \sigma_{r_1} \sigma_{r_4} \Delta_{1_{calc}} \Delta_{4_{calc}}(t) \\
& + \rho_{23} \sigma_{r_2} \sigma_{r_3} \Delta_{2_{calc}}(t) \Delta_{3_{calc}} \\
& + \rho_{24} \sigma_{r_2} \sigma_{r_4} \Delta_{2_{calc}}(t) \Delta_{4_{calc}}(t) \\
& + \rho_{34} \sigma_{r_3} \sigma_{r_4} \Delta_{3_{calc}} \Delta_{4_{calc}}(t)
\end{aligned}$$

Figure 7. Comparison of normalized camber and normalized deflection due to subsequently applied load with suggested values.

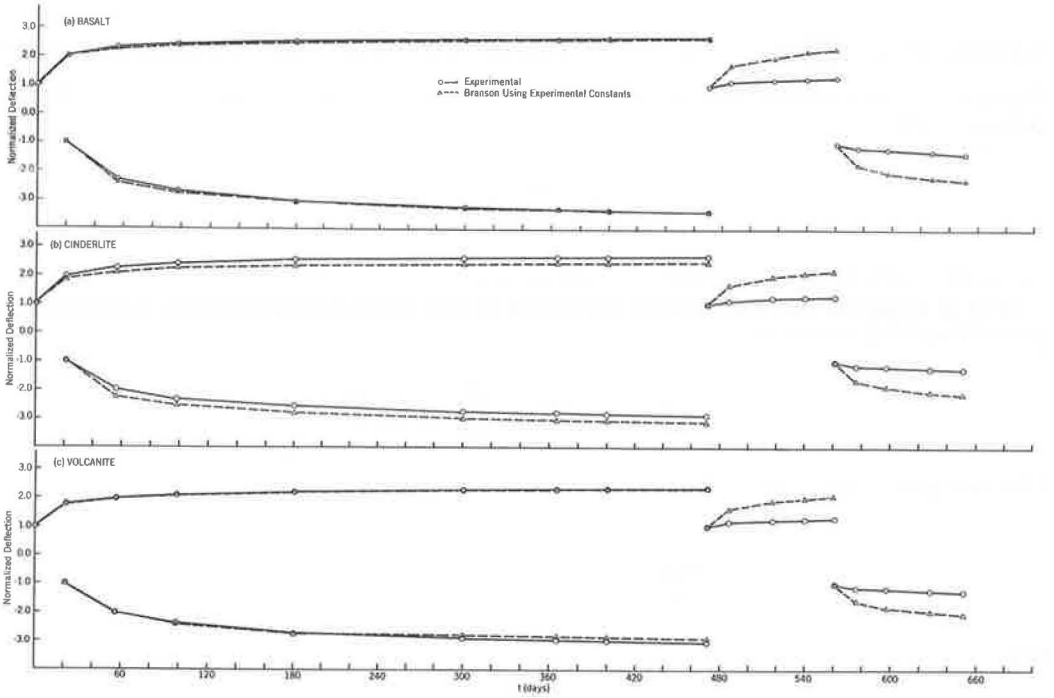

Table 5. Comparison of experimental and suggested values for ultimate shrinkage strains and ultimate creep coefficients.

	Ultimate Shrinkage Strain ($\times 10^{-6}$ in./in.)		Ultimate Creep Coefficient		
Aggregate	Experimental[a]	Meyers (8, 16)	Experimental[a]	Hamada (9)[b]	Meyers (8, 16)
Basalt	1,050	714	3.7	3.84	2.69
Cinderlite	938	714	3.3	2.20	2.34
Volcanite	878	726	3.0	2.54	2.33

[a]Obtained from beams. [b]Average values obtained from cylinders under various constant stress levels.

Figure 8. Correction factor versus loading age.

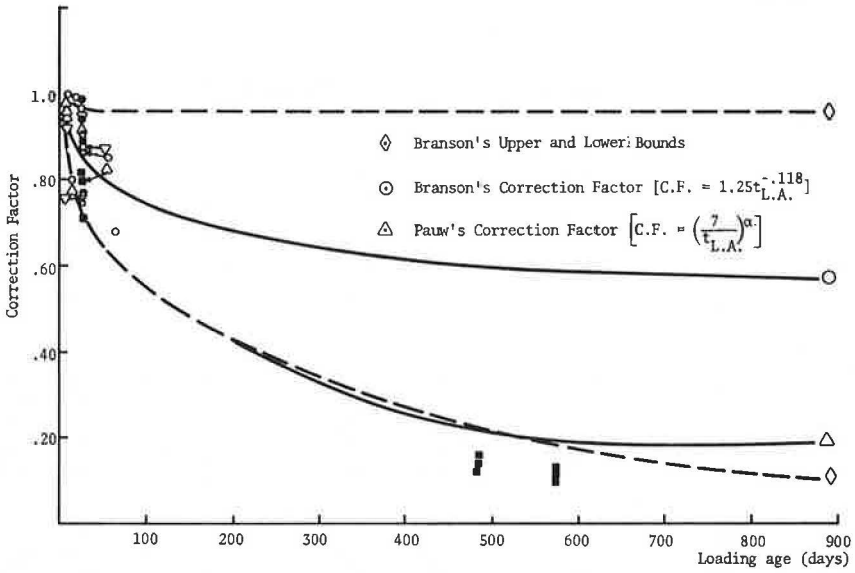

Table 6. Statistical analysis of the deflection components.

Aggregate	Time (days after stressing)	Average Deflection Components (in.)				Standard Deviation				Coefficient of Variation			
		$\bar{\Delta}_1$	$\bar{\Delta}_2$	$\bar{\Delta}_3$	$\bar{\Delta}_4$	σ_1	σ_2	σ_3	σ_4	v_1	v_2	v_3	v_4
Basalt	0	0.426				0.200				0.0469			
	21		0.440	0.495			0.0271	0.0174			0.0616	0.0352	
	56		0.578		0.683		0.0358		0.0085		0.0619		0.0124
	98		0.633		0.879		0.0393		0.0156		0.0621		0.0177
	180		0.685		1.054		0.0419		0.0164		0.0612		0.0156
	300		0.716		1.148		0.0444		0.0195		0.0620		0.0170
	365		0.731		1.190		0.0450		0.0200		0.0616		0.0168
	400		0.736		1.204		0.0454		0.0220		0.0617		0.0183
	471		0.744		1.230		0.0454		0.0225		0.0610		0.0183
Cinderlite	0	0.599				0.0250				0.0417			
	21		0.558	0.705			0.0173	0.0110			0.0337	0.0156	
	56		0.721		0.683		0.0225		0.0032		0.0312		0.0047
	98		0.809		0.915		0.0250		0.0104		0.0309		0.0114
	180		0.875		1.083		0.0275		0.0205		0.0314		0.0189
	300		0.920		1.202		0.0286		0.0205		0.0311		0.0170
	365		0.934		1.244		0.0291		0.0211		0.0311		0.0170
	400		0.942		1.258		0.0296		0.0217		0.0314		0.0172
	471		0.957		1.291		0.0296		0.0241		0.0309		0.0187
Volcanite	0	0.740				0.0356				0.0482			
	21		0.556	0.804			0.0259	0.0523			0.0661	0.0623	
	56		0.711		0.876		0.0333		0.0056		0.0468		0.0064
	98		0.787		1.193		0.0368		0.0125		0.0467		0.0105
	180		0.856		1.460		0.0403		0.0246		0.0471		0.0168
	300		0.906		1.634		0.0412		0.0336		0.0455		0.0206
	365		0.923		1.702		0.0428		0.0365		0.0464		0.0214
	400		0.928		1.724		0.0432		0.0376		0.0465		0.0218
	471		0.945		1.764		0.0441		0.0394		0.0467		0.0223

Table 7. Statistical analysis of $r_i = \frac{\Delta_{i_{meas}}}{\Delta_{i_{calc}}}$ using experimental constants.

Aggregate	Time (days after stress-ing)	Mean				Standard Deviation				Correlation Coefficient					
		$\bar{r}_1$	$\bar{r}_2$	$\bar{r}_3$	$\bar{r}_4$	σ_1	σ_2	σ_3	σ_4	ρ_{12}	ρ_{13}	ρ_{14}	ρ_{15}	ρ_{16}	ρ_{17}
Basalt	0	1.002				0.0470									
	21		1.034	0.977			0.0639	0.0342		0.979	0.836				
	56		1.073		1.033		0.0665		0.0129	0.978		0.585	0.702	0.402	0.935
	98		1.066		1.063		0.0662		0.0189	0.980		0.384	0.709	0.193	0.828
	180		1.057		1.087		0.0647		0.0169	0.978		0.304	0.704	0.101	0.778
	300		1.043		1.078		0.0647		0.0183	0.979		0.487	0.708	0.301	0.887
	365		1.043		1.085		0.0642		0.0183	0.979		0.449	0.705	0.256	0.867
	400		1.042		1.084		0.0643		0.0198	0.980		0.454	0.711	0.269	0.869
	471		1.038		1.084		0.0633		0.0198	0.980		0.466	0.711	0.282	0.875
Cinderlite	0	1.066				0.0445									
	21		1.156	1.060			0.0371	0.0194		0.295	0.681				
	56		1.180		0.905		0.0368		0.0043	0.289		-0.921	0.897	-0.632	-0.900
	98		1.195		0.969		0.0369		0.01106	0.298		-0.825	0.901	-0.289	-0.152
	180		1.185		0.980		0.0372		0.0185	0.305		-0.0477	0.905	0.937	0.699
	300		1.173		0.990		0.0365		0.0169	0.293		-0.484	0.899	0.696	0.311
	365		1.163		0.995		0.0364		0.0169	0.287		-0.589	0.897	0.605	0.191
	400		1.169		0.994		0.0367		0.0172	0.299		-0.391	0.902	0.761	0.408
	471		1.168		0.999		0.0367		0.0186	0.299		-0.599	0.902	0.583	0.178
Volcanite	0	1.239				0.0596									
	21		1.203	1.186			0.0568	0.0738		-0.0916	0.684				
	56		1.208		1.206		0.0566		0.0077	-0.0632		-0.762	0.771	-0.608	0.0398
	98		1.207		1.314		0.0564		0.0138	-0.0820		-0.682	0.783	0.788	1.0000
	180		1.200		1.373		0.0566		0.0231	-0.0838		-0.529	0.784	0.889	0.979
	300		1.193		1.399		0.0543		0.0288	-0.0532		-0.410	0.765	0.933	0.946
	365		1.193		1.415		0.0553		0.0304	-0.0569		-0.374	0.767	0.947	0.933
	400		1.191		1.415		0.0553		0.0309	-0.0665		-0.416	0.773	0.936	0.949
	471		1.191		1.418		0.0556		0.0317	-0.0727		-0.472	0.777	0.913	0.965

Table 8. Statistical analysis of $r_i = \frac{\Delta_{i_{meas}}}{\Delta_{i_{calc}}}$ using ACI constants.

Aggregate	Time (days after stress-ing)	Mean				Standard Deviation				Correlation Coefficient					
		$\bar{r}_1$	$\bar{r}_2$	$\bar{r}_3$	$\bar{r}_4$	σ_1	σ_2	σ_3	σ_4	ρ_{12}	ρ_{13}	ρ_{14}	ρ_{23}	ρ_{24}	ρ_{34}
Basalt	0	0.973				0.0614									
	21		1.562	1.000			0.0766	0.0351		0.0447	0.836				
	56		1.260		2.575		0.1001		0.212	0.995		-0.961	0.777	-0.984	-0.651
	98		1.175		2.335		0.0812		0.162	0.998		-0.921	0.868	-0.895	-0.556
	180		1.095		2.314		0.0844		0.142	0.995		-0.918	0.888	-0.872	-0.549
	300		1.004		2.115		0.0726		0.116	0.985		-0.901	0.917	-0.814	-0.515
	365		0.976		2.058		0.0711		0.112	0.987		-0.897	0.913	-0.815	-0.507
	400		0.970		2.044		0.0704		0.110	0.983		-0.887	0.922	-0.781	-0.478
	471		0.957		2.032		0.0672		0.106	0.977		-0.883	0.934	-0.760	-0.479
Cinderlite	0	1.056				0.0754									
	21		1.630	1.092			0.0496	0.0200		-0.143	-0.440				
	56		1.362		2.176		0.0238		0.129	-0.977		0.214	0.227	0.00826	-0.972
	98		1.308		2.020		0.0183		0.0975	-1.000		0.0449	0.434	-0.0400	-0.919
	180		1.224		1.960		0.0197		0.0620	-0.994		-0.202	0.326	0.317	-0.793
	300		1.133		1.818		0.0173		0.0660	-0.996		-0.153	0.328	0.272	-0.821
	365		1.098		1.764		0.0129		0.0652	-0.980		-0.169	0.616	-0.423	-0.814
	400		1.093		1.741		0.0128		0.0589	-0.979		-0.175	0.615	-0.0372	-0.809
	471		1.085		1.748		0.0124		0.0654	-0.958		-0.184	0.684	-0.116	-0.804
Volcanite	0	1.210				0.0710									
	21		1.537	1.225			0.131	0.0763		-0.123					
	56		1.258		2.500		0.135		0.155	0.261		-0.715	0.526	-0.862	-0.0217
	98		1.194		2.386		0.120		0.101	0.246		-0.832	0.539	-0.744	0.162
	180		1.131		2.411		0.101		0.0824	0.241		-0.920	0.543	-0.605	0.340
	300		1.047		2.253		0.0816		0.0677	0.229		-0.977	0.553	-0.436	-0.508
	365		1.019		2.202		0.0855		0.0626	0.229		-0.984	0.554	-0.404	0.536
	400		1.012		2.186		0.0834		0.0633	0.210		-0.984	0.569	-0.383	0.541
	471		1.006		2.180		0.0812		0.0650	0.216		-0.984	0.564	-0.388	0.542

For basalt aggregate at t = 300 days, using Branson's model (11) with the recommended values of the constants from Table 7 gives estimates of

$$\overline{\Delta(t)} = -0.501 \text{ in.}$$
$$\Delta(t) = 0.0029 \text{ in.}^2$$
$$\sigma\Delta(t) = 0.053 \text{ in.}$$

This means that, with the assumption of normality, there is 68 percent probability that the deflection values will be within the interval -0.448 to -0.554 or that there is 95 percent probability that the deflection values will be within -0.395 and -0.607 in. This statement could be further refined by assuming other probability distributions (i.e., lognormal, beta, or the like) and by increasing the number of sample points. The small amount of sample points available do not merit further investigations at this time. Measured deflection values were

$$\Delta(t)_{1-A} = -0.542 \text{ in.}$$
$$\Delta(t)_{1-B} = -0.520 \text{ in.}$$
$$\Delta(t)_{1-C} = -0.441 \text{ in.}$$

with a mean of -0.501 in., variance of 0.0029 in.^{2}, and standard deviation of 0.053 in.

Therefore the mean value and possible ranges are well predicted. If these results are to be extrapolated to actual practice, it should be noted that an unevaluated uncertainty exists between laboratory results and those expected in actual field conditions.

CONCLUDING REMARKS

The following statements can be made on the basis of the results from this experimental study:

1. The linear superposition assumption for developing a mathematical model to represent the experimental data for initial loading and subsequent loading and unloading is valid for Hawaiian aggregate concretes.
2. The modulus of elasticity for normal Hawaiian aggregate concrete is slightly lower than the elastic modulus suggested in ACI 318-71. For the two lightweight aggregates, the moduli of elasticity are approximately 10 to 15 percent lower.
3. For the first 450 days after casting, Hawaiian aggregate concretes exhibit a fairly constant elastic modulus instead of the expected increase with age.
4. All Hawaiian aggregate concretes show larger ultimate shrinkage strains when compared with the data in published literature. However, Hawaiian lightweight concretes have smaller ultimate shrinkage strains than the Hawaiian normal-weight concrete.
5. The creep coefficient for basalt concrete is larger than the creep coefficients for cinderlite and volcanite concretes. However, this does not necessarily mean that the basalt concrete creeps more because the creep strain is determined from the product of the creep coefficient and initial strains.
6. Equation 1 is a good representation of the creep data for Hawaiian aggregate concretes.
7. The effect of loading age is well represented by Eq. 9 for loading prior to approximately 56 days. Beyond this time more data should be gathered.
8. The ultimate creep coefficient for Hawaiian aggregate concretes is stress-independent in the range of stresses from 0 to 60 percent of the 28th day compressive strength.
9. It is recommended that the deflections of the prestressed concrete beams should be modeled as the sum of individual components described in this paper.
10. Statistical analysis of the limited data showed that the coefficient of variation of the deflection components ranges from 2 to 10 percent.

11. A method is proposed to evaluate the expected deflection range, centered about computed values, which can be easily applied by the designer.

ACKNOWLEDGMENT

This investigation has been carried out at the Civil Engineering Department, University of Hawaii. It forms part of a research program on the time-dependent behavior of concrete made from Hawaiian aggregates supported by the Hawaii Department of Transportation and the Federal Highway Administration, U.S. Department of Transportation.

REFERENCES

1. Ross, A. D. Concrete Creep Data. The Structural Engineer, London, Aug. 1937, p. 314.
2. Lorman, W. R. The Theory of Concrete Creep. Proc. ASTM, Vol. 40, 1940, p. 1082.
3. Shank, J. R. The Plastic Flow of Concrete. Ohio State Univ., Bull. 91, 1935.
4. Thomas, F. G. A Conception of the Creep of Unreinforced Concrete and an Estimation of the Limiting Values. Structural Engineer, London, Vol. 11, No. 2, Feb. 1933.
5. Hansen, T. C. Creep and Stress Relaxation of Concrete, A Theoretical and Experimental Investigation. Proc., Swedish Cement and Concrete Research Institute, Stockholm, 1960, p. 98.
6. McHenry, D. A New Aspect of Creep in Concrete and Its Application to Design. Proc. ASTM, Vol. 43, 1943, p. 1069.
7. Watari, J. Shrinkage and Constant-Stress Creep Tests of Hawaiian Aggregate Concrete. Univ. of Hawaii, MS thesis, 1971.
8. Meyers, B. L., Branson, D. E., Schumann, C. G., and Christiason, M. L. The Prediction of Creep and Shrinkage Properties of Concrete. Iowa State Highway Commission, Res. Rept. 70-5, Aug. 1970.
9. Hamada, H. S., Zundelevich, S., and Chiu, A. N. L. Time-Dependent Behavior of Concrete Made With Hawaiian Aggregates. Highway Research Record 400, 1972, pp. 37-54.
10. Branson, D. E. Design Procedures for Computed Deflections. ACI Jour., Proc. Vol. 65, No. 9, Sept. 1968, p. 730.
11. Branson, D. E., Meyers, B. L., and Kripanarayan, K. M. Loss of Prestress Camber and Deflection of Non-Composite and Composite Structures Using Different Weight Concretes. Iowa State Highway Commission, Res. Rept. 70-6, Aug. 1970.
12. Pauw, A. Time-Dependent Deformations of Concrete. Missouri Cooperative Highway Research Program, Rept. 71-1.
13. Zundelevich, S. Statistical Studies on Deflections of Reinforced Concrete Beams. Civil Engineering Dept., Stanford Univ., engineer's thesis, Feb. 1968.
14. Variability of Deflections of Simply Supported Reinforced Concrete Beams. ACI Jour., Proc. Vol. 69, No. 1, Jan. 1972, p. 29.
15. Zundelevich, S., and Benjamin, J. R. Probabilistic Analysis of Deflections of Reinforced Concrete Beams. ACI, Publ. SP-31, 1972.
16. Branson, D. E., and Christiason, M. L. Time Dependent Concrete Properties Related to Design—Strength and Elastic Properties, Creep and Shrinkage. ACI, Publ. SP27-13, 1971.
17. Reichard, T. W. Creep and Drying Shrinkage of Lightweight and Normal-Weight Concretes. National Bureau of Standards, Monograph 74, March 4, 1964.

COMPARISON OF BRIDGE STRESS HISTORY RESULTS WITH DESIGN-RELATED ANALYSES

David W. Goodpasture and Edwin G. Burdette, University of Tennessee

Six bridges at three bridge sites located near a weigh station were investigated with respect to the stress ranges caused by normal traffic. The summation of these stress ranges for each bridge is presented, and comparisons are made with calculated stresses. The main objective of the stress comparisons is to introduce a workable method for the design engineer to use in predicting probable maximum and "typical" girder stresses due to normal traffic. Two AASHO design vehicles are considered in the analysis, and the stress resulting from this load, considering equal distribution of the moment to each girder, was shown to exceed almost all stress ranges measured in the field. One-half of this stress compares favorably with a significant number of stress ranges encountered on the most highly stressed girder. This type of analysis is intended to furnish a method for enabling the design engineer to utilize the results of the many stress history research efforts currently in progress or recently completed. The results presented are for particular bridges and should not be used generally until additional verification is obtained by using the stress history results of other researchers.

•DURING the past few years, the behavior of actual highway bridges subjected to truck traffic has been under investigation. In particular, the loading or stress history of bridges has been of interest with the ultimate goal of providing the bridge design engineer with a workable method to use in designing bridges relative to their fatigue strength or life. During the past 3 years, a stress and loading history study has been in progress at the University of Tennessee under a contract with the Tennessee Department of Transportation, Bureau of Highways, in cooperation with the Federal Highway Administration. This paper is based primarily on a portion of the results of that research project. The main objective of the research project was the collection and correlation of large amounts of strain and vehicle weight data so that the stress history and loading history of the bridges considered could be determined. Only the stress history portion of the data will be used here. A brief description of the bridges and testing procedure follows.

Six bridges at three locations were included in the investigation, and a brief description of these bridges is given in Table 1. A more complete description of the bridges may be found elsewhere (1). These bridges were chosen because they are representative of a large number of bridges in use today and because of their proximity to a weigh station on the Interstate System. The steel bridge serves as a control for comparison to other stress and loading history studies, whereas the reinforced concrete bridges were chosen to expand our knowledge in an area relatively untouched by other stress history researchers.

The data collection system consisted of a minicomputer with a magnetic tape unit, teletype, multiplexer interface, and strain gauge conditioning and amplification units, all housed in an office trailer. The trailer was moved to each bridge site for the col-

Sponsored by Committee on Dynamics and Field Testing of Bridges.

lection of data. The strain caused by the passage of a truck was digitized at a rate of 300 samples/sec/gauge, and the data were stored on magnetic tape. These strains were reduced to stress ranges of a later time, which enabled two types of stress range history to be considered. First, only the maximum stress range per truck was considered, and, second, all stress ranges above 1,000 psi were considered. Tables 2, 3, and 4 give the results obtained.

Inspection of the A and B columns in each of the three tables reveals very little difference above a stress level of 2,000 psi. In fact, only in three cases do the two columns differ at all for stresses greater than 3,000 psi. This result is in agreement with the comparison reported by Galambos and Heins (2). Galambos and Heins reported that at the 95 percent confidence level there was no significant difference in the means of the two sets of data above 3,000 psi. Their two sets of data correspond to columns A and B in the tables. The t-test was also used in the present study for each girder for stresses greater than 2,000 psi. As a result of these statistical tests, it may be concluded that at the 95 percent confidence level there was no significant difference between columns A and B. A word of caution is in order, however, because both statistical analyses were performed on small sets of data.

Consider girder W-3 in Table 4 where a large number of vehicles caused numerous stress ranges even at the higher stress levels. The discrepancy between columns A and B at the lower stress ranges is much larger than for the other girders. Therefore, as more data are accumulated over longer periods of time, the difference in the methods of stress range measurement may be significant at the medium stress ranges. Whether this is an academic question will have to await the results of laboratory fatigue tests where low stress ranges are being used to learn whether there is a measurable fatigue limit for steel. If the fatigue limit, if one exists, is established near 3,000 psi, then stress ranges below that level need not be considered, and any difference in the methods of determining stress ranges below that level is not important.

ESTIMATION OF EXPECTED STRESS RANGE

Because the program of stress measurement in highway bridges necessarily includes only a minute percentage of the total number of bridges in use, a method to predict analytically the maximum stresses to which a given bridge may be subjected would be most useful. Such a method would, ideally, be characterized by two attributes: It would predict, with "reasonable accuracy," both the maximum stress range and a more "typical" stress range that the bridge could be expected to experience; and it would be easy to apply.

It should be emphasized here that this paper makes no claim of having developed a method that precisely meets these criteria. The development of an analytical method was not included in the scope of the research project from which this paper has evolved. However, an attempt was made to predict, approximately, the stresses that the study bridges might be expected to experience. The method used and the results obtained are described in the following paragraphs.

Loading

The AASHO HS20 loading with one truck in each traffic lane was used to calculate the maximum moment at midspan for each bridge.

Moment Calculation

The bending moment at midspan was calculated from statics for the simple span steel bridge (bridge 1). The STRUDL II subset of the ICES program was used to calculate midspan bending moments for the three-span continuous, reinforced concrete beam bridges (bridges 2 and 3). The spans were divided into several segments with different moments of inertia to account for the nonprismatic cross section due to the beam haunches. The moment of inertia for each section was computed on the basis of an uncracked section, and the entire bridge cross section, including curbs, was considered.

Stress Calculation

Stresses at midspan were calculated for all three bridges on the basis of a uniform lateral distribution of the applied loads. This assumption is not considered unreasonable for the prediction of maximum stress, which occurs under the condition of one truck in each lane. For the case of only one truck on a bridge, however, the only justification that can be made for this assumption is its simplicity.

As suggested in the previous paragraph, two stresses were calculated for each bridge: first, the maximum expected stress due to one truck in each traffic lane and, second, a "typical" stress due to one truck on the bridge taken to be one-half of the maximum expected stress. The moment of inertia used in each stress calculation was that obtained on the basis of the entire bridge cross section at midspan, including curbs. A cracked section was assumed in the calculation of stress in the reinforced concrete bridges.

Results

The expected stress levels, calculated as described, are as follows:

Bridge Site	Maximum Expected Stress (psi)	"Typical" Stress (psi)
1	3,980	1,990
2 (eastbound)	4,560	2,280
3	3,700	1,850

The calculated stress levels are shown on the stress range histograms (Figs. 1, 2, and 3). These histograms were obtained from the data given in Tables 2, 3, and 4, considering only the maximum stress range for each truck.

Discussion

The results shown in Figures 1, 2, and 3 suggest the following observation: Using the relatively simple analytical approach described previously makes it possible to predict with "reasonable" accuracy (a) the approximate maximum stress range that a bridge may be expected to experience a significant number of times during its life and (b) the stress range that may be thought of as an approximate "average" for the stresses produced by loaded trucks crossing the bridge.

The preceding observation is particularly well supported by data shown in Figure 3 for bridge 3. There were a few stress ranges higher than the predicted maximum; however, the percentage of occurrences of these higher stress ranges was insignificant. The results shown in Figures 1 and 2 for bridges 1 and 2 indicate that the calculated maximum stress range was somewhat higher than the highest stress range recorded in the field. However, the calculated maximum stress is "in the ballpark"; that is, it does provide a reasonable, conservative prediction of the maximum expected stress range.

The reason for the somewhat higher observed stresses in bridge 3 is not entirely clear. One factor that might provide a partial explanation is that each bridge at site 3 is located at the bottom of a sag vertical curve. This could lead to higher stresses in the bridge girders because the dynamic impact factor would tend to be higher and there would be a greater likelihood that two heavily loaded trucks might be on the bridge at the same time. The fact that bridge 3 was 40 ft curb to curb, as opposed to 30 ft for the other bridges, could also be a factor, inasmuch as the lateral distribution of load would be affected by the roadway width and girder spacing.

The "typical" stress calculated for all three bridges fitted, reasonably well, the stress history data shown in Figures 1, 2, and 3. In each case, the calculated stress range gave a reasonable indication of the stress range, high enough to be of interest from the viewpoint of fatigue damage, that could be expected to occur under the action of a relatively high percentage of trucks.

Figure 1. Percentage of occurrences versus stress range at bridge site 1 (both bridges).

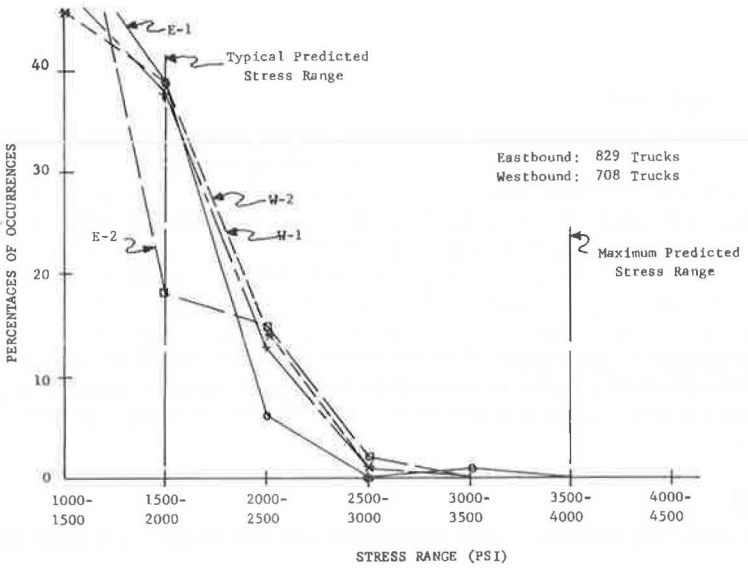

Figure 2. Percentage of occurrences versus stress range at bridge site 2 (eastbound).

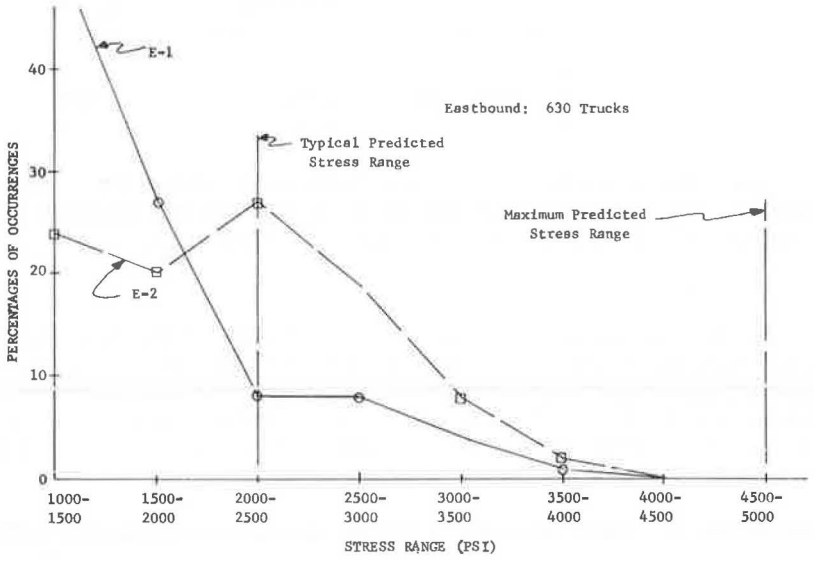

Figure 3. Percentage of occurrences versus stress range at bridge site 3 (both bridges).

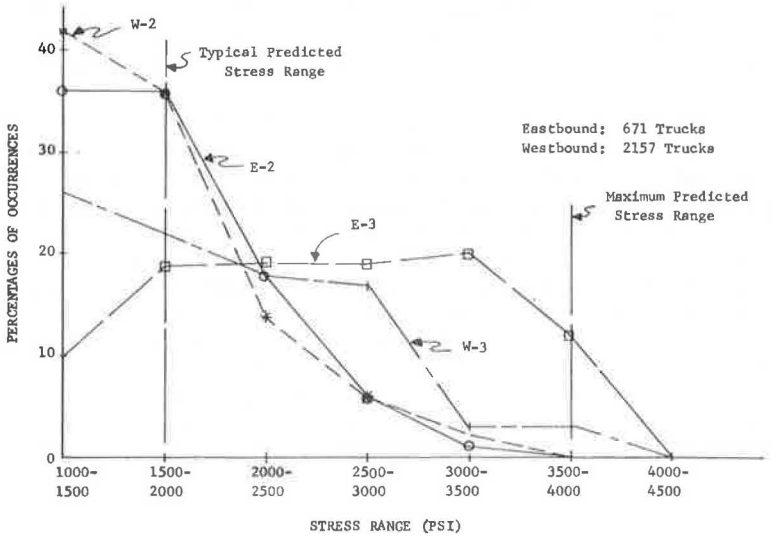

Table 1. Description of bridges.

Bridge No.	Direction	General Description	Span (ft)	Girder Spacing (ft, in.)	Skew (deg)	Location
1	E and W	Simple span steel girders with composite concrete deck, five W 36 x 170 girders with partial length cover plates	70	7 0	70	I-40 over Tenn-95
2	E	Three-span continuous, reinforced concrete deck girder, four girders	47, 66, 47	8 10	75	I-40 and I-75 over Everett Road
	W	Three-span continuous, reinforced concrete deck girder, five girders	58, 72, 58	6 8	75	
3	E and W	Three-span continuous, reinforced concrete deck girder, five girders	41, 60, 41	9 2	60	I-40 and I-75 over Campbell Station Road

Table 2. Stress ranges for bridge site 1.

Stress Range Level (psi)	Girder E-1		Girder E-2		Girder W-1		Girder W-2	
	A	B	A	B	A	B	A	B
1,000 to 1,500	270	367	280	307	196	355	206	265
1,500 to 2,000	196	206	78	82	157	184	176	186
2,000 to 2,500	29	30	64	64	52	54	62	63
2,500 to 3,000	1	1	7	7	5	5	3	3
3,000 to 3,500	3	3	1	1	1	1	0	0
3,500 to 4,000	1	1	—	—	—	—	1	1
Total	500	608	430	461	411	599	448	518

Note: A = one stress range per truck; B = all stress ranges ≥1,000 psi. Number of trucks eastbound was 829; westbound, 708.

Table 3. Stress ranges for bridge site 2.

Stress Range Level (psi)	Girder E-1		Girder E-2		Girder W-2		Girder W-3	
	A	B	A	B	A	B	A	B
1,000 to 1,500	196	295	96	261	153	594	180	451
1,500 to 2,000	103	114	82	121	143	220	147	182
2,000 to 2,500	31	35	110	120	95	107	77	80
2,500 to 3,000	31	32	79	80	48	50	14	14
3,000 to 3,500	17	19	31	34	15	15	3	3
3,500 to 4,000	2	2	10	10	0	0	—	—
4,000 to 4,500	—	—	—	—	1	1	—	—
Total	380	497	408	626	455	987	421	730

Note: Number of trucks eastbound was 630; westbound, 623.

Table 4. Stress ranges for bridge site 3.

Stress Range Level (psi)	Girder E-2		Girder E-3		Girder W-2		Girder W-3	
	A	B	A	B	A	B	A	B
1,000 to 1,500	171	204	58	340	527	653	475	819
1,500 to 2,000	160	164	101	151	454	471	400	471
2,000 to 2,500	81	81	101	111	176	185	315	337
2,500 to 3,000	24	24	106	108	71	73	313	326
3,000 to 3,500	4	4	109	109	19	19	232	244
3,500 to 4,000	—	—	64	64	6	6	51	52
4,000 to 4,500	—	—	6	6	2	2	15	15
4,500 to 5,000	—	—	1	1	—	—	5	5
5,000 to 5,500	—	—	—	—	—	—	3	3
5,500 to 6,000	—	—	—	—	—	—	4	4
Total	440	477	546	890	1,255	1,409	1,813	2,276

Note: Number of trucks eastbound was 671; westbound, 2,157.

CONCLUSIONS

The stress history study that formed the basis of this paper was a part of a continuing national effort to extend the state of existing knowledge relative to the fatigue life of bridges designed under existing specifications. Some of the results of this study are given in Tables 2, 3, and 4. These results agree very well with similar published results from other studies. As noted earlier, this study supports the observation (2) that, for stress ranges above approximately 3,000 psi, it makes little difference in the data whether one stress range per truck is considered or all stress ranges caused by each truck are considered.

As more stress history data are accumulated, effort must be directed toward relating these data to bridge design. For example, it would be most helpful if a bridge designer could calculate, with at least approximate accuracy, the maximum stress range that a bridge might be expected to experience a "significant" number of times during its life. It would be of further help if the designer could decide, on the basis of available information, whether the predicted stress range would be "acceptable" from the viewpoint of expected fatigue life.

The stress calculations described in this paper represent at least a tentative step toward the prediction of the maximum stress range referred to earlier. The method presented needs considerable refinement, a task that requires not only additional computational effort but also additional field test data for comparison purposes. If one then moves beyond the problem of stress range prediction to the question of "acceptability" of the predicted stress range, a gap in existing knowledge becomes evident. Needed to fill this gap are more laboratory data on high-cycle, variable stress range fatigue. Thus, it would appear to be desirable in the future to broaden the scope of research on stress history to include specific efforts to relate research results to bridge design.

ACKNOWLEDGMENTS

Appreciation is expressed to the Tennessee Department of Transportation, Bureau of Highways, for assistance in the performance of the research studies described. The contents of this report reflect the views of the authors who are responsible for the facts and the accuracy of the data. The contents do not necessarily reflect the official views or policies of the state of Tennessee or the Federal Highway Administration. This report does not constitute a standard, specification, or regulation.

REFERENCES

1. Goodpasture, D. W. Final Report on Stress History of Highway Bridges. Dept. of Civil Engineering, Univ. of Tennessee, 1972.
2. Galambos, C. F., and Heins, C. P., Jr. Loading History of Highway Bridges: Comparison of Stress Range Histograms. Highway Research Record 354, 1971, pp. 1-12.

DYNAMIC ANALYSIS OF BEAM-SLAB HIGHWAY BRIDGES

W. S. Peterson and C. N. Kostem, Lehigh University

The findings of an analytical study on the determination of vehicle-induced dynamic response of highway bridge superstructures are presented. The investigation utilized the finite element displacement approach. In contrast to the traditional one-dimensional modeling, which assumes the superstructure to be a single beam, the superstructure is here assumed to be two-dimensional, a composition of discrete beam and slab elements. The reported investigation was carried out for a simply supported bridge superstructure with a 71½-ft span length and no skew. The system consists of six 24/45 prestressed concrete I-beams and a 7½-in. thick concrete deck. An AASHO HS20-44 design vehicle was simulated by using a constant force system in the dynamic analysis. Damping was neglected, and the bridge surface was assumed to be free of imperfections. Numerical studies were carried out for various lane loadings and various vehicular speeds. Deflection and bending moment time histories for beams and deflection contour graphs for the deck slab corresponding to the 50-mph vehicular speed are provided. Analytical results were compared with the data obtained from field tests performed on the actual bridge. A good correlation was observed. This paper does not include the experimental study, which is presented in another publication. Conclusions were drawn and reported based on this investigation. [AUTHOR]

•THE DYNAMIC RESPONSE of bridge superstructures to moving loads has been a problem of interest for many years and has been studied by many investigators. The induced dynamic behavior produces a response spectrum indicating stresses and deformations that may be greater or less than those of the static load case for a given configuration (5). Most early investigations were aimed at the definition of the resonance characteristics of the bridge superstructure. In these early studies the entire bridge superstructure, which is composed of several girders and a slab, was idealized as a single beam for the analytical determination of the dynamic response (2, 3). This simplified model will only predict the gross behavior of the overall bridge superstructure. To establish the dynamic interaction of the components of the superstructure requires that a more refined model be employed. For the reported investigation the finite element method is used in which the system is assumed to consist of beam and plate elements. Advantages of the finite element method over the single beam model are the following:

1. A more realistic model that treats the entire cross section as a plate with several stiffeners is obtained,
2. The dynamic behavior of the superstructure can be obtained in both longitudinal and lateral directions,
3. Individual beam behavior can be investigated,
4. The slab response is obtained,
5. Interaction between the various beams and the slab may be studied, and
6. Dynamic load distribution factors can be predicted.

Sponsored by Committee on Dynamics and Field Testing of Bridges.

BRIDGE IDEALIZATION

Numerical studies were performed using an existing bridge near Lehighton, Pennsylvania, as the test structure (4, 5). The superstructure has a 71½-ft simply supported span with no skew. A field test of this structure subjected to static and dynamic loadings has been reported (5). The bridge cross section is shown in Figure 1.

The bridge superstructure was discretized into 20 plate elements and 24 beam elements connected at the node points as shown in Figure 2 (1). A lumped mass model is used in which the contributions to each node point by the bridge slab, beams, parapet section, curb section, and truck are considered to be concentrated at the node points. Experiments carried out on prestressed concrete bridges indicated that damping is negligible for the short-term response spectrum (2, 3). Therefore, damping has been neglected in this study. In the analysis it was assumed that the bridge roadway was free of surface irregularities.

VEHICLE IDEALIZATION

In this investigation a constant force model is used. Consequently, each wheel group is idealized as a time-independent concentrated load that is linearly distributed to the nearest node points. The front, drive, and rear axle groups applied a total constant force of 10.2, 32.2, and 32.67 kip respectively. This model simulates the AASHO HS20-44 design vehicle with spacing of 13.0 ft between front and drive axles and 20.4 ft between drive and rear axles.

ANALYTICAL RESULTS

Analytical studies were conducted for the following cases:

Truck Position	Speed (mph)
Lane 3	25
Lane 3	50
Lane 3	300
Lane 5	50

[The 300-mph speed was close to resonant speed of bridge superstructure (3).] For the sake of brevity, the discussions will be confined to the 50-mph lane 3 case. A nondimensional distance ratio defined by the ratio of the (front-wheel distance)/(bridge length) is used to locate the truck position. Displacements in the upward direction and moments that produce tension on the bottom fibers are considered positive.

Displacement and bending moment time histories show the response of a particular node point or group of node points as the truck crosses the bridge. Figures 3 and 4 show the displacement and bending moment time histories of nodal points 22, 23, and 24 on beam B. The dynamic and static nodal point responses are plotted on these graphs so that comparisons can be made. The dynamic response appears as an almost symmetric oscillation about the smooth static response curve. In the 50-mph case, the vehicle traverses the span in approximately 1½ sec. At a distance ratio of 1.467, the rear axle of the vehicle leaves the span and the static response becomes zero. After a ratio of 1.467, the dynamic oscillations still persist and would theoretically continue indefinitely inasmuch as damping was not included in the analysis.

Figures 5 and 6 show the displacement and bending moment time histories of the midspan section (node points 3, 8, 13, 18, 23, and 28 located on beams F, E, D, C, B, and A respectively). Beams A, B, C, D, and E have maximum deflections in the downward direction and maximum moments that produce tension in the bottom fibers. Beam F deflects upward and is under a negative bending moment producing tension in the top fibers. This is caused primarily by the unsymmetrical lane 3 loading.

Figure 7 shows the midspan deflection diagrams for the 50-mph lane 3 loading. The diagrams are numbered in sequence and show the displaced shape of the cross section at midspan for distance ratio intervals of 0.1231 (0.12 sec). The cross section deflects

Figure 1. Cross section of test bridge.

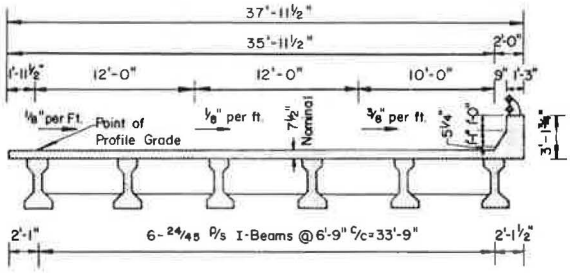

Figure 2. Finite element mesh.

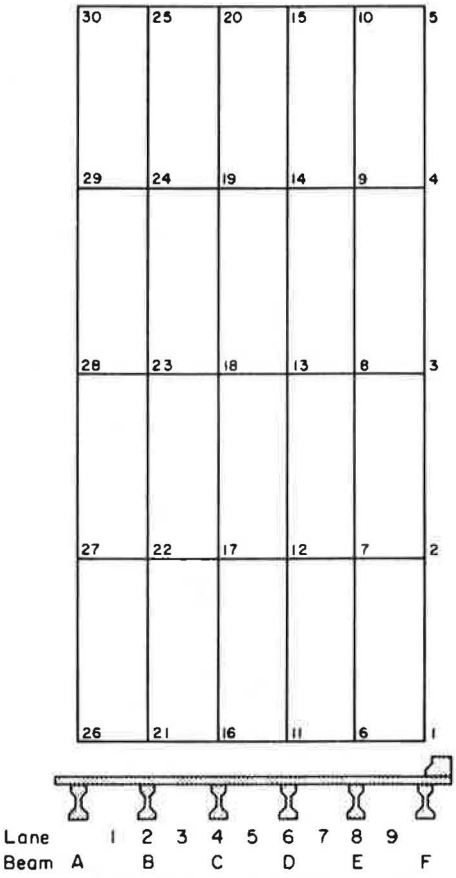

Figure 3. Displacement time history, 50-mph lane 3 case.

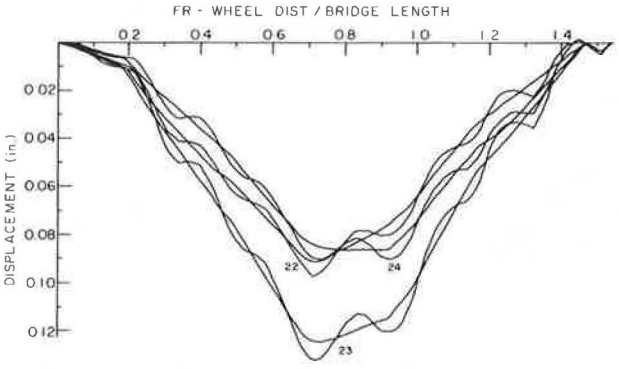

Figure 4. Bending moment time history, 50-mph lane 3 case.

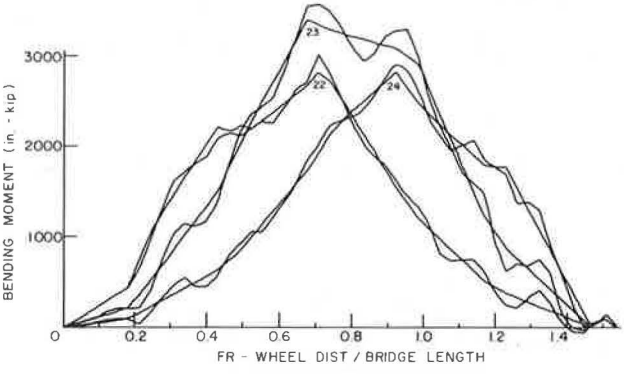

Figure 5. Displacement time history, 50-mph lane 3 case.

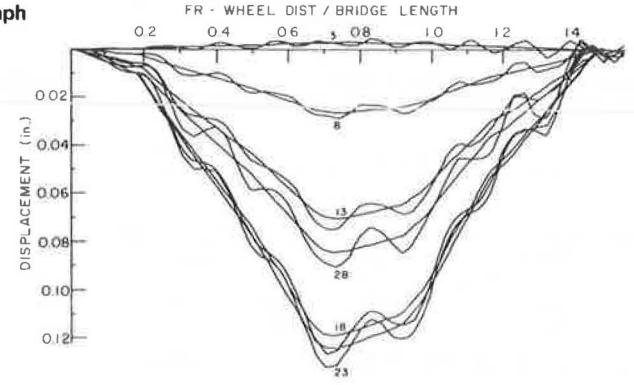

Figure 6. Bending moment time history, 50-mph lane 3 case.

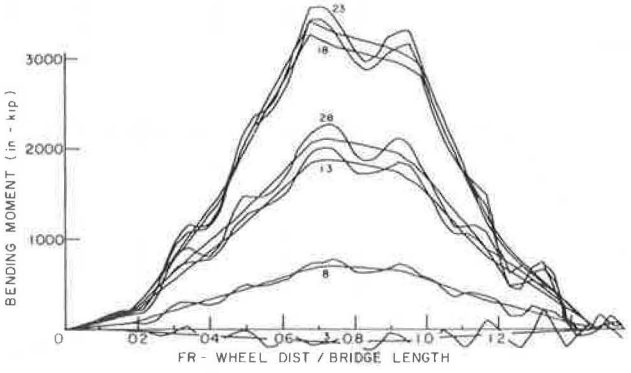

Figure 7. Displacement diagrams, 50-mph lane 3 case.

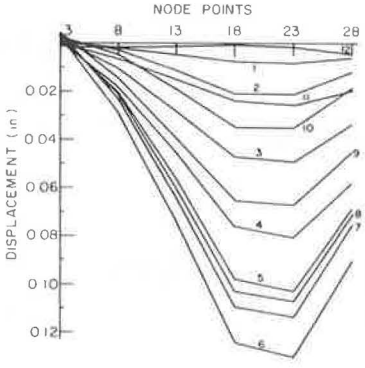

Figure 8. Displacement contours at distance ratio of 0.7076, 50-mph lane 3 case.

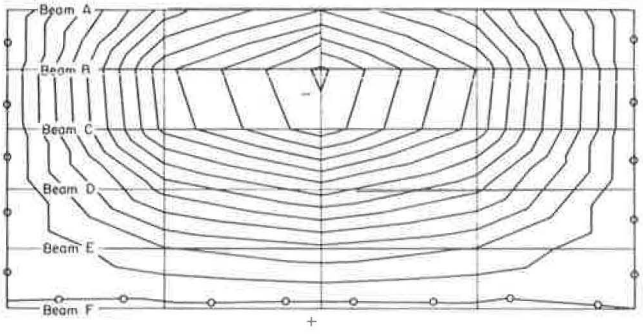

Figure 9. Displacement contours at distance ratio of 1.4153, 50-mph lane 3 case.

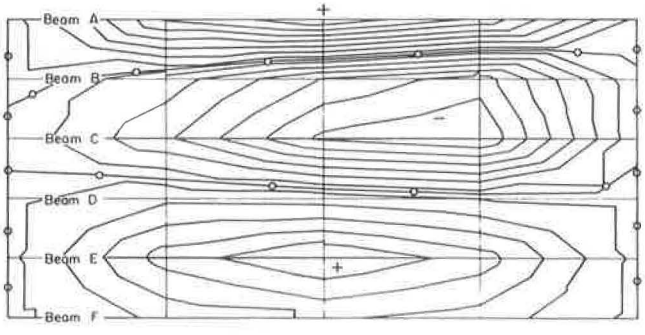

Figure 10. Displacement contours at distance ratio of 1.4462, 50-mph lane 3 case.

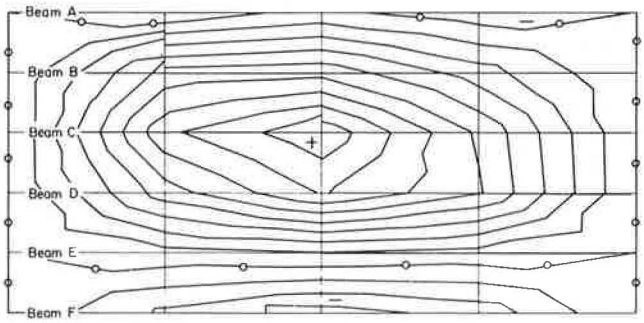

Table 1. Experimental and computed static midspan girder deflections and moments with corresponding ratios.

		Deflection (in.)			Moment (in.-kip)		
Beam	Node	Computed	Experimental	Computed/Experimental[a]	Computed	Experimental	Computed/Experimental[b]
A	28	-0.0842	-0.068	+1.24	+2,107	+1,905	+1.11
B	23	-0.1241	-0.090	+1.34	+3,350	+3,530	+0.95
C	18	-0.1188	-0.080	+1.48	+3,259	+3,168	+1.03
D	13	-0.0702	-0.052	+1.35	+1,879	+1,922	+0.98
E	8	-0.0260	-0.021	+1.24	+699	+772	+0.91
F	3	+0.0027	-0.004	-0.67	-150	+184	-0.82

[a]Average percentage of difference is 34.5. [b]Average percentage of difference is 8.0.

Table 2. Computed midspan girder deflections and moments and corresponding computed and experimental dynamic load factors for the 50-mph lane 3 case.

		Deflections			Moments		
Beam	Node	Computed (in.)	Computed $(DLF)_d$	Experimental[a] $(DLF)_d$	Computed (in.-kip)	Computed $(DLF)_m$	Experimental[b] $(DLF)_m$
A	28	-0.0910	1.081	0.93	+2,282	1.083	1.06
B	23	-0.1321	1.064	1.02[c]	+3,573	1.067	1.05
C	18	-0.1261	1.061	0.96	+3,431	1.053	1.03
D	13	-0.0749	1.067	0.97	+2,011	1.070	1.02
E	8	-0.0289	1.108	1.00	+773	1.106	1.21
F	3	+0.0046	1.704	1.33[c]	-256	1.707	-2.24
			1.075	0.96		1.080	1.06

Note: DLF = dynamic load factor = $\frac{\text{maximum dynamic response}}{\text{maximum static response}}$; total $(DLF)_d = \frac{\Sigma^* \text{ dynamic deflection}}{\Sigma^* \text{ static deflection}}$ where $\Sigma^* = 0.86D_A + D_B + D_C + D_D + D_E + 1.41\ D_F$ (5); total $(DLF)_m = \frac{\Sigma \text{ dynamic moment}}{\Sigma \text{ static moment}}$.

[a]For 52.6 mph, lane 2.
[b]For 50.7 mph, lane 2.
[c]Values were calculated by the authors and are different from those in an earlier report (5).

downward during the intervals 1 through 6 then upward as the truck leaves the bridge span during the intervals 6 through 12.

Displacement contours (i.e., lines connecting points of equal displacement) are shown in Figures 8, 9, and 10. A positive sign indicates a region of upward deflection, whereas a negative sign indicates a downward deflected region. The contours of zero displacement are marked with a 0. Figure 8 shows the displacement contours of the bridge superstructure at a distance ratio of 0.707 at which time the maximum displacement occurs at node 23. It can be noted that beam F is deflecting upward.

A contour displacement sequence (Figs. 9 and 10) is presented as the rear axle of the vehicle leaves the bridge. These figures illustrate the bridge vibration characteristics as the response of the superstructure approaches the state of free vibration. From the displacement contours it is apparent that the bridge deck vibrates in elliptical dish-shaped patterns with the major axis of the ellipse parallel to the longitudinal axis of the bridge. A line parallel to the major axis of the ellipse is seen to correspond to the first modal shape of a simply supported beam.

COMPARISON WITH EXPERIMENTAL RESULTS

The analytical results are compared to the Lehighton Bridge field test results (4, 5). Experimental and analytical static deflection and moment values are given in Table 1. Theoretical results show beam F deflecting upward for a lane 3 loading, as in the case of an experimental lane 2 load, but opposite to an experimental lane 3 case. Beams A, B, C, D, and E exhibit deflection ratios greater than 1.0, indicating that the stiffness has been underestimated, whereas for beam F the stiffness has been overestimated. A deflection ratio is defined as the analytic result divided by the corresponding experimental result.

The computed dynamic midspan deflections and bending moments for the 50-mph lane 3 loading, along with the corresponding theoretical and experimental dynamic load factors, are given in Table 2. The total dynamic load factor, as defined in Table 2, provides a measure of the overall dynamic amplification of the static response. Beams not directly under the load (A, D, E, and F) tend to have higher amplification factors than those beams directly under the load (B and C). The maximum dynamic load factors exceed the AASHO impact factor of 1.255 (6) and occur at beam F in both the experimental and analytical investigations. Experimental values obtained for the response of beam F may be in doubt due to the lack of sensitivity of the data logging equipment associated with measuring such small relative deflections. Also uncertainties may exist in the analytical model due to the difficulty in estimating the stiffness contribution made by the curb and parapet sections to beam F.

The average frequencies of vibration for the bridge superstructure are as follows:

1. Natural unloaded theoretical (single beam model) = 5.7 cps,
2. Loaded experimental (52.6 mph lane 2) = 5.5 cps, and
3. Loaded theoretical (finite element model, 50 mph lane 3) = 4.9 cps.

The loaded frequency is the frequency of vibration of the bridge superstructure when the mass of the loading vehicle is included in the system, whereas for the unloaded frequency the mass of the loading vehicle is not included in the system. The experimental and theoretical loaded frequencies were determined by finding the average loaded frequency of forced vibration for beam B. The natural unloaded frequency of free vibration was estimated by considering the entire superstructure cross section as a single beam (3). The single beam model gave the highest estimated frequency, whereas that from the finite element technique gave the lowest (1).

CONCLUSIONS

A two-dimensional finite element model rather than the one-dimensional single beam model was employed in the dynamic analysis of a beam-slab highway bridge superstructure. This two-dimensional model enabled the authors to obtain the static and dynamic response of the individual beams and slab sections. The analytical study including all the vehicle speeds shown previously and the available field test data has indicated the following:

1. The variation of the dynamic load factor is a nonlinear function of the vehicle speed.
2. The dynamic load factors for the exterior beams were consistently higher than those for the interior beams. Depending on the location of the vehicle, in some cases, they were also greater than the AASHO impact factor of $1 + \frac{50}{L + 125}$, which for the test bridge was 1.255.
3. Beams that are not directly under the load tend to have higher amplification of moment than those beams directly under the load. It should not be inferred from this that the maximum dynamic stresses necessarily occur in the beam with the maximum amplification factor. The maximum stress is, of course, a function of the maximum live load stress as well as the amplification factor.
4. The dynamic response of the beams tends to oscillate about the static response.

REFERENCES

1. Clough, R. W., and Felippa, C. A. A Refined Quarilateral Element for Analysis of Plate Bending. Proc. Second Conf. on Matrix Methods in Structural Mechanics, Wright-Patterson AFB, Ohio, 1969, pp. 399-440.
2. Fenves, S. J., Veletsos, A. S., and Siess, C. P. Dynamic Studies on Bridges on the AASHO Road Test. HRB Spec. Rept. 71, 1962.
3. Linger, D. A., and Hulsbos, C. L. Dynamics of Highway Bridges. Iowa Eng. Exp. Station, Iowa State Univ., Proj. 370-S, Pt. I, July 1960.
4. Peterson, W. S., and Kostem, C. N. Dynamic Analysis of Highway Bridges Using the Finite Element Method. Fritz Eng. Laboratory, Lehigh Univ., Rept. 400.7, May 1972.
5. VanHorn, D. A., and Chen, C. H. Structural Behavior of a Prestressed Concrete I-Beam Bridge, Lehighton Bridge. Fritz Eng. Laboratory, Lehigh Univ., Rept. 349.4, Oct. 1971.
6. Standard Specifications for Highway Bridges. AASHO, 1969.

LOADING HISTORY OF SPAN 10 ON YELLOW MILL POND VIADUCT

David G. Bowers, Connecticut Department of Transportation

Two simple-span structures on heavily traveled Interstate 95 in Bridgeport, Connecticut, were tested electronically to determine the magnitude and frequency of stress ranges induced by normal live loading. The bridges were designed in accordance with composite-action techniques and consisted of 7½-in. concrete decking on rolled cover-plated beams. Strain gauges were mounted at the critical ends of cover plates and at midspan on selected beams and on one diaphragm. A computer-controlled data acquisition system made it possible to record strains continually. As a supplement to strain data, lane counts were made and truck classifications and weights and measurements obtained. Gross truck weights were fairly evenly distributed between 10,000 and 70,000 lb with maximum weight recorded at between 90,000 and 100,000 lb. Distribution of truck traffic was approximately 55 percent in the outer lane, 45 percent in the middle lane, and less than 1 percent in the inner lane. On the basis of current popular methods of fatigue analysis, which tend to neglect stress ranges below 3 ksi, fatigue failure of the beams tested would be considered a remote possibility for the near future. The numerous low stress ranges induced by live loading, although their effect on the integrity of cover-plated beams is unknown, could perhaps drastically shorten the service lives of these members.

•IN LATE 1970, catastrophic failure of an internal, cover-plated steel beam occurred in span 11 of the 14-span Yellow Mill Pond Viaduct on Interstate 95 in Bridgeport. The failure, shown in Figure 1, originated as a crack at the toe of the fillet weld along the end of the primary cover plate and propagated through the flange and 16 in. up into the web before detection and subsequent repair. Also noted in connection with this failure was a high incidence of missing bolts in the diaphragm-to-beam connections. Follow-up inspection of other cover-plated beams in other bridges on I-95 revealed the presence of extremely small cracks (less than 1 in. long) along the weld toes at the cover plate ends.

Certain investigators suggested that the cracking might have resulted from fatigue action generated by normal live loading. In this connection, a study was undertaken to determine (a) the frequency of ranges of dynamic stresses induced in selected bridges by normal live loading and (b) the general composition and weight of the traffic causing these stresses and to estimate (c) the fatigue lives of the structures from the data acquired in (a) and (b). This report is devoted to discussion of the equipment and methods employed to acquire appropriate strain data and to the findings derived therefrom.

TEST BRIDGES

Two simple-span, cover-plated, steel-beam bridges were selected for acquisition of data that would permit assessment of structural behavior under normal loading. These test bridges were the eastbound and westbound structures in span 10 of the Yellow Mill Pond Viaduct. Selection of these bridges was based on the following:

Sponsored by Committee on Dynamics and Field Testing of Bridges.

1. Span length and steel types similar to those in span 11,
2. Live loading the same as on span 11, and
3. Easy access to the underside of the bridge.

Figure 2 shows a plan view of the layout of beams and diaphragms in span 10; Table 1 gives data on beam detail. As can be seen, the internal beams are the same in both eastbound and westbound structures. The fascia beams, however, vary not only in size but also in cover plate detail. The ends of the partial cover plates are not tapered but are rounded to a radius of 3 in. at the corners. Fillet welds 1½ in. in size extend across and around the ends and along the edges of the plates for a distance of 2 ft, at which point $^{5}/_{16}$-in. fillet welds begin and continue along the remainder of the edge.

Both bridges carry three lanes of traffic on 7¼-in. concrete decks. The roadways in span 10 are on tangent and have a positive gradient of approximately 1 percent to the west. In 1969, a "thick" two-course bituminous concrete overlay was placed on the concrete deck in both roadways. The bridges were built between 1956 and 1957 and were opened to traffic in January 1958.

INSTRUMENTATION

Strain Gauges

Electrical-resistance strain gauges were mounted at various points on the tension flanges and tension flange cover plates, as well as at the midpoint on one of the diaphragms. Strain gauge placement is shown in Figure 2. As can be seen, gauges were placed primarily at two locations on the beams: on the tension flange cover plate at midspan and on the tension flange 4 in. off the leading edge (with respect to traffic flow) of the primary cover plate. Auxiliary gauges were mounted at the secondary plate terminus on beam 3 on the westbound structure and on the full-length primary plate 4 in. off the secondary plate on the external fascia beam in the westbound roadway.

The gauges were paper-backed and were cemented to the beam after recommended preparation of the steel. After waterproofing, the gauges were connected via transducer cable to electronic strain-monitoring equipment housed in an FHWA trailer.

Strain-Monitoring Equipment

The data acquisition system employed in the tests was developed for the FHWA by Scientific Data Systems. The system is largely automated and is computer controlled. It has been employed successfully in a number of loading history tests conducted by the FHWA on various bridges throughout the country.

Briefly, the equipment takes variations in analog voltages produced in a maximum of 10 resistance strain gauges, digitizes the magnitude of this variation for each gauge, stores the values and tabulates them as strains within certain preselected ranges, and prints out the total number of strains that fall within these ranges for each gauge over a specified time interval. The levels of strain that define the individual ranges can be manipulated to produce a meaningful picture of the stress events that take place under a given set of conditions.

TEST PROCEDURES

Acquisition of Strain Data

Strain-range data were acquired and printed out during 64-min cycles. The computer was programmed to classify and count strain ranges for 60 min and print out the stored data during the last 4 min of the cycle. Stress ranges were manipulated so that minimum stress range, i.e., the stress below which the computer will disregard an event, was set at 0.6 ksi; thus, negligible strains produced from passage of light vehicles and damped vibrations induced by heavy trucks were eliminated from the count. In the eastbound span, stress levels were increased in increments of 0.45 ksi from 0.6 to 4.65 ksi, whereas in the westbound span levels increased in increments of 0.6 ksi from 0.6 to 6.0 ksi. One exception to this rule occurred at midspan of the external fascia beam in the westbound roadway where higher stress levels were encountered.

Figure 1. Failure in internal cover-plated steel beam.

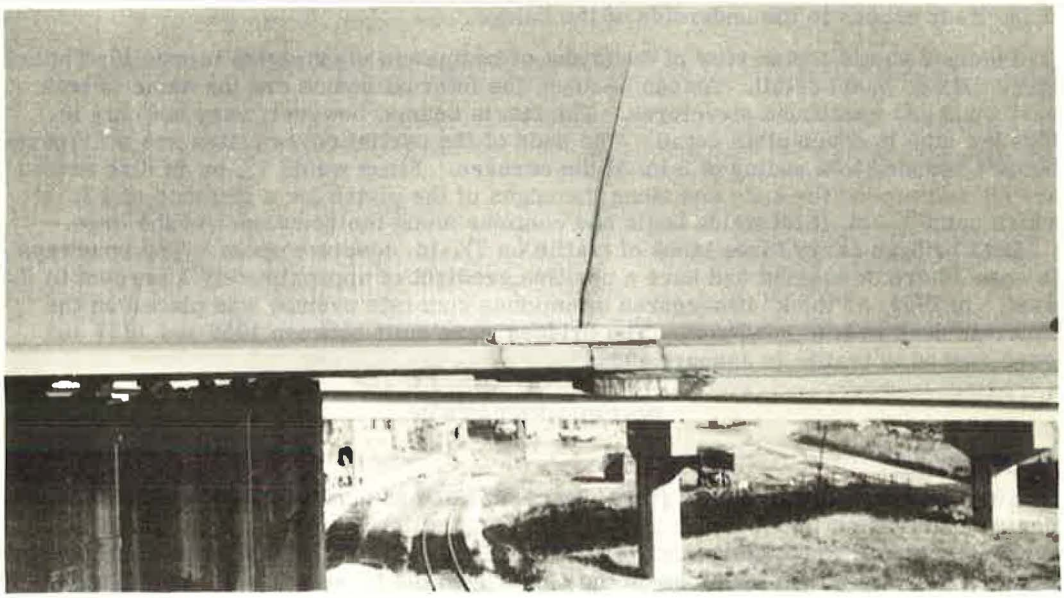

Figure 2. Framing plan of span 10 with locations of strain gauges.

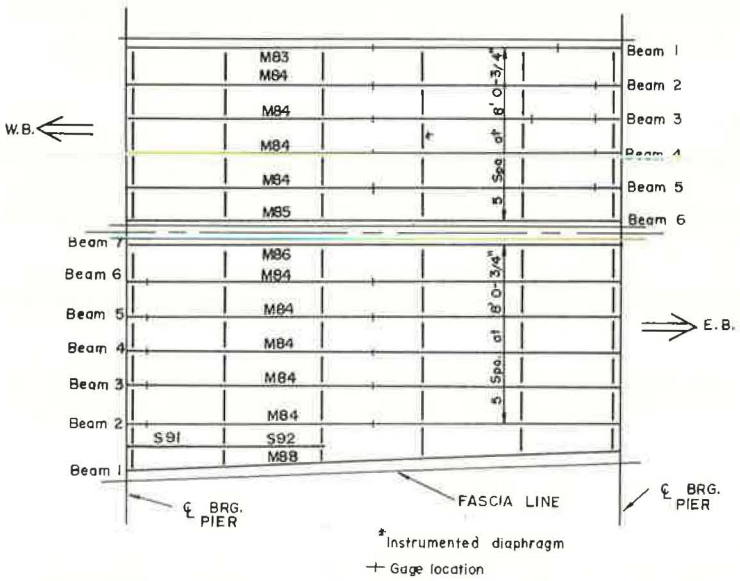

In this case, the initial stress range was 0.6 to 2.4 ksi with successive ranges increased in increments of 0.6 ksi to 7.2 ksi. Thus, the computer was programmed to scan for a peak stress whenever the analog voltage exceeded that corresponding to the minimum test level of 0.6 ksi. Once the peak strain was sensed, the computer would scan for a valley only when the signal voltage dropped below that corresponding to a no-load situation. The resulting stress range would therefore be the absolute value measured between the peak and valley and would be counted in the appropriate stress category. Secondary ranges were counted only when the minimum and zero stress levels were exceeded.

Original plans called for 24-hour data acquisition for a period of 5 to 6 days on each structure. Problems with the computer, however, reduced actual strain-sensing time to 33 and 65 hours on the eastbound and westbound structures respectively. Despite this reduction, the volume of data acquired was quite adequate to develop a clear picture of the loading to which the individual members are subjected.

Truck Classification and Lane Counts

All trucks and buses with more than four tires were classified and counted according to the lane in which they crossed the test spans. Normal highway lighting provided sufficient illumination for dark-hour classification and counting. Thus, a continual record of truck crossings was obtained over a 6-day period for both eastbound and westbound spans. Data on multiple truck crossings, i.e., instances where any part of more than one truck was on the span at one time, were obtained for shorter time intervals on each bridge. Truck-count periods corresponded to computer recording intervals, e.g., counting for 1 hour followed by a 4-min lapse during which the computer printed out strain data.

Truck Weights

Unfortunately, off-highway space for truck-weighing operations in the Bridgeport area was limited to the Stratford Toll Station. The truck-weighing site selected was a rest area in Westport, approximately 9.25 miles, and 10 exits, west of the test spans. At Westport, weighing in both roadways was carried out over three nonconsecutive 8-hour shifts. Trucks were flagged down at random and driven across portable scales that weighed individual axles. Axle spacings were measured simultaneously with the weighing. A traffic count was also conducted at the Westport site during the weighing operations. This count took into consideration all types of vehicles, including passenger cars and motorcycles, but did not classify vehicles according to lane traveled.

TEST RESULTS

Eastbound Structure

Table 2 gives the output of the 11 gauges monitored in the eastbound span and also the number of trucks that traversed the structure during the total recording period. As previously indicated, malfunctions in the computer system resulted in intermittent recording of stress ranges, which totaled 33 hours for the majority of gauges.

As can be seen from the table, 94 to 99 percent of the stress ranges occurring at the end of the cover plates fell within the 0.60- to 1.95-ksi levels for all beams. Very few events were recorded in excess of 2.40 ksi, and only a single even above 3.3 ksi (beam 3). Total events divided by the total trucks indicates to some extent the distribution of loading across the span at the ends of the cover plate. It should be noted that beams 3 and 4, which are directly under the outside and middle lanes, sustained the highest value of stress events per truck at this location.

As for the midspan gauges, approximately 97 to 99 percent of all stress ranges recorded fell within the limits 0.60 to 2.85 ksi. As is apparent, the value of events per truck increases with increasing beam number from outside to inside of the bridge; the number of events greater than 2.85 ksi is also much higher than expected in the higher numbered beams (5 and 6). The distribution of high stress ranges would indicate that beam 4, which would normally be expected to carry 25 to 30 percent of the

total internal live load moment generated in the five beams in question, is now sustaining considerably less than its share of high-stress events. Conversely, beam 6, which is under the inside lane and would normally carry approximately 12 to 20 percent of the live load moment induced in these five members, is sustaining about 33 percent of the events greater than 2.85 ksi. Assignation of one specific cause of this unusual distribution is difficult inasmuch as a combination of effects, e.g., bridge and traffic dynamics, interaction of longitudinal and torsional motions, and construction differences, could make themselves felt in unpredictable ways.

During computer operation, approximate lane distribution of all trucks in the eastbound roadway of span 10 (Table 2) was as follows: 55 percent in the outer lane, 45 percent in the middle, and less than 1 percent in the inner. Weekday truck volume was high and exhibited a certain periodicity with peak volume occurring at about 900 to 1,000 hours. Weekend truck traffic was low and favored the outside lane. Multiple crossings were generally less than the number of total commercial vehicles by an order of magnitude. Considerable jumps in multiple crossings occurred during peak-hour traffic flows on the weekdays. Most of the multiple crossings involved single trucks in the outer and middle lanes.

In Westport, a total of 845 trucks were weighed and measured. The majority of gross truck weights were fairly uniformly distributed between 20 and 70 kip, with no loading exceeding 100,000 pounds. As for overweight vehicles, 21 of the 845 trucks weighed exceeded the allowable maximum weights for their respective classes as established in the Connecticut code. It is interesting to note, however, that the greatest percentage of illegal overweights was not in gross loadings but in the single drive axles on the 2S-1 and 2S-2 vehicles. Of the 311 2S-2 trucks weighed for example, 56, or 18 percent, carried excessive weight on the single drive axle.

Westbound Structure

Table 3 gives the output of the 13 gauges monitored in the westbound span and also the number of trucks that traversed the structure during the total recording period. Computer recording time for the gauges varied from 65 hours 10 min to 15 hours 10 min due to channel sharing and, in certain cases, gauge failure. In the table, the a gauges are those placed on the flange next to the primary cover plate, and the e gauges are those mounted on the primary plate just off the secondary one. As in the eastbound structure, recording of stress ranges was not continuous as planned but intermittent due to minor system malfunctions. According to the table, from 88 to 97 percent of the total stress events occurring at the end of the primary cover plates fell within the 0.6- to 1.8-ksi range. Only 35 events greater than 3.0 ksi were recorded at these locations, and, of these, 28 occurred on beam 2. In the case of the two e gauges, the one mounted on the fascia beam (beam 1) produced considerably more high stress ranges than the one on beam 3, despite the significantly greater section modulus and exterior position of beam 1.

As for midspan gauges, approximately 95 to 99.9 percent of all stress ranges recorded fell within the limits 0.60 to 3.6 ksi. It follows from Table 3 that the number of stress events greater than 3.0 ksi decreases with increasing beam number (outside to inside). It will be noted that the frequency of high-stress events occurred in just the opposite manner: increasing with increasing beam number.

The output of the gauge on the diaphragm between beams 3 and 4 produced some of the most surprising results. Each truck that traversed the test span during the recording period gave rise to an average of 1.9 stress-range events in this member. More surprising yet was the magnitude of the stress ranges. In 63 hours, the bottom flange at midspan of the diaphragm was stressed to 3.0 ksi more than 2,400 times. Included among these were 27 stress events greater than 5.4 ksi. This might explain the high incidence of bolt failures in the diaphragm-to-beam connections that have occurred in this viaduct.

Like the eastbound roadway, percentage of trucks on the outer, middle, and inner lanes in the westbound roadway averaged 55, 45, and 1 percent respectively, with variations of 4 to 5 percent occurring in the outer and middle lanes depending on hours of

Table 1. Details of beams shown in Figure 2.

Member	Cover Plate Dimensions (ft) Top	Bottom	Size	Center-to-Center Bearing (ft, in.)
M88	14 × 1¼ × 64	15 × 1¼ × F. L. 14 × 1 × 77	36WF300	113 7 13/16
M84	14 × 1 × 65	15 × 1¼ × 95 14 × 1⅛ × 77	36WF230	113 6
M86		14 × ¾ × 75	36WF280	113 6
M85	14 × ⅞ × 58½	15 × 1 × 87 14 × ¾ × 74	36WF280	113 6
M83	14 × 1¼ × 64	15 × 1¼ × F. L. 14 × 1 × 76	36WF300	113 6
S91			18WF60	
S92			18WF60	

Table 2. Total number of events at each stress range.

Item	End of Cover Plate 2a	3a	4a	5a	6a	Midspan 2d	3d	4d	5d	6d
Stress level and stress, ksi										
0 at >4.65	0	0	0	0	0	0	0	0	0	0
1 at 4.65	0	0	0	0	0	0	0	0	1	2
2 at 4.20	0	0	0	0	0	2	5	2	5	8
3 at 3.75	0	1	0	0	0	9	23	11	17	41
4 at 3.30	0	6	0	0	1	67	151	36	103	171
5 at 2.85	0	91	2	3	0	278	464	245	302	396
6 at 2.40	9	176	19	34	1	644	635	858	485	724
7 at 1.95	110	897	251	384	55	1,022	1,094	1,266	940	1,783
8 at 1.50	937	1,307	1,827	1,236	444	1,931	1,798	1,963	2,032	3,428
9 at 1.05	2,154	1,947	2,542	2,221	1,013	1,906	1,726	1,835	1,357	2,023
Minimum 0.60										
Total	3,210	4,425	4,641	3,878	1,514	5,859	5,896	6,216	5,242	8,576
Total trucks	7,783	7,783	7,783	7,783	3,792	7,783	7,783	7,783	6,543	7,783
Events/truck	0.41	0.57	0.60	0.50	0.40	0.75	0.76	0.80	0.80	1.10
Total recording time, hours	33	33	33	33	17	33	33	33	28	33

Table 3. Total number of events at each stress level.

Item	End of Cover Plate 5a	4a	3a	2a	1e	3e	Dia-phragm	Midspan 4d	3d	2d	1d	Stress for 1d (ksi)
Stress level and stress, ksi												
0 at >6.0	0	0	0	0	0	0	2	0	0	1	3	>7.2
1 at 6.0	0	0	0	0	7	0	25	0	0	11	5	7.2
2 at 5.4	0	0	0	0	9	0	79	0	0	21	13	6.6
3 at 4.8	0	0	0	0	30	0	248	0	10	54	32	6.0
4 at 4.2	0	1	1	3	72	0	673	7	26	241	57	5.4
5 at 3.6	0	3	2	25	146	17	1,375	42	124	556	99	4.8
6 at 3.0	1	34	8	106	402	96	2,797	392	452	801	225	4.2
7 at 2.4	36	331	127	838	1,027	516	5,077	1,412	992	1,559	415	3.6
8 at 1.8	662	1,946	1,244	2,654	3,064	1,184	9,122	4,091	2,223	4,358	689	3.0
9 at 1.2	3,551	5,127	3,756	4,807	3,839	1,527	8,304	6,323	3,263	5,001	7,908	2.4
Minimum 0.6												0.6
Total	4,270	7,442	5,138	8,431	8,596	3,340	27,702	12,267	7,090	12,603	9,452	
Total trucks	14,877	14,582	7,654	14,582	10,538	3,386	14,582	14,582	8,393	14,385	7,744	
Events/truck	0.29	0.51	0.67	0.58	0.82	0.99	1.90	0.84	0.84	0.88	1.22	
Total recording time, hour:min	65:10	63:10	34:10	63:10	45:00	15:10	63:10	63:10	36:10	62:10	30:00	

computer operation. Periodic fluctuation in commercial traffic and in multiple crossings also followed closely the patterns that developed in the eastbound flow. Commercial vehicles accounted for approximately 13.5 percent of the total traffic flow.

In Westport, 588 trucks were sampled for gross and axle weights in the westbound roadway. In the popular truck classes, the average gross weights were generally equal to, or less than, those measured in the eastbound roadway. Distribution of gross truck weights was fairly uniform between 30 and 70 kip. Approximately 10 percent more westbound trucks weighed between 20 and 30 kip than eastbound trucks. Gross truck weights in excess of 70 kip were about 8 percent of the total trucks weighed; this percentage was about double that in the eastbound roadway. Average westbound gross truck weight was, however, slightly lower than the eastbound as a result of the higher percentage of trucks weighing 20 to 30 kip.

As in the eastbound roadway, the majority of illegal loadings occurred in the single drive axle on the 2S-2 trucks. Approximately 10.3 percent of the 3S-2 vehicles were above the maximum allowable gross weight of 73,000 pounds, which amounted to three times the overweight trucks in this class in the eastbound roadway. Percentages of overweights in other classes were similar in both roadways.

FATIGUE CONSIDERATIONS

In analysis of the fatigue lives of the two spans under consideration, various assumptions were made. First, the percentage of trucks in the total traffic stream was considered constant from 1958 to 1971 (about 13.5 percent). Second, the 1967 ADT was assumed to represent the average ADT for the period 1958 to 1971. Third, the stress conditions given in Tables 2 and 3 were assumed to prevail since 1958. Fourth, the stress level below which there would be a negligible effect on fatigue was assumed to be 2.85 and 3.0 ksi for the eastbound and westbound roadways respectively. Following these assumptions, estimated values of total stress ranges greater than 2.85 (eastbound) and 3.0 (westbound) ksi that have occurred since 1958 were obtained for each gauge.

The results of this exercise indicate that, based on present behavior under live loading, the two test structures are adequately designed to resist fatigue for some time to come. For example, the critical end-of-cover-plate location monitored by gauge 1e in the westbound roadway was subjected to more than 586,000 events greater than 3.0 ksi, the greatest number sustained for this location on both bridges. Even if it is assumed that all 586,000 events were registered at the maximum range recorded (6.0 ksi), this particular detail would be in no immediate danger of fatigue failure because the 95 percent lower confidence limit for cycles to failure has been estimated at about 4×10^6 cycles at S = 6 ksi for beams with end-welded cover plates.

Considering the results obtained from the tests and subsequent fatigue analyses on span 10, it is difficult to comprehend the apparent fatigue failure in adjacent span 11. The two spans are almost identical in detail and completely identical with regard to length, traffic, age, environment, and steel. There are, however, conjectural differences, such as construction technique and workmanship, that may very well have entered into the failure in span 11.

If we disregard the popular theory that the effect of low stress levels on beam-fatigue failure is negligible, another possibility exists. The shape of the S-N curve below S = 3 ksi is not known for cover-plated steel beams. All known laboratory tests in this area have been carried out above this stress level. Thus, if the S-N curve does not flatten out below S = 3 ksi as is currently assumed but maintains the same slope, it is entirely possible that the large number of low-level stress events, say from 3.0 to 0.6 ksi, that have occurred at critical points in the members may exert a considerable influence on the fatigue lives of the structures in span 10. The number of these events, together with the low-amplitude stress cycles that occurred in the damping phase and were not recorded as events in this study, can be estimated at close to 200,000,000 for certain members.

From the test data obtained in this study, it is safe to assume that the fatigue behavior of one bridge cannot necessarily be used to assess the fatigue behavior of a similar bridge subject to the same loading and environmental conditions.

SPONSORSHIP OF THIS RECORD

GROUP 2—DESIGN AND CONSTRUCTION OF TRANSPORTATION FACILITIES
John L. Beaton, California Division of Highways, chairman

BRIDGE SECTION
Arthur L. Elliott, California Division of Highways, chairman

Committee on Bridge Design
Richard J. Posthauer, New York State Department of Transportation, chairman
William L. Armstrong, N. H. Bettigole, Louis M. Bjorn, J. N. Clary, Daniel E. Czernik, A. L. Elliott, Frede Gloersen, George G. Goble, Theodore R. Higgins, Nelson C. Jones, William A. Kline, Heinz P. Koretzky, Robert J. McDonagh, Robert M. Olson, Adrian Pauw, Donald A. Recchio, W. Jack Wilkes

Committee on Concrete Superstructures
Cornie L. Hulsbos, University of New Mexico, chairman
W. E. Baumann, Russell L. Chapman, Jr., Hotten A. Elleby, John M. Hanson, Norris L. Hickerson, Francis J. Jacques, Daniel P. Jenny, Alan H. Mattock, J. L. Norris, Robert A. Norton, Emile G. Paulet, Paul F. Rice, Dominick L. Somma, David A. Van Horn, Earle E. Wilkinson

Committee on Dynamics and Field Testing of Bridges
Robert F. Varney, Federal Highway Administration, chairman
James W. Baldwin, Jr., Edwin G. Burdette, Michael E. Fiore, Charles F. Galambos, Egbert R. Hardesty, Conrad P. Heins, Jr., Cornie L. Hulsbos, Henry L. Kinnier, Kenneth H. Lenzen, Norman G. Marks, Fred Moses, W. H. Munse, Leroy T. Oehler, Ronald R. Salmons, W. W. Sanders, Jr., Chester P. Siess, William H. Walker, Robert K. L. Wen, G. W. Zuurbier

Lawrence F. Spaine, Highway Research Board staff

The sponsoring committee is identified by a footnote on the first page of each report.

The contents of this report reflect the views of the author who is responsible for the facts and the accuracy of the data presented herein. The contents do not necessarily reflect the official views or policies of the state or the Federal Highway Administration. This report does not constitute a standard, specification, or regulation.